

*Stochastic Resonance in Vision: Models and
Data*

Tham, Carole

2006

MIMS EPrint: **2007.7**

Manchester Institute for Mathematical Sciences
School of Mathematics

The University of Manchester

Reports available from: <http://eprints.maths.manchester.ac.uk/>

And by contacting: The MIMS Secretary
School of Mathematics
The University of Manchester
Manchester, M13 9PL, UK

ISSN 1749-9097

Stochastic Resonance in Vision: Models and Data

A thesis submitted to the university of Manchester for the degree of
Doctor of Philosophy
in the Faculty of Engineering and Physical Sciences.

2006

Carole Tham

School of Mathematics

Contents

Abstract	8
Declaration	9
Copyright Statement	10
Dedication	11
Abbreviations	12
1 Introduction	13
1.1 What Is Stochastic Resonance?	13
1.2 It All Begins With Climate Change	17
1.3 Applications of Stochastic Resonance	18
1.3.1 Electrical and Optical Applications	18
1.3.2 Biological Applications	20
1.3.3 Stochastic Resonance in Vision	22
2 The Retina and a Simple Model of SR	26
2.1 A Brief Introduction to the Retina	26
2.2 The Rod Pathway	26
2.2.1 Noise	27
2.2.2 Rods	28
2.2.3 Synapses and Thresholds	28
2.2.4 Horizontal Cells	29
2.2.5 Bipolar Cells	29
2.2.6 Amacrine Cells	30
2.2.7 Ganglion Cells	30

2.2.8	Summary of the Rod Pathway	31
2.3	A Simple Threshold Model Due to Simonotto	31
3	Statistical Decision Theory and SR	33
3.1	Statistical Decision Theory and ROC Curves	33
3.2	A Simple Mathematical Model	36
3.2.1	A Discretely Sampled System	36
3.2.2	A Signal Detection Task	38
3.2.3	Detecting the Signal I: no nonlinearity and Gaussian noise	39
3.2.4	Detecting the Signal II: after the threshold	42
4	Experimental Evidence for Stochastic Resonance	49
4.1	Introduction: What is Psychophysics?	49
4.1.1	Psychophysics and Statistical Decision Theory	51
4.2	Experimental Design	52
4.2.1	Experimental Conditions and Dark Adaptation	52
4.2.2	The Experiments	54
4.2.3	Equipment	64
4.2.4	Software Review	65
4.2.5	Calibration Procedure	66
4.2.6	Bayesian Adaptive Method for Determination of CDT	66
4.2.7	Generating the Noise	67
4.2.8	Observers	69
4.3	Results	70
4.3.1	Grating Experiment	71
4.3.2	Angled Grating Experiment	74
4.3.3	Oriented Triangle Experiment	76
4.3.4	Square Detection Experiment	79
4.3.5	Displaced Square Discrimination Experiment	81
4.3.6	Square Wave Discrimination Experiment	82
4.3.7	Grating with Time Varying Noise Experiment	84
4.3.8	Triangle with Time Varying Noise Experiment	85
4.4	Discussion	87

5	Conclusions	89
A	The Variance of the Power Spectrum	91
A.1	Constructing formulae	91
A.2	Verifying the results	93
B	Implementation of Bayesian Adaptive Method	95
C	Creating Normally Distributed Noise From Uniformly distributed Noise	97
D	Bayesian Estimation of Frequencies	99
D.1	Case I - Make no assumptions about p	100
D.2	Case II - p lies in the range $\frac{1}{2} \leq p \leq 1$	100
D.3	Error Bar Construction	102
E	Watson's Model of Early Vision	103
E.1	The Model	103
E.1.1	Input	103
E.1.2	Contrast sensitivity Filter	103
E.1.3	Channels	104
E.1.4	Pooling	105

Word count 21,335

List of Figures

1.1	Schematic diagram of a non-linear signal processor	14
1.2	The double well potential	15
1.3	An excitable system	16
1.4	The Schmitt Trigger	18
1.5	ISIH's measured by Douglass for the crayfish mechanoreceptor	21
1.6	Threshold against added noise. Reproduced from Simonotto [48]	23
2.1	A slice through the retina	27
2.2	Relationship between rhodopsin content and rod sensitivity.	29
2.3	The nature of response from a bipolar cell	30
2.4	The flow of information in the retina.	31
2.5	A simple threshold model	32
3.1	An example of a ROC curve	35
3.2	A schematic diagram for the threshold system.	38
3.3	A periodic signal lying slightly below a threshold.	39
3.4	A series of ROC curves	42
3.5	The probability that the x_j is one as a function of time	43
3.6	Expected power spectra obtained from an analytic expression and numerical trials.	45
3.7	Expected power at the signal frequency as a function of the noise strength	46
3.8	Numerical and approximate parametric representations of the distributions for the power	47
3.9	ROC curves and power spectra for both linear and non linear systems with different values of added noise	48
4.1	Gustav Theodor Fechner (1801-1887)	50

4.2	An example of a psychometric function	51
4.3	Dark Adaptation Curve, taken from [11]	53
4.4	A typical pair of images used to determine a CDT	56
4.5	A typical pair of images used for an SR experiment	57
4.6	A typical pair of images used for angled grating experiment	59
4.7	A typical pair of images used for the oriented triangle experiment	60
4.8	A typical square stimulus	61
4.9	A typical pair of images used for the displaced square discrimination experiment	62
4.10	A square wave and its fundamental frequency	63
4.11	A pair of images used for the square wave discrimination experiment	64
4.12	CDT measurement using an adaptive Bayesian approach	67
4.13	Observer A's results for the grating experiment	71
4.14	Observer A's results for the grating experiment cont.	72
4.15	Observer B's results for the grating experiment	72
4.16	Observer B's results for the grating experiment cont.	72
4.17	Observer C's results for the grating experiment	73
4.18	Observer C's results for the grating experiment cont.	73
4.19	Observer A's results for the angled grating experiment	74
4.20	Observer A's results for the angled grating experiment cont.	75
4.21	Observer A's results for the angled grating experiment cont.	75
4.22	Observer B's results for the angled grating experiment	76
4.23	Observer A's results for the oriented triangle experiment	77
4.24	Observer A's results for the oriented triangle experiment cont.	77
4.25	Observer B's results for the oriented triangle experiment	78
4.26	Observers A and C, results for the oriented triangle experiment	78
4.27	Observer C's results for the square experiment	80
4.28	Observer A's results for the square experiment	80
4.29	Observer A's results for the Displaced Square Discrimination Experiment	81
4.30	Observer B's results for the Displaced Square Discrimination Experiment	83
4.31	Observer A's results for the square wave discrimination experiment	83
4.32	Observer B's results for the square wave discrimination experiment	83
4.33	Observer A's results for the grating with time varying noise experiment	84

4.34	Observer B's results for the grating with time varying noise experiment	85
4.35	Results for observers A and B in the triangle experiment with time varying noise	86
4.36	Observer A's results for the triangle experiment with time varying noise	86
4.37	CDT against time for the grating and triangle experiments	88
5.1	Stages of the retina model	90
C.1	Illustration of the transform method for generating normal deviate form a uniform deviate	98
D.1	The prior distribution over the hypotheses	100
D.2	The posterior distribution.	101
D.3	The prior distribution over the hypotheses, with the restricted range of probabilities $\frac{1}{2} \leq p \leq 1$	101
D.4	The posterior distribution with the restricted range of probabilities $\frac{1}{2} \leq p \leq 1$	102
E.1	Watson's model for early vision	104

List of Tables

3.1	Relation of outcomes to states of the world	34
4.1	Detection and discrimination experiments.	55
4.2	Observers used for experiments	70

Abstract

Stochastic resonance (SR) is a phenomenon whereby small amounts of additive noise can greatly enhance the performance of a non-linear signal processing system. It is well known that many sensory systems are non-linear in nature and the phenomenon of SR has been widely studied in them. Perhaps one underexplored area of research is the visual system, in particular the retina and this project aims to explore to what extent SR is or could be utilised in the retina.

The thesis is organised as follows: In chapter one I look at the historical development of SR from its conception as an explanation of the periodic occurrence of ice ages to applications in sensory systems. The structure of the retina is explored in chapter two and I explain why SR might be expected to occur in visual systems. The mathematics of the problem is detailed in chapter three, showing why SR arises in systems containing a threshold type non-linearity. The phenomenon is extensively studied experimentally in chapter four, with many different stimuli being tested. These are broadly organised into two types of task, detection and discrimination, with each stimulus carefully designed to probe a different aspect of the phenomenon. In the final chapter overall conclusions are drawn, the scope for future work is explored, including the description of a retina model and the possibilities for practical applications are raised.

The thesis contains novel receiver operating characteristic (ROC) curves, used to demonstrate that SR can occur in systems containing a threshold type non-linearity. I go on to show that noise can be used to enhance the perceptibility of some signals. However, this enhanced perception is shown to be limited to low level visual tasks.

Declaration

No portion of the work referred to in this thesis has been submitted in support of an application for another degree or qualification of this or any other university or other institute of learning.

Copyright Statement

Copyright in text of this thesis rests with the author. Copies (by any process) either in full, or of extracts, may be made **only** in accordance with instructions given by the author and lodged in the John Rylands University Library of Manchester. Details may be obtained from the librarian. This page must form part of any such copies made. Further copies (by any process) of copies made in accordance with such instructions may not be made without the permission (in writing) of the author.

The ownership of any intellectual property rights which may be described in this thesis is vested in The University of Manchester, subject to any prior agreement to the contrary, and may not be made available for use by third parties without the written permission of the University, which will prescribe the terms and conditions of any such agreement.

Further information on the conditions under which disclosures and exploitation may take place is available from the Head of School of Mathematics.

Dedication

I would like to dedicate this thesis to my son Daniel, who has grown from a baby into a wonderful little boy during its construction. He has been there to provide a necessary distraction and much amusement when otherwise I may have become buried under the workload. It is also dedicated to my husband Yun Kiong, who has been a constant support.

I would like to express many thanks to Mark Muldoon my mathematics supervisor for his continued help in getting me this far and to Richard Abadi, my optometry supervisor, for his wonderful insights into the retina and experimental practice.

Abbreviations

CDF Cumulative Density Function

CDT Contrast Detection Threshold

CSF Contrast Sensitivity Function

DAC Digital-to-Analogue-Converter

DFT Discrete Fourier Transform

DoG Difference of Gaussians

IID Independent and Identically Distributed

ISIH InterSpike Interval Histogram

NSR Noise to Signal Ratio

PSD Power Spectral Density

RGB Red, Green, Blue

ROC Receiver Operating Characteristic curve

SDT Statistical Decision Theory

SNR Signal to Noise Ratio

SR Stochastic Resonance

2AFC Two Alternative Forced Choice

VDU Visual Display Unit

Chapter 1

Introduction

1.1 What Is Stochastic Resonance?

Stochastic resonance (SR) is a phenomenon whereby small amounts of additive noise can significantly enhance the performance of a non-linear signal processing system. The phenomenon has been extensively studied and comprehensive reviews are given by McNamara and Wiesenfeld [27] and Gammaitoni *et al.* [14]. In order to exhibit SR a system should have three basic properties: a non-linearity, usually a barrier or threshold¹; a coherent signal, for example a periodic signal; and a source of additive noise. Such a system is shown below (figure 1.1).

To understand how the phenomenon works, consider the double well (bistable) potential system shown in figure 1.2 (a) and imagine that some form of detector reports the position of the particle (as being either in the left well, L, or the right well, R) at a specified time. The system has two stable states at $\pm s$ and an unstable state at 0, so that a particle released into the system will come to rest in one of the stable states. The potential of the particle at any position x is given by $U(x)$. Once the particle has come to rest it will not move unless acted on by an external force. If a weak periodic force is applied to the system the particle will move up and down

¹Bezrukov and Vodyanoy [5, 6] have modeled SR in a threshold free system (an example of which is a voltage dependent ion channel), where pulses are dependent exponentially on the signal, creating the non-linearity

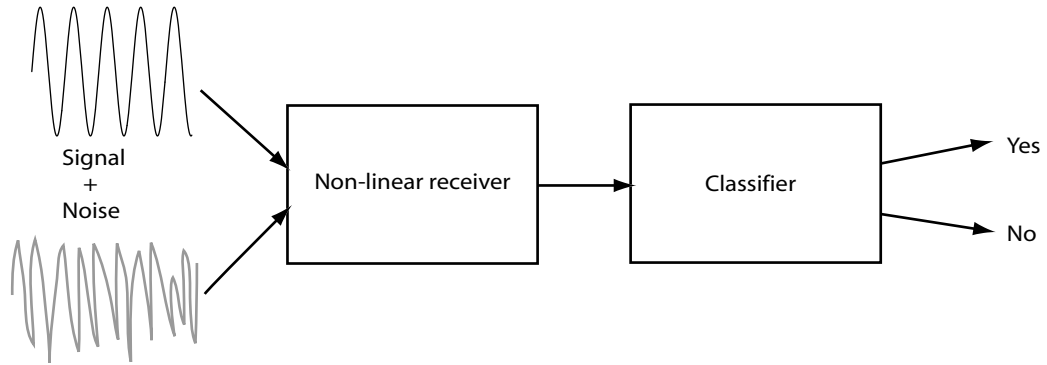


Figure 1.1: Schematic diagram of a non-linear signal processor. The receiver converts the input (signal + noise) into a form used by the classifier. The classifier makes decisions, yes-signal present or no-signal absent, based on what it receives.

the sides of its well. If the force is strong enough, the particle will jump the barrier (that is the unstable state) periodically, at odd integer multiples of the period, and will spend some time in each of the stable wells. At regular intervals the position of the particle is recorded giving rise to a sequence of the form $LLRR\dots$ as in figure 1.2 (b), from which the frequency of the periodic signal can be recovered. The height of the barrier will provide information about the minimum amplitude of signal required to surmount it.

Consider now the case when the signal is too weak to push the particle over the barrier. In the absence of other effects, the particle will bob about in its well. The receiver will record the same position ($LLLLLL\dots$ for example) and the detector will not be able to classify the signal. If enough noise is added to the system, it may in cooperation with the signal push the particle over the barrier. Since the noise and the periodic signal work together to cross the barrier, peaks in the signal will still correspond to crossings and frequency information can again be recovered. However, the noise must lie within a particular (relative to the signal and the barrier) range: too weak and it will not aid the particle in crossing the barrier, too strong and the crossings will not correspond to the peaks of the periodic signal.

Frequency information can be recovered from the response recording by use of Fourier analysis. The first task is to compute the discrete Fourier transform of the recording at discrete values of the frequency. The *power spectral density* (PSD) at each frequency can be calculated as twice the square of the Fourier transform at that

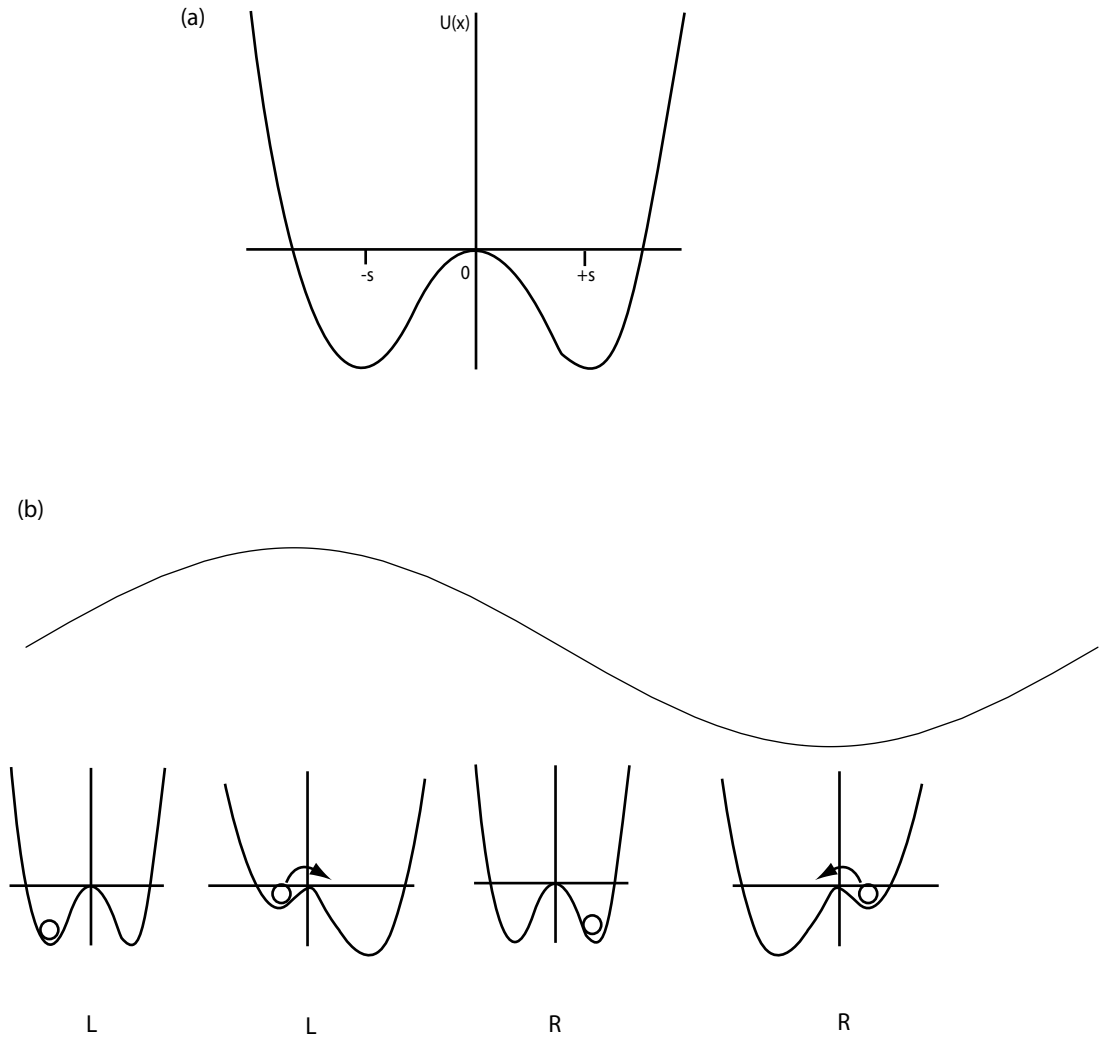


Figure 1.2: (a) The double well potential. (b) A particle placed in the double well will cross the barrier when the periodic signal (above) reaches its peak. An example of a signal recording is shown under each double well.

frequency. The PSD provides the distribution of power over frequency in the recorded response. If a periodic signal is detected it will show as a peak in the PSD at the frequency of the signal.

Another example of a system, often found in neuronal circuits, that exhibits SR is an *excitable system*. Unlike the double well, this system has a single rest state and an unstable excited state that is reached by crossing a barrier. An example of an excitable system is shown in figure 1.3. The system has an inbuilt threshold and monitors (over time) whether an input crosses this threshold. If, when the receiver is looking at the input it lies above the threshold, a pulse is emitted (see figure 1.3 (b))

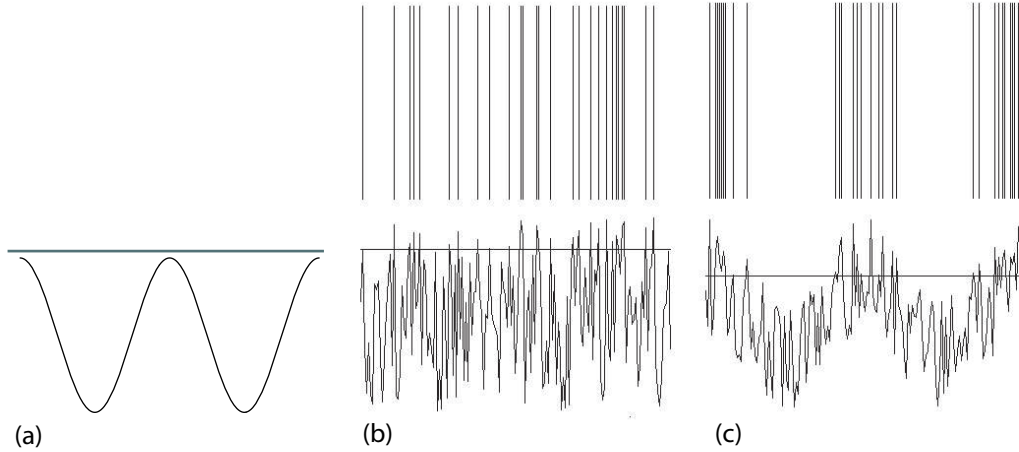


Figure 1.3: An excitable system. (a) A periodic signal lying below the threshold. (b) If pure noise is added to a system, threshold crossings are random and no information is contained in the pulse train (above). (c) If the noise and signal are both added to the system the threshold crossings and hence the pulse train correspond to peaks of the signal and frequency information can be recovered.

and (c)). If, on the other hand, the input lies below the threshold, no pulse is emitted. The pattern of pulses can be used by the detector to determine frequency information about the signal. Again, when the whole signal lies below the threshold, no pulses are emitted and it will not be detected. If noise is added to this sub-threshold signal it may push the input above the threshold, this is most likely to happen at the peaks of the signal. Information about the signal frequency is contained in the emitted pulse train and can be recovered by the detector.

Although it appears that we are performing a little magic or getting something for nothing, possibly even contravening certain information theoretic forms of the second law of thermodynamics [52], this is not the case. What SR does provide is a method of improving the performance of a pre-existing non-linear system, which is itself counter intuitive, since the non-linearity has often been introduced as a method of suppressing low level (again relative to the signal) noise in an inherently noisy signal².

²In their paper [2], Apostolico et al. describe a system where adding noise to an above threshold signal caused residual SR effects. This was extended by Stocks [51] who demonstrated SR in systems with significantly suprathreshold signals, which can outperform systems built to a standard design.

1.2 It All Begins With Climate Change

The theory of stochastic resonance evolved from the marrying of two ideas used to explain the periodic occurrence of ice ages. The theory was developed independently in the early 1980's by two groups: Nicolis and Nicolis [34, 33], and Benzi *et al.* [4, 3]. In fact it is Benzi who gave the phenomenon its name, saying [4]

our approach indicates the possibility of a new type of resonance, namely *stochastic resonance* between a deterministic external forcing of a climatic model and a stochastic internal mechanism.

He justifies the name, saying [4]

The word resonance is appropriate because if the noise is too small there is no correlation between the jumping time and the periodic change of the insolation. The same is true if the noise is too strong.

It was known that ice ages occurred periodically with the same frequency as the variation in the eccentricity of the Earth's orbit. This variation was however weak and insufficient to cause ice ages [33]. A rival theory proposed that pseudorandom fluctuations in oceanic conditions and solar radiation (called the internal mechanism by Benzi) were the cause. The genius was to combine the two theories giving rise to a new area of research, the theory of stochastic resonance.

The theory pictures the Earth's climate as a double well potential (see 1.1), with a cold 'ice age' state and warmer 'temperate' state being the stable solutions. These are separated by an unstable barrier lying along the 10K temperature difference between the stable states. At any time the Earth's temperature varies slightly as it moves up and down the sides of the well. Every 50,000 years the Earth's orbit reaches its most elongated state, and the Earth is at its closest position to the Sun. The increase in heat energy, combined with the natural peaks in radiation (the sun spot cycle has an 11 year periodicity and is the most probable cause of this noise [33]) provides enough energy to jump the barrier into the alternative well, where it will remain until astronomical conditions again favor a jump.

1.3 Applications of Stochastic Resonance

Since its conception SR has found applications in all areas of science. The first field where its properties were tested was electronics. When later applied to the naturally non-linear neuronal circuits found in biological systems research into SR “took off”. Below I review some historically important examples of SR.

1.3.1 Electrical and Optical Applications

The Schmitt Trigger

The first demonstration of stochastic resonance was carried out by Fauve and Heslot [12] in 1983 using an electrical circuit called a Schmitt trigger. The output of the circuit can be likened to a double well potential [12, 27, 14]. A diagram of the circuit and its response is shown in figure 1.4 below. The following explanation of

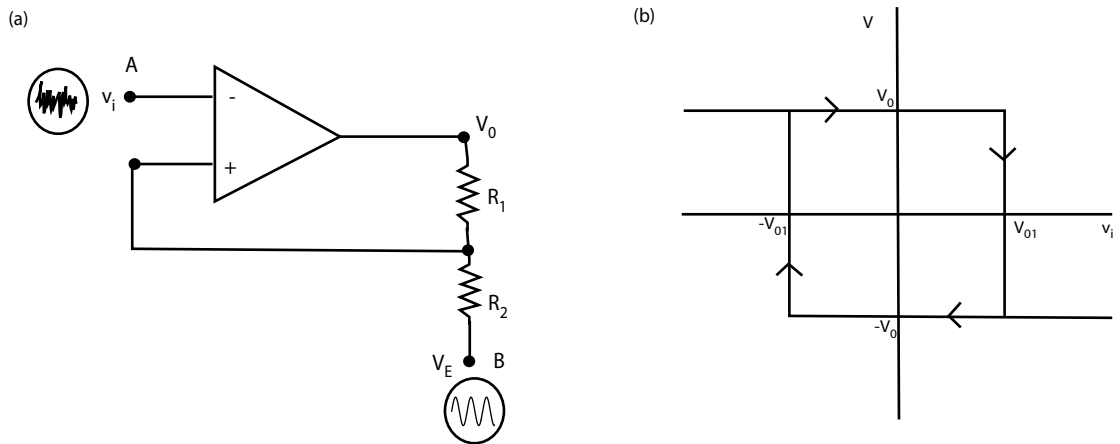


Figure 1.4: (a) A circuit diagram for the Schmitt Trigger. (b) A representation of the response of the system, the loop is indicative of a hysteresis effect.

the Schmitt trigger and how it was used to demonstrate SR is based on that given by Fauve [12] and uses his notation.

The Schmitt trigger operates by comparing its + and - inputs. Suppose initially that the input to the negative terminal v_i is less than V_{01} . It is clear from figure 1.4 (b) that the output of the system is V_0 . Now, if v_i is increased, the output will remain V_0 until $v_i = V_{01}$ when the output will switch to $-V_0$ where it will stay with further

increases in v_i . Suppose now we decrease v_i , the output will continue to be $-V_0$ until $v_i = V_{02} = -V_{01}$ when the output will again switch back to V_0 . The values V_{01} and V_{02} can be thought of as thresholds, since changing the value of v_i doesn't affect the output until it (v_i) crosses one of these values. Notice that the thresholds are not equal and the system exhibits hysteresis (memory), so that when v_i lies between $\pm V_{01}$ the output may take a value of either $+V_0$ or $-V_0$. Thus, the system has two stable states and must overcome a barrier (or threshold) to switch between them.

In order to demonstrate SR, Fauve initially applied white noise to the inverting ($-$) terminal, so that the output switched randomly between $+V_0$ and $-V_0$. The power spectrum was lorentzian in shape, with no discernable peak. Next he applied a time-dependent voltage V_E to terminal B (figure 1.4), which was fed back through the positive terminal. This had the effect of increasing and decreasing the threshold voltages V_{01} and V_{02} . The voltage alone was insufficient to enable jumping between the two states. However, when the amplitude of the noise was increased, switching did occur. Fauve found that the power spectrum of the output showed a sharp peak at the frequency of the periodic voltage V_E . He furthermore found that noise of a particular variance produced a greater difference between the power spectrum at the forcing frequency and a neighboring frequency, thus demonstrating SR.

The Bistable Ring Laser

The next demonstration of SR used a bistable ring laser [28, 27, 14], a model of which is developed in [54]. The system uses a laser whose beam is forced to travel in a ring by the use of (at least three) mirrors. The beam can be forced to travel in either a clockwise or counterclockwise direction around the ring by a *signal*. Noise can also be added to the system to induce random switching. The system can be likened to a double well potential whose output (the direction of travel of the beam) is similar to that of the Schmitt trigger (see 1.4 (b)). Again, the system experiences hysteresis with an area where, for a particular amplitude of input (signal plus noise), the beam can potentially travel in either direction and must overcome a *barrier* to change direction.

The results of McNamara *et al.* [28] show a peak in the PSD at the signal frequency and a peak in the signal to noise ratio (SNR) for a non-zero noise, demonstrating SR.

These results were reinforced by Vemuri and Roy [54] in their model.

1.3.2 Biological Applications

Crayfish Mechanoreceptors

In 1993 Douglass *et al.* [10] were the first group to demonstrate SR in sensory neurons. They (surgically) isolated single mechanoreceptor neurons from crayfish tailfins, along with the associated nerve roots and abdominal ganglions, and immersed them in crayfish saline. The neuron was mounted vertically on an electromagnetic motion transducer activated by the sum of a signal and a random noise. In crayfish, mechanoreceptors are responsible for transducing the movements of small hairs into signals (spikes) that propagate along the nerve. Douglass carefully chose the most effective signal which, unlike in many SR experiments, was presented slightly above threshold. The group recorded spike trains similar to those shown in the upper half of figure 1.3 from which *interspike interval histograms* (ISIHS) and PSDs could be calculated.

ISIHS calculated by Douglass for three noise amplitudes are shown in figure 1.5. The ISIH's assess the coherence of spiking activity with signal frequency. The results show an increased coherence between ISIH peaks and integer multiples of the stimulus period T_0 (the first five multiples of T_0 are marked with arrow heads), for an optimum noise level see figure 1.5(b). For no noise the spike rate was low see figure 1.5(a) and higher (than optimum) noise levels gave rise to increased randomisation of the peaks see figure 1.5(c). Douglass also measured a significant enhancement in the PSD at the signal frequency for non-zero noise. When the noise was increased, the magnitude of this peak was reduced. The group showed noise-induced signal enhancement in ten out of the eleven mechanoreceptor cells tested. They concluded that they had demonstrated that biological systems had the ability to use SR and they raised the question of whether organisms had evolved to exploit SR.

Paddle Fish Feeding Behavior

The question of whether organisms had evolved to exploit SR was answered in 1999 by Russell *et al.*[45, 32] in their study of paddle fish feeding. Paddle fish are

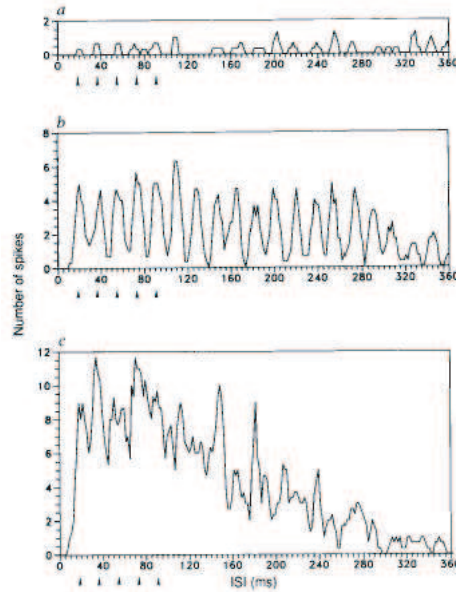


Figure 1.5: ISIH's measured by Douglass for the crayfish mechanoreceptor (a) with no noise peaks of ISIH are of low magnitude (b) with an optimum amount of noise, peaks in ISIH correspond to integer multiples of the signal period (c) when noise is increased beyond the optimum, peaks in ISIH no longer coincide with the period of the signal. Reproduced from Douglass [10]

weakly electric fish that live in the rivers of North America where muddy water limits visibility. Instead of using visual cues they sense their prey, the zooplankton *Daphnia*, electrostatically.

In this experiment Russell recorded the feeding patterns of paddle fish via a video camera. Using a pair of electrodes noise was added to the water surrounding both the fish and its prey, *Daphnia*, which themselves provide the 'signal'. The study showed that the paddle fish fed from a wider area when an optimal amount of noise was added to the system, compared to both the control, when no noise was added, and the case when high (above optimal) noise was added.

The paper [45] suggests that paddle fish have evolved to use the *noise* produced by the sum of signals from individual *Daphnia* in a dense swarm to highlight the presence of a single *Daphnia* emitting its own signal.

Stochastic Resonance and Hearing

The possibility of SR in auditory (and visual cortex) neurons was first raised by Longtin [23]. He compared interspike interval histograms (ISIH) outputs from a Schmitt trigger, stimulated by a periodic signal and random noise, with those recorded from an auditory nerve fibre from a monkey. The similarity of the two results suggested the possibility of SR in auditory systems.

In the human ear, rows of hair cells spiral up the cochlea, and movement of these hairs causes a hearing sensation. A sound of particular frequency will stimulate hairs in a specific region of the cochlea, carrying frequency information to the processing areas of the brain. These hairs are subject to Brownian motion, a random movement, creating a natural form of noise. Gebeshuber [15] modeled the effect of this noise on frequency information transmitted in pulse trains. She showed an increase in information when noise was added to a periodic signal. Jaramillo and Wiesenfeld [19] demonstrated that, for extracted frog hair cells, the noise level that produced a peak in the SNR corresponded to the level of naturally occurring Brownian motion in the hair cells. This again suggests that hearing apparatus may have evolved to exploit SR.

Psychophysics (see 4.1) experiments on human subjects were carried out by Zeng et al. [59]. The experiments measured detection thresholds on normal hearing and cochlea implant subjects and showed a reduction in threshold with added noise. This reduction was more significant in cochlea implant observers suggesting that noise should be added to improve performance of these implants.

Morse and Evans [30] have studied the effect of noise on vowel coding in cochlea implants and showed that the addition of an optimal level of noise gave rise to the greatest enhancements of the key features of a vowel. Moss *et al.*[31] have suggested that the addition of noise to cochlea implants may be the first practical application of SR.

1.3.3 Stochastic Resonance in Vision

Historical Development

There has been little study on the role of noise in the visual system. Early work includes that of Rovamo *et al.* [43, 44] where the *contrast detection threshold* (CDT) of

a sinusoidal signal was measured while varying various parameters (viewing distance, angle and signal luminance etc.) both in the presence and absence of externally added noise. They were not looking for SR and did not demonstrate it. However, this is not surprising since they used only a single example of noise (of a given mean amplitude) and other SR studies have shown a need for the fine tuning of noise.

The first study to look specifically for SR in the visual system was that by Simonotto [48], this work examined the effect of time varying noise on feature detection. Subjects were shown a series of strips of decreasing contrast, each containing the same noisy signal and were asked to identify the strip where the feature first disappeared. This contrast was taken to be the threshold for that particular noise intensity. In all ten noise intensities were tested. The results suggest a significant SR effect (see figure 1.6) which shows a reduction in threshold with added noise.

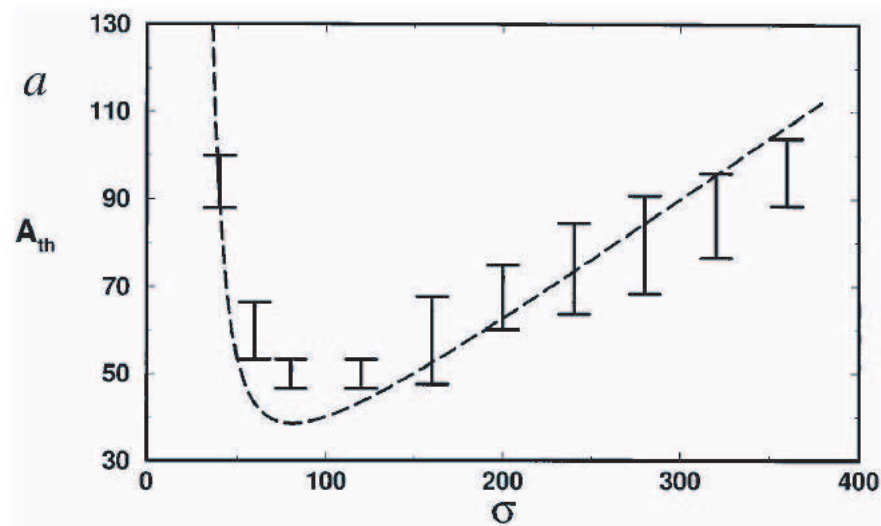


Figure 1.6: Threshold against added noise. Reproduced from Simonotto [48]

The experiment of Simonotto, while intriguing, does not follow an accepted psychophysics protocol. Observers can see all the information (stimuli) at once and may use differing criteria to judge whether they can see a feature. In other words, Simonotto relied on an observer making a consistent judgement, without testing this consistency. Because of this, it is difficult to draw conclusive evidence for SR from this experiment or to make comparisons between its results and the results of later experiments.

A more comprehensive study was carried out by Blackwell [7]. She used a two

alternative forced choice (2AFC) method, where an observer is forced to choose between two options, to measure the effect of static noise on the CDT of sinusoidal gratings of various frequencies. Blackwell's results show that noise had a facilitatory effect on detection for low (<10 cpd) frequency sinusoids. Furthermore for subjects whose CDT's were relatively high (compared to the other subjects in the study), a wider range of noise contrasts were seen to be facilitatory.

Blackwell extended her research to look at filtered noise. When the noise was high pass filtered she showed lower CDT at low sinusoid frequencies and when the signal was low-pass filtered she showed reduced CDT for high frequencies. Blackwell did these experiments to eliminate the well-documented [1] phenomenon of *sub-threshold summation* as an explanation for SR. Sub-threshold summation is a consequence of the existence of independent spatial frequency channels in early perception and explains why the superposition of two subliminal stimuli may—if the two have similar harmonic content—be perceived as a supra-threshold signal at the shared spatial frequency. Blackwell also suggests that SR may, at least in part, be explained in terms of reduced observer uncertainty [38] about when the stimulus is present.

More Recent Research

A current area of research has focused on demonstrating SR within the brain. This work focuses on the visual system, but bypasses the eyes by presenting the signal to one eye and the noise to the other. The two inputs remain separate until they meet at the optic chiasm within the brain. Thus, any improvement in detecting the signal in the presence of the noise must arise from some function within the brain.

Results were initially reported by Mori and Kai [29], where they recorded a peak in the PSD of brain wave recordings for an optimum amount of non-zero added noise, for all five subjects in their study.

The phenomenon reached the popular press [18] with a review of the work of Kitajo *et al.* [20]. This work enhanced that of Mori and Kai by comparing the results of psychophysics experiments (see 4.1) for the above case of presenting the signal to one eye and noise to the other, with the case of presenting the signal and noise to the same eye. Their results likewise showed an increase in detecting the signal for a non-zero noise. A comparison of the *two eyed* versus *one eyed* experiments showed an SR effect for both cases with an increase effect for the *one eyed* case. This result

suggests the possibility of SR within the retina although this is not raised by the authors themselves.

This Project

Further to the work described in this section, this study aims to extend the work of Blackwell to look at the detection of sub-threshold signals in both static and time-varying noise. The work will also examine some simple discrimination tasks.

Chapter 2

The Retina and a Simple Model of SR

2.1 A Brief Introduction to the Retina

In order to gain an understanding of how SR might occur in the retina I feel it is important to understand how the retina works. In this section I will describe the various structures that compose the retina, where noise might be added and how thresholds might act.

2.2 The Rod Pathway

Much is known about the retina, Dowling [11] refers to it as “the approachable part of the brain”. It is divided up into distinct layers, each containing a specialised cell (see figure 2.1). These cells have been accurately described, enabling a picture of the passage of information (light) to be drawn.

Light traveling through the eye must pass through all the layers of the retina before impinging on the photoreceptors (or being absorbed and discarded in the pigment epithelium layer). Photoreceptors fall into two categories, rods active in low light (scotopic) conditions and cones active in higher light level (photopic) conditions. There are three different varieties of cone receptor and these generate high acuity colour vision, while the single type of rod receptor absorbs light over the wavelength

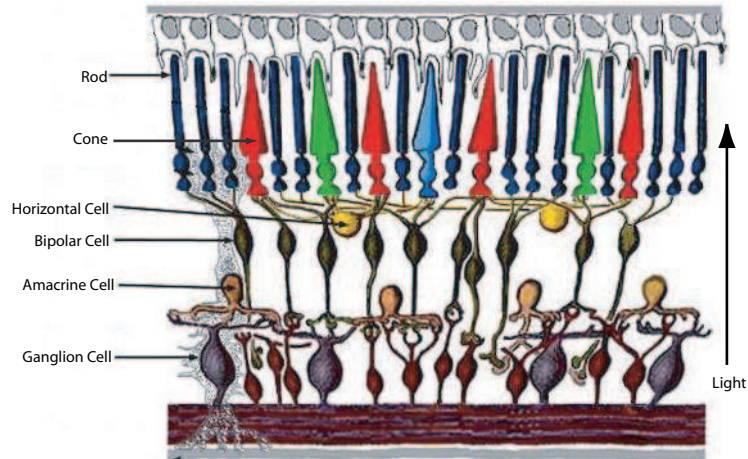


Figure 2.1: A diagram of a slice through the retina, showing the retinal layers and the types of cells that compose the retina, diagram modified from [21].

range 400-700nm and maximally at 525nm, to give sensitive monochromatic vision. Since SR is a near threshold phenomenon, in this project I will concentrate on the low light level rod mediated system.

2.2.1 Noise

There are many reasons why noise may be present in signals transmitted through the visual system. Firstly, noise arises in the environment, before it enters the eye light may bounce off many objects carrying a little information of each. In order to limit the effects of this type of noise, the visual system filters the signal it receives. This preserves only the high frequency part of the signal, containing detailed information about the scene. Secondly, photoreceptors may respond as though they have been stimulated when no light has provoked them. The level of this thermal noise is low and in daylight it is imperceptible, however in low light level conditions when just a few photons are stimulating the retina, it can be a significant feature of the signal reaching the brain (see 4.2.1). This can be seen as bright flashes when the eyes are closed, the so called *dark light*. Since dark light is indistinguishable from real photon activations, it cannot be eliminated from a signal. A further source of noise is due to eye movements (microsaccades) that occur continuously without being noticeable during normal vision, the possibility that this type of noise gives rise to SR in visual cortex neurons is discussed by Henning et al. [17]. Finally, noise can arise at the

synaptic connections between elements of the visual system. If small in comparison with the signal, this type of noise can be eliminated by threshold mechanisms acting between neurons.

2.2.2 Rods

In the retina there are around 110-125 million rods [49] Within each rod there are many (600-1000) [49] membranous disks. These disks contain the rod photopigment *rhodopsin* (10^9 molecules per rod [11]) which becomes bleached upon the absorption of a photon and then transparent to light until, in time, it returns to its unbleached state. One rod can absorb many photons, but is limited by the number of rhodopsin molecules it contains. However, the quantity of unbleached rhodopsin is not the only factor affecting a rods sensitivity (sensitivity = $1/\text{threshold}$) as is demonstrated in fig 2.2¹, taken from Dowling [11]. This sensitivity also deviates (if less significantly) from the log-linear relationship predicted by Weber's law 4.1.

As well as their immense photon catching abilities, Dowling [11] argues that rods can communicate between themselves. This increases the probability of detecting a single photon and is demonstrated by the recording of single photon absorbtions in rods neighboring the absorber.

2.2.3 Synapses and Thresholds

The junctions between different cells are called synapses and information must pass through them to be transferred from one cell to another. In the retina there are two types of synapse; chemical, where neurotransmitters pass between cells, and

¹Dowling's original caption reads: Relationship between rhodopsin content and final log sensitivity of receptor potentials measured extracellularly from the skate retina (open circles), intracellularly from toad rods (filled circles), and extracellularly from single toad rods with suction electrodes (filled squares). All of these data systematically deviate from an exact log-linear relationship (solid line). That is with bleaches below about 50 percent the data points fall above the line, whereas with larger bleaches the data points fall below the line. The dashed line in the figure plots the rise of threshold expected if the only factor limiting were the quantum-catching ability of the receptor as rhodopsin levels are reduced.

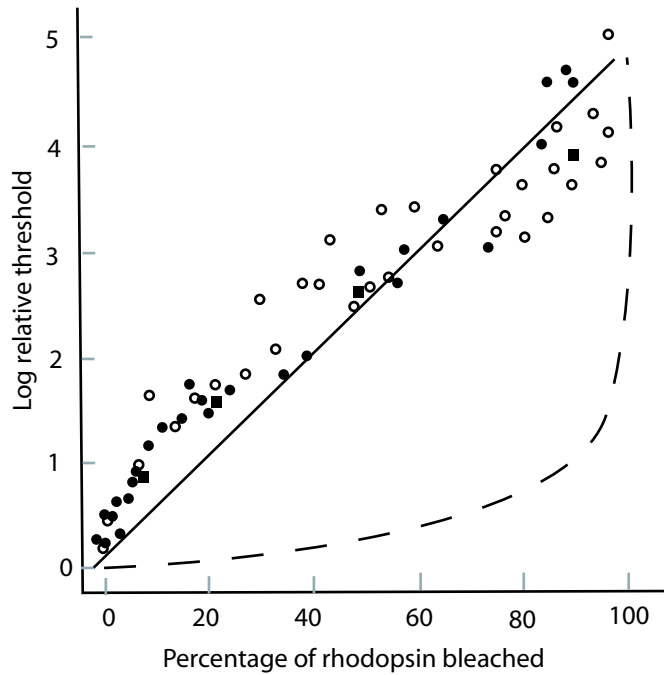


Figure 2.2: Relationship between rhodopsin content and rod sensitivity.

electrical, where charged ions are transmitted.

These synapses are a potential site for the introduction of noise into a signal. In an attempt to limit this noise, transmitted signals are thresholded, that is only signals above a certain amplitude are transmitted. The threshold determines the sensitivity of a cell.

2.2.4 Horizontal Cells

The role of horizontal cells in the rod pathway is not entirely clear. Dowling [11] and Malik [24] say that horizontal cells contribute to the inhibitory surround of rod bipolars (see 2.2.5) and the rods themselves form the centre part. While Webvision [21] in their section devoted to the rod pathway, don't mention horizontal cells at all.

2.2.5 Bipolar Cells

Of the three types of bipolar cell found in the visual system, only one is found in the rod pathway. The rod bipolar cell has an antagonistic centre-surround nature,

where a bright spot of light focussed on photoreceptors impinging on the centre of its receptive field stimulates the cell, this signal is inhibited if the stimulus also falls on photoreceptors feeding into the surround region (see figure 2.3). All rod bipolars exhibit this on-centre structure, meaning they are maximally stimulated by a bright spot covering their centre and a dark surround. This cell is perfectly suited to the detection of grating patterns.

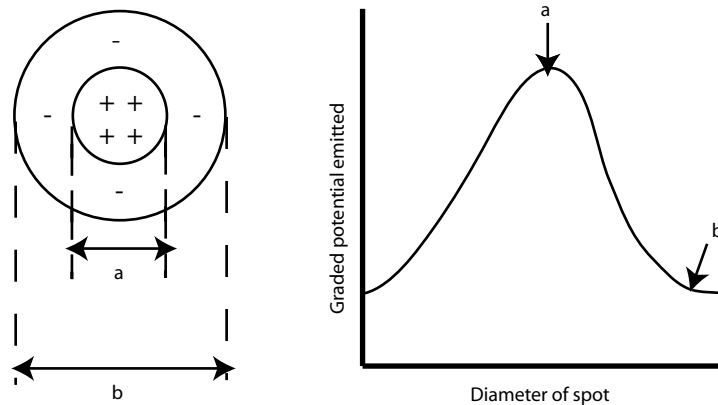


Figure 2.3: The nature of response from a bipolar cell. Indicates how the graded potential emitted from a cell is affected by the size of a spot of light exciting it. Based on figures from [46].

2.2.6 Amacrine Cells

Rod bipolar cells do not synapse directly onto ganglion cells (although some cone bipolars do), but instead pass information through amacrine cells. Amacrine cells carry information horizontally through the retina and feed signals back to bipolar cells and on to ganglion cells.

2.2.7 Ganglion Cells

Ganglion cells share the same nature as the cells that impinge on them. So ganglions that receive input from cone bipolars have a centre-surround nature. However in the rod pathway, where ganglions receive input from amacrine cells they inherit their nature from these amacrine cells. They exhibit a transient response to stimulation,

emitting action potentials at both the onset and termination of stimulation. As a result of this they are highly sensitive to movement within the visual field.

It is the processes of the ganglion cells that leave the eye (through the optic disk) to form the optic nerve and transmit information to the brain for further processing. Approximately one million ganglion cells [49] form the optic nerve, this represents a great contraction of information from the 100 million or so rods. To achieve this, significant processing of visual signals must occur in the retina itself, before these signals are transmitted to the brain.

2.2.8 Summary of the Rod Pathway

A summary of the flow of information through the retina is given in figure 2.4

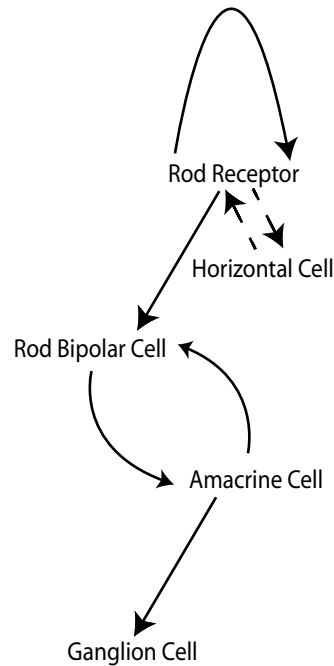


Figure 2.4: The flow of information in the retina.

2.3 A Simple Threshold Model Due to Simonotto

As part of his report on SR in the visual system, Simonotto [48] produced a set of three images to demonstrate the effect. Following a dithering technique [55], these show a picture where each pixel has had noise (drawn from a Gaussian distribution) added and then has been thresholded, with an output pixel having value 0 if it lies

above the threshold and value 1 if below. The images indicated that an optimum noise exists, producing the *clearest* output image, although this is subjective. A similar set of images has been reproduced in figure 2.5.

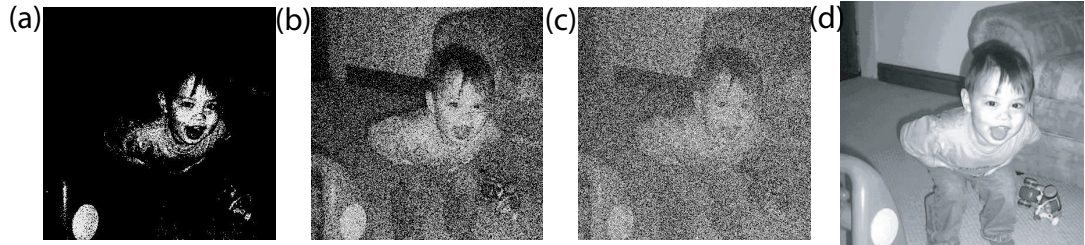


Figure 2.5: A simple threshold model. (a)-(c) Images with differing amounts of added noise, the amplitude of noise increases from left to right, passed through a threshold non-linearity. Where max is the maximum pixel value in the original image, the added noise was (a) $0.25 \cdot \text{max}$, (b) $1.0 \cdot \text{max}$ and (c) $2.0 \cdot \text{max}$. The original picture is shown in (d).

Chapter 3

Statistical Decision Theory and SR

In this chapter I will demonstrate that SR is possible (mathematically) in systems that contain a threshold non-linearity. To do this I will introduce statistical decision theory (SDT) which I will then apply to produce receiver operating characteristic curves (ROC). Although the SDT behind the production of these ROC curves is long established [9] the ROC curves themselves are a novel aspect of this thesis. All simulations in this chapter were carried out using *Mathematica* [42].

3.1 Statistical Decision Theory and ROC Curves

In systems or experiments where there are large amounts of error prone data a decision maker (part of the system or an external observer) makes choices based on the evidence he has. He must analyse the statistics of the data and the likely repercussions of possible outcomes, before making a decision on what the information he has received truly represents. This type analysis is called *statistical decision theory* and is best explained by application to an experiment.

The simplest question one can ask is one that requires a yes or no answer. Imagine a simple experiment where an observer is presented with a series of stimuli, a proportion of which contain a signal, the observer is asked to indicate whether or not the signal was present in each stimulus. For this type of experiment there are four possible outcomes:

hit corresponding to correct identification of the signal

miss saying signal was absent when in fact it was present

correct rejection correctly saying the signal was absent

false alarm incorrectly identifying the signal as present when it was absent

The choice of outcome is dependent on the form of the stimulus that has been presented. For example; there are only two alternatives (or states of the world [16]) for each presentation, either the signal was present, or it was not. The outcomes related to these presentation alternatives are given in table 3.1, from which we can derive the

State of the World	Possible Outcomes
Signal	hit or miss
No signal	correct rejection or false alarm

Table 3.1: Relation of outcomes to states of the world

relationships

$$P(\text{hit}) + P(\text{miss}) = 1 \tag{3.1}$$

$$P(\text{false alarm}) + P(\text{correct rejection}) = 1$$

which illustrate the interdependence of the quantities in table 3.1 and the existence of only two independent variables, usually taken to be $P(\text{hit})$ and $P(\text{false alarm})$.

In any yes-no experiment it is desirable to increase the hit rate while reducing the false alarm rate, however, such a strategy is not generally achievable. Instead the observer must evaluate the *costs* associated with different decisions. For example, if ten million people have to be evacuated every time a hurricane warning is raised, the cost of raising such an alarm in error (a false alarm) is high. On the other hand, incorrectly answering a question on an exam has a low cost relative to not answering the question. If the *cost* of a false alarm is β , then a reasonable strategy would be to maximise

$$\alpha = P(\text{hit}) - \beta P(\text{false alarm}) \tag{3.2}$$

To implement this strategy an observer must define under which conditions to identify a positive event: he or she might, for example, choose to apply a threshold to some summary statistic derived from the observable information. Such a threshold could be set either by the objectives of the task (determined by the cost of a false alarm

β in 3.2) or, arbitrarily, by the observer him/herself. Psychometric functions (see section 4.1) can be plotted for yes-no tasks; these curves depend on the criterion used to identify a positive event.

A useful way of analysing yes-no tasks is through receiver operating characteristic (ROC) curves. A ROC curve is produced by plotting the probability of a hit against the probability of a false alarm. All ROC curves begin at (0,0), the case of reporting no signal for all stimuli and end at (1,1), the case of reporting the signal as always being present. Intermediate points are found by applying different criteria. Guessing or chance results, produce a curve that lies along the diagonal from (0,0) to (1,1), while a near-perfect classifier will produce a curve joining the points (0,0), $(0+\delta, 1-\delta)$ and (1,1), where $\delta \ll 1$. An optimal classifier (*ideal observer*) will give rise to a convex curve falling between these two lines, see figure 3.1. Here optimal [53] is meant in the

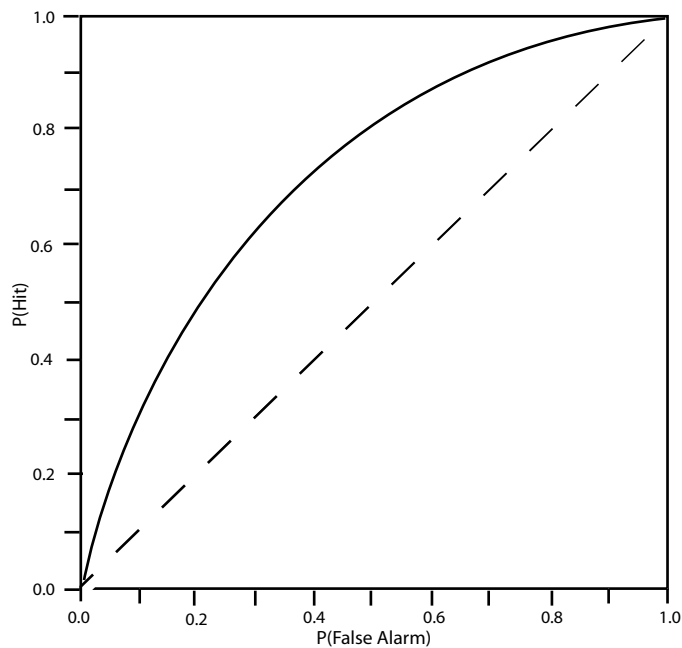


Figure 3.1: An example of a ROC curve

sense that the hit rate is maximised for a given false alarm rate. Thus, the optimal ROC curve gives the best possible performance of the classifier for a given signal and noise.

In the remainder of this chapter I will explore SR analytically, using SDT to give a fairly complete account of the effect in a simple setting.

3.2 A Simple Mathematical Model

The basis of the work in this section is a paper by François Chapeau-Blondeau [9] in which he formulates an expression for the PSD of a discretely sampled input (signal plus noise) crossing a threshold non-linearity. In his paper Chapeau-Blondeau considers an arbitrary periodic signal and an arbitrary noise. In order to obtain more explicit models I will consider specific realisations of the noise and a sinusoidal signal. I will begin by developing explicit expressions for the distributions required to sketch ROC curves, first obtaining exact results in the case when no threshold is applied and then a circle of approximate expressions that apply when a threshold is included. I conclude with some numerical experiments for the latter case.

3.2.1 A Discretely Sampled System

Consider a periodic signal sampled N (where N is even) times. The sampled points are given by

$$x_0, x_1, \dots, x_{N-1}$$

The fixed time interval of the sampling process is Δt so that the total sampling period is given by $N\Delta t$.

Since we wish to investigate statistical problems associated with detecting a sinusoidal signal in background noise we need to compute the *discrete Fourier transform* (DFT) $X(f_k)$ of the signal at discrete values of the frequency

$$f_k = \frac{k}{N\Delta t} \quad k = 0, \dots, N-1$$

In order to do this, instead of integrating over the total time period, we sum over the time epoch $t_n = n\Delta t$ ($n = 0, \dots, N-1$) at which each sample was taken, to give

$$\begin{aligned} X(f_k) &= \int_{-\infty}^{\infty} x(t) e^{2\pi i f_k t} dt \\ &\approx \sum_{n=0}^{N-1} x(t_n) e^{2\pi i f_k t_n} \Delta t \\ &= \Delta t \sum_{n=0}^{N-1} x_n e^{2\pi i \frac{k n}{N}} \end{aligned}$$

The DFT is then given by

$$X_k = \frac{1}{\sqrt{N}} \sum_{n=0}^{N-1} x_n e^{2\pi i \frac{kn}{N}} \quad (3.3)$$

where the factor $\frac{1}{\sqrt{N}}$ is added for convenience. The inverse Fourier transform is

$$x_n = \frac{1}{\sqrt{N}} \sum_{k=0}^{N-1} X_k e^{-2\pi i \frac{kn}{N}}$$

If the X_k are real valued, then

$$X_{-k} = X_k^*$$

but, here we go from 0 to N-1, over one period, so we have

$$X_{N-k} = X_k^* \quad (3.4)$$

The power spectral density (PSD) of x , at each frequency $f_k = \frac{k}{N\Delta t}$ ($k = 1, \dots, \frac{N}{2}$), is then

$$P_k = |X_k|^2 + |X_{N-k}|^2 = 2|X_k|^2 \quad (3.5)$$

where equation 3.4 has been used.

We will not generally be interested in the whole spectrum, but a few representative frequencies, and so it is useful to formulate a version of 3.5 that depends only on real valued quantities. Define

$$a_k = \frac{1}{\sqrt{N}} \sum_{n=0}^{\frac{N}{2}-1} x_n \cos\left(2\pi n \frac{k}{N}\right) \quad \text{and} \quad b_k = \frac{1}{\sqrt{N}} \sum_{n=0}^{\frac{N}{2}-1} x_n \sin\left(2\pi n \frac{k}{N}\right) \quad (3.6)$$

so that for $x_n \in \mathbb{R}$

$$a_k + ib_k = X_k$$

$$a_k - ib_k = X_{N-k}$$

and,

$$|X_k|^2 = a_k^2 + b_k^2 \quad (3.7)$$

Now let

$$\begin{aligned} \mathbf{u}_k &= \sqrt{\frac{2}{N}} \left(1, \dots, \cos\left(2\pi n \frac{k}{N}\right), \dots, \cos\left(2\pi \left(\frac{N}{2} - 1\right) \frac{k}{N}\right) \right) \\ \mathbf{v}_k &= \sqrt{\frac{2}{N}} \left(0, \dots, \sin\left(2\pi n \frac{k}{N}\right), \dots, \sin\left(2\pi \left(\frac{N}{2} - 1\right) \frac{k}{N}\right) \right) \end{aligned} \quad (3.8)$$

It can be shown that the vectors $\mathbf{u}_k, \mathbf{v}_k$ for $k = 1 \dots, \frac{N}{2}$ form an orthonormal basis for \mathbb{R}^N . That is

$$\begin{aligned} \mathbf{u}_j \cdot \mathbf{u}_k &= \delta_{j,k} \\ \mathbf{v}_j \cdot \mathbf{v}_k &= \delta_{j,k} \\ \mathbf{u}_j \cdot \mathbf{v}_k &= 0, \end{aligned} \tag{3.9}$$

The vectors $\mathbf{u}_k, \mathbf{v}_k$ also allow one to compute the power spectrum, since

$$(\mathbf{x} \cdot \mathbf{u}_k)^2 + (\mathbf{x} \cdot \mathbf{v}_k)^2 = 2(a_k^2 + b_k^2) = 2|X_k|^2$$

using equation 3.7.

3.2.2 A Signal Detection Task

We will be interested in detecting a sinusoidal signal with added noise, which is passed through a step non-linearity. The result is processed using discrete Fourier transforms to give a peak in the PSD at the signal frequency. This scheme is illustrated in figure 3.2.

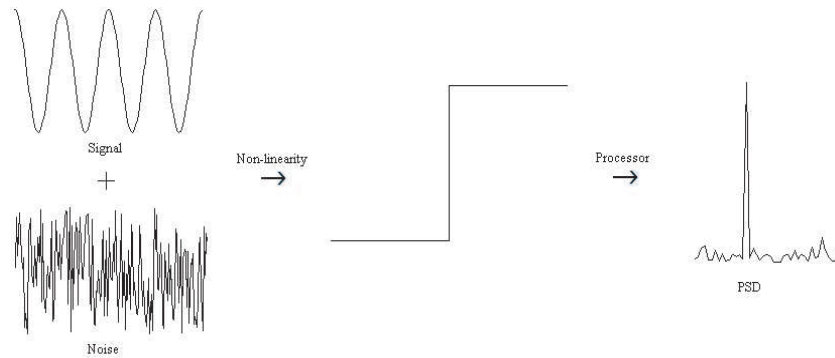


Figure 3.2: A schematic diagram for the threshold system.

To fix terms, consider the problem of distinguishing between a vector of pure noise and a sampled signal of the sort illustrated in figure 3.3:

$$y_j = (1 - \delta) \cos(2\pi j(f_0 \Delta t)) + \sigma_0 \xi_j$$

where the ξ_j are noise terms with

$$\langle \xi_j \rangle = 0 \quad \text{and} \quad \langle \xi_j \xi_k \rangle = \delta_{j,k} \tag{3.10}$$

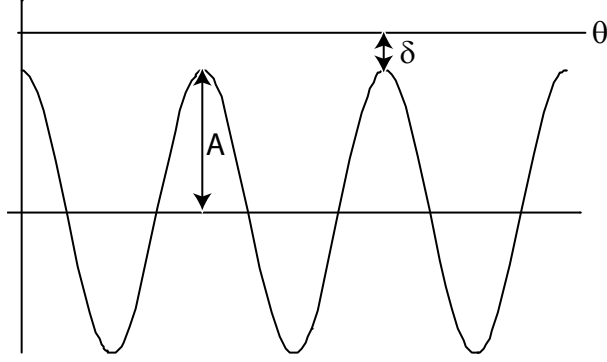


Figure 3.3: A periodic signal lying slightly below a threshold. In the calculations that follow, $\theta = 1$ and so $A = 1 - \delta$.

where angle braces indicate averages over realisations the noise process. Eventually we will apply a threshold nonlinearity and sample this signal to obtain

$$x_j = \Theta(y_j)$$

where $\Theta(y)$ is the threshold nonlinearity satisfying

$$\Theta(y) = \begin{cases} 1 & \text{If } y \geq 1 \\ 0 & \text{Otherwise} \end{cases}$$

But to being with, I'll consider the somewhat simpler problem of detecting the sinusoidal signal by analysing the power spectrum of the y_j .

3.2.3 Detecting the Signal I: no nonlinearity and Gaussian noise

To apply statistical decision theory one needs to know something about the distribution of the entries in the power spectrum. For the sake of convenience, let us imagine that the sampling frequency $1/\Delta t$ is a multiple of the signal frequency f , so that

$$f_0 = f_{k_0} = k_0/(N\Delta t) \tag{3.11}$$

for some integer $0 < k_0 < N/2$. In the remainder of this section we'll also imagine that the noise terms ξ_j are normally distributed with zero mean and unit variance.

Then we need only work out the distribution of the PSD at two frequencies: the signal frequency and some other frequency, say f_{k_1} . Consider the latter case first, we want the expected value of

$$2|Y_{k_1}|^2 = (\mathbf{y} \cdot \mathbf{u}_{k_1})^2 + (\mathbf{y} \cdot \mathbf{v}_{k_1})^2$$

Both terms give rise to similar calculations, so consider $\mathbf{y} \cdot \mathbf{u}_{k_1}$:

$$\begin{aligned}
\mathbf{y} \cdot \mathbf{u}_{k_1} &= \sum_{j=0}^{N-1} y_j u_{k_1,j} \\
&= \sum_{j=0}^{N-1} ((1 - \delta) \cos(2\pi j(f_0 \Delta t)) + \sigma_0 \xi_j) u_{k_1,j} \\
&= (1 - \delta) \sum_{j=0}^{N-1} \cos(2\pi j \frac{k_0}{N}) u_{k_1,j} + \sigma_0 \sum_{j=0}^{N-1} \xi_j u_{k_1,j}
\end{aligned}$$

But, the first of these sums vanishes on account of the orthogonality relations (3.9).

Simplifying further:

$$\mathbf{y} \cdot \mathbf{u}_{k_1} = \sigma_0 \sum_{j=0}^{N-1} \xi_j u_{k_1,j}$$

Now, as the ξ_j are independent and normally distributed, the dot product $\mathbf{y} \cdot \mathbf{u}_{k_1}$, which is just a weighted sum of the ξ_j , is also normally distributed, with mean given by

$$\begin{aligned}
\langle \mathbf{y} \cdot \mathbf{u}_{k_1} \rangle &= \langle \sigma_0 \sum_{j=0}^{N-1} \xi_j u_{k_1,j} \rangle \\
&= \sigma_0 \sum_{j=0}^{N-1} \langle \xi_j \rangle u_{k_1,j} \\
&= 0
\end{aligned} \tag{3.12}$$

and variance

$$\begin{aligned}
\langle (\mathbf{y} \cdot \mathbf{u}_{k_1})^2 \rangle &= \langle \sigma_0^2 \left(\sum_{j=0}^{N-1} \xi_j u_{k_1,j} \right)^2 \rangle \\
&= \sigma_0^2 \left(\sum_{j=0}^{N-1} \langle \xi_j^2 \rangle u_{k_1,j}^2 + 2 \sum_{j < m} \langle \xi_j \xi_m \rangle u_{k_1,j} u_{k_1,m} \right) \\
&= \sigma_0^2 \sum_{j=0}^{N-1} u_{k_1,j}^2 \\
&= \sigma_0^2
\end{aligned} \tag{3.13}$$

where I have used the properties of the noise (3.10) and the orthogonality relations (3.9). Essentially identical calculations show that $\mathbf{y} \cdot \mathbf{v}_{k_1}$ is also normally distributed, with mean zero and variance σ_0^2 . Defining

$$c_{k_1} = \mathbf{y} \cdot \mathbf{v}_{k_1}$$

$$d_{k_1} = \mathbf{y} \cdot \mathbf{v}_{k_1}$$

we are interested in the distribution of $P_{k_1} = c_{k_1}^2 + d_{k_1}^2$. As c_{k_1} and d_{k_1} are uncorrelated (this follows from the orthogonality of u_{k_1} and v_{k_1}) the sum of their squares has a χ^2 distribution with two degrees of freedom, whose density is

$$g_{k_1}(\rho) = \frac{e^{-\rho/(2\sigma_0^2)}}{2\sigma_0^2} \quad (3.14)$$

Similar calculations apply for the channel that includes the signal, but with the results that

$$\begin{aligned} c_{k_0} &= \mathbf{y} \cdot \mathbf{u}_{k_0} \sim N((1 - \delta)\sqrt{N/2}, \sigma_0) \\ d_{k_0} &= \mathbf{y} \cdot \mathbf{v}_{k_0} \sim N(0, \sigma_0) \end{aligned}$$

The nonzero mean for c_{k_0} means that the power at the signal frequency, $P_{k_0} = c_{k_0}^2 + d_{k_0}^2$, has a *non-central χ^2 distribution* whose density is given by:

$$g_{k_0}(\rho) = \frac{e^{-\frac{(\rho+\mu^2)}{2\sigma_0^2}} I_0\left(\frac{\mu\sqrt{\rho}}{\sigma_0^2}\right)}{2\sigma_0^2} \quad (3.15)$$

where $\mu = (1 - \delta)\sqrt{N/2}$ and $I_0(x)$ is a *modified Bessel function of the first kind*.

Signal detection strategies and ROC curves

Suppose now that one is presented with a single vector of observations y_j and asked whether it appears to contain the sinusoidal signal. If the signal is present the power at its frequency f_{k_0} will be drawn from the g_{k_0} computed above. If the signal is absent, the power at the signal frequency will be distributed in the same way as all the other frequencies, as g_{k_1} .

Strategies for signal detection now reduce to the choice of a cutoff ϕ : if, for a particular observed y_j , the power at the signal frequency exceeds this cutoff, then the signal is said to be present, otherwise it is said to be absent. Combining this policy with the expressions for g_{k_0} and g_{k_1} , it is easy to work out the probabilities required to draw a ROC curve:

$$\begin{aligned} P(\text{hit} \mid \phi) &= \int_{\phi}^{\infty} g_{k_0}(\rho) d\rho \\ P(\text{false alarm} \mid \phi) &= \int_{\phi}^{\infty} g_{k_1}(\rho) d\rho \end{aligned} \quad (3.16)$$

where the first line gives the probability that the observed power will exceed ϕ when the signal is present and the second is the probability that it will do so by chance,

even when the signal is absent. A ROC curve is then traced out as the image of a function $\gamma : [0, \infty) \rightarrow [0, 1]^2$ with

$$\gamma(\phi) = (P(\text{false alarm} \mid \phi), P(\text{hit} \mid \phi)) \quad (3.17)$$

Figure 3.4 shows ROC curves for a variety of noise amplitudes. In the caption there, and in the rest of this chapter, noise amplitudes will be characterised by the noise-to-signal ratio (NSR)

$$\eta = \frac{\sigma_0 \sqrt{2}}{1 - \delta} \quad (3.18)$$

where $(1 - \delta)/\sqrt{2}$ is the root-mean-squared amplitude of the sinusoidal signal, and σ_0 is the root mean squared amplitude of the noise terms.

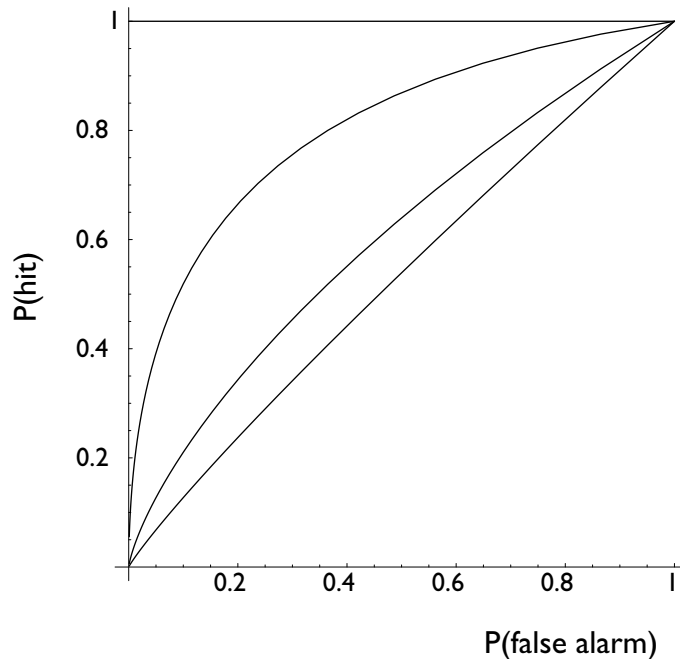


Figure 3.4: ROC curves traced using equation 3.16 for a system with $\delta = 0.05$, $N = 240$ and $k_0 = 15$. The four curves are for noise levels $\eta = 2, 4, 8$ and 16 .

3.2.4 Detecting the Signal II: after the threshold

Once the threshold has been applied the signal has a markedly different character: it assumes only the values 0 or 1. The statistical properties of the x_j are thus very different, and in some ways simpler, than those of the y_j . We have chosen our signal to be subliminal, so in the absence of noise it never crosses the threshold, $x_j = 0 \forall j$.

When noise is present we have

$$\begin{aligned}
P(x_j = 1) &\equiv p_j \\
&= P(y_j \geq 1) \\
&= P((1 - \delta) \cos(2\pi j(f_0 \Delta t)) + \sigma_0 \xi_j \geq 1) \\
&= P(\sigma_0 \xi_j \geq 1 - (1 - \delta) \cos(2\pi j(f_0 \Delta t))) \\
&= P(\xi_j \geq (1/\sigma_0) [1 - (1 - \delta) \cos(2\pi j(f_0 \Delta t))]) \\
&= 1 - \Phi((1/\sigma_0) [1 - (1 - \delta) \cos(2\pi j(f_0 \Delta t))])
\end{aligned} \tag{3.19}$$

where the first line should be read as a definition of the symbol p_j and $\Phi(x)$ is the *cumulative density function* (CDF) for the distribution of the noise. Figure 3.5 shows p_j as a function of noise amplitude for a set of NSR ratios η .

For computational ease the noise here is uniformly distributed over an interval $-a \leq \xi \leq a$ whose size a is chosen so as to achieve the desired value of η

$$a = \sqrt{\frac{3}{2}} (1 - \delta).$$

Note that, for very small noise amplitudes $p_j = 0$ except for a brief interval near the peak of the underlying sinusoidal oscillation. By contrast when the η is very large all the p_j tend to $1/2$, which is simply the probability that $\xi_j > 0$.

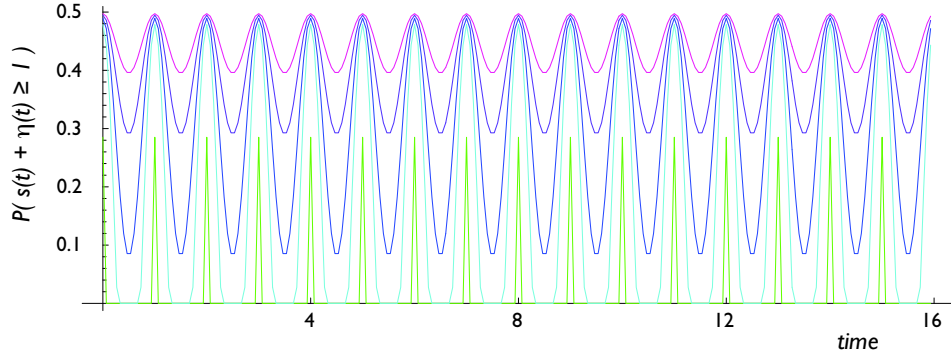


Figure 3.5: The probability that the x_j is one as a function of time for various noise levels $\eta = 0.1, 1, 2, 4$ and 8 . Here $\delta = 0.05$, $N = 240$, $\Delta t = 1/15$ and the sinusoidal signal has frequency $f_0 = 1.0$. The p_j are plotted with connecting line segments to guide the eye, but are really only defined at the sampling times $j\Delta t$.

As in the previous section, we would like to work out the distribution of the entries in the power spectrum. Here we will work with the p_j defined above, and so we no

longer need to make any special distinction between the channel corresponding to the signal frequency and the other. Conceptually, this is straightforward: the space of possible vectors \mathbf{x} is simply $\{0, 1\}^N$ and, armed with (3.19), we can compute the probability of each possible string of 0's and 1's. But this is an $O(2^N)$ process and not remotely feasible for the sorts of signals considered above.

Fortunately, one need not resort to direct enumeration of every possible \mathbf{x} . Instead consider $\langle a_k^2 \rangle$ for some arbitrary $0 < k \leq N/2$.

$$\begin{aligned} \langle a_k^2 \rangle &= \left\langle \left(\sum_{j=0}^{N-1} x_j u_{k,j} \right)^2 \right\rangle \\ &= \left\langle \sum_{j=0}^{N-1} x_j^2 u_{k,j}^2 + 2 \sum_{j < m} x_j x_m u_{k,j} u_{k,m} \right\rangle \\ &= \sum_{j=0}^{N-1} \langle x_j^2 \rangle u_{k,j}^2 + 2 \sum_{j < m} \langle x_j x_m \rangle u_{k,j} u_{k,m} \end{aligned}$$

Now, if $j \neq m$, the expected value of the product $x_j x_m$ is just $p_j p_m$. But the expected value of x_j^2 is just p_j . Indeed, $\langle x_j^r \rangle = p_j \forall r \neq 0$, so the expected contribution to the power spectrum is

$$\begin{aligned} \langle a_k^2 \rangle &= \sum_{j=0}^{N-1} \langle x_j^2 \rangle u_{k,j}^2 + 2 \sum_{j < m} \langle x_j x_m \rangle u_{k,j} u_{k,m} \\ &= \sum_{j=0}^{N-1} p_j u_{k,j}^2 + 2 \sum_{j < m} p_j p_m u_{k,j} u_{k,m} \\ &= (\mathbf{p} \cdot \mathbf{u}_k)^2 - \sum_{j=0}^{N-1} p_j^2 u_{k,j}^2 + \sum_{j=0}^{N-1} p_j u_{k,j}^2 \end{aligned} \tag{3.20}$$

The last line provides a computationally efficient way to evaluate $\langle a_k^2 \rangle$ and, as the calculations don't depend on any special properties of \mathbf{u}_k , one can compute $\langle b_k^2 \rangle$ in the same way and so obtain $\langle P_k \rangle$.

Figure 3.6 shows a comparison between the expected power spectrum based on (3.20) and a direct numerical experiment. Note that for very low noise levels the power spectrum includes peaks at all the harmonics of the signal frequency: for such weak noise the only nonzero x_j correspond to the peaks in the underlying sinusoid and so appear more like a periodic delta function. Notice also that the power at frequencies other than the signal frequency (and its harmonics) rises steadily with increasing noise, while the power at the signal frequency has a maximum for some intermediate noise level. This point is illustrated more clearly in figure 3.7, which

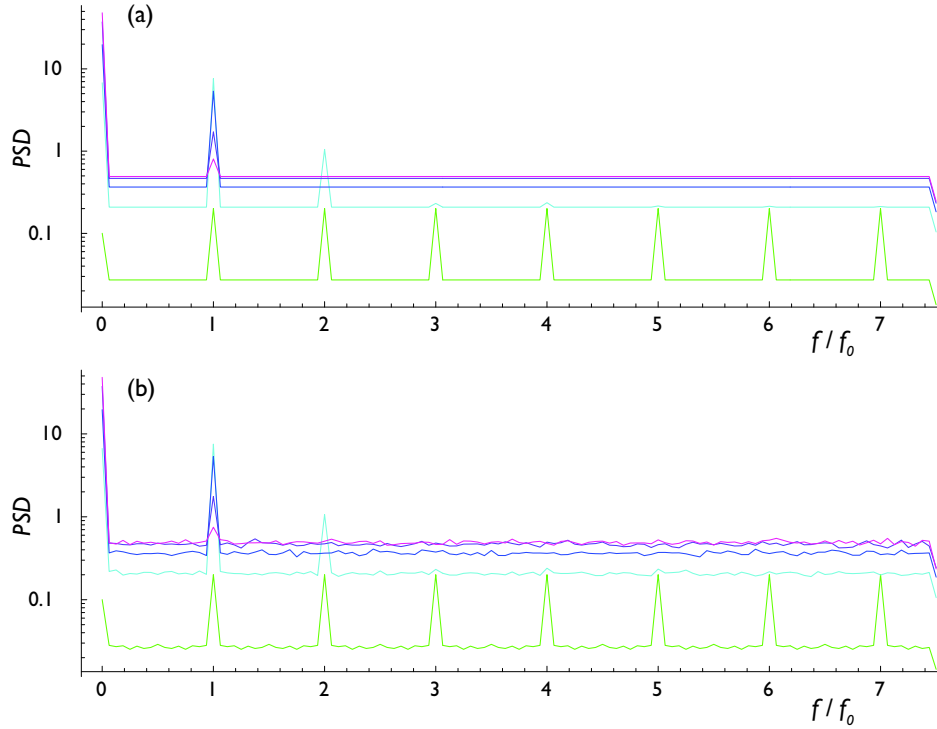


Figure 3.6: Expected power spectra for the same sets of parameters as illustrated in figure 3.5. Panel (a) shows $\langle P_k \rangle = \langle a_k^2 \rangle + \langle b_k^2 \rangle$ computed using (3.20) while the lower panel, (b), shows the results of averaging the spectra of 512 realisations of \mathbf{x} . For the latter case the spectra were computed via the DFT using *Mathematica*'s built-in `Fourier` function. The parameters and colour scheme are the same as described in the caption to figure 3.5.

shows the expected power at the signal frequency as a function of the noise-to-signal ratio η : there is a peak at about $\eta = 1.5$.

ROC curves

We have computed the mean of the entries in the power spectrum, but to draw ROC curves we need details of the distributions of the entries in the power spectrum. These are unlikely to be well-known, or simply defined, but in this section we propose some approximate approaches. The main ingredient is a formula for $\langle P_k^2 \rangle$ (for details, see appendix A) which enables one to compute the variance of the entries in the power spectrum. It agrees with simulation about as well as the formula for the mean did and enables one to approximate the distribution of the P_k with parametric distributions.

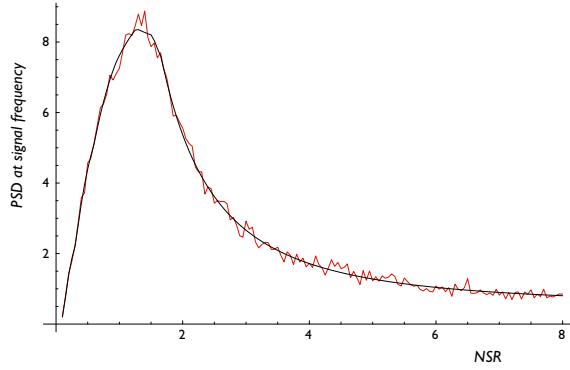


Figure 3.7: Expected power at the signal frequency as a function of the noise strength η . The smooth black curve is based on (3.20) while the jagged red curve shows, for each η the mean over 64 realisations of \mathbf{x} . Parameters other than η are as in figure 3.5.

Figure 3.8 shows both numerically-produced densities and approximate parametric distributions. The panels in the left column show histograms of P_k at a frequency away from the signal peak. Each plot also includes a solid black curve showing the density function for an exponential distribution with the same mean as the P_k . The panels at right show the distribution of power at the signal frequency, as well as the density for a normal distribution that has the same mean and variance as expected for P_k .

The normal approximation appears reasonable for modest noise, though the histograms appear a bit skewed to the right, but at high noise levels the approximation is poor. However, we are primarily interested in the lower noise levels for, as figure 3.7 illustrates, it is around $\eta = 1.5$ that the power at the signal channel peaks.

Finally, the data in histograms such as those in figure 3.8 are, in themselves very good representatives of the distribution of the power spectrum and can be used directly to compute ROC curves. In figure 3.9 ROC curves (far right) are drawn for simulations based on 1000 realisations of \mathbf{x} . In the central columns the power spectrum for a single example realisation of the process is shown both before (second column) and after the threshold nonlinearity (third column). The first column shows a single realisation of the input stimulus, \mathbf{y} .

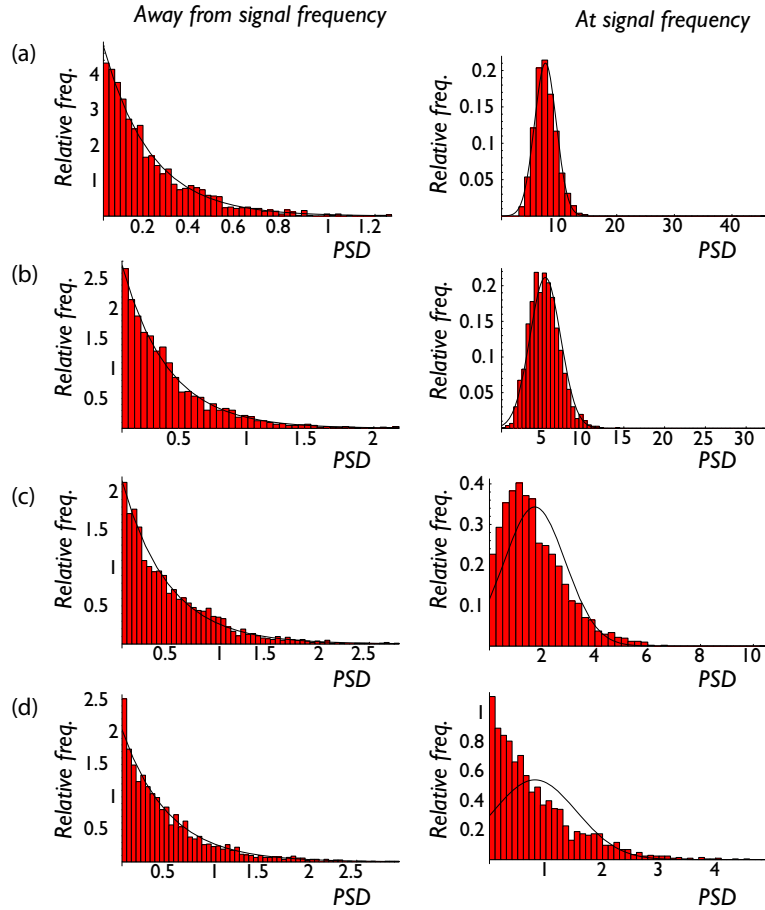


Figure 3.8: Numerical and approximate parametric representations of the distributions for the power at the signal frequency (right column) and at a frequency away from the signal peak (left column). The black curves are plots of the densities given in equations 3.14 and 3.15, with mean and variance chosen to match the histograms. The panels in row (a) come from simulations with $\eta = 1$ while those in (b) - (d) had $\eta = 2, 4,$ and $8,$ respectively. Histograms are based on 2048 realisations of \mathbf{x} and the remaining parameters are as in figure 3.5.

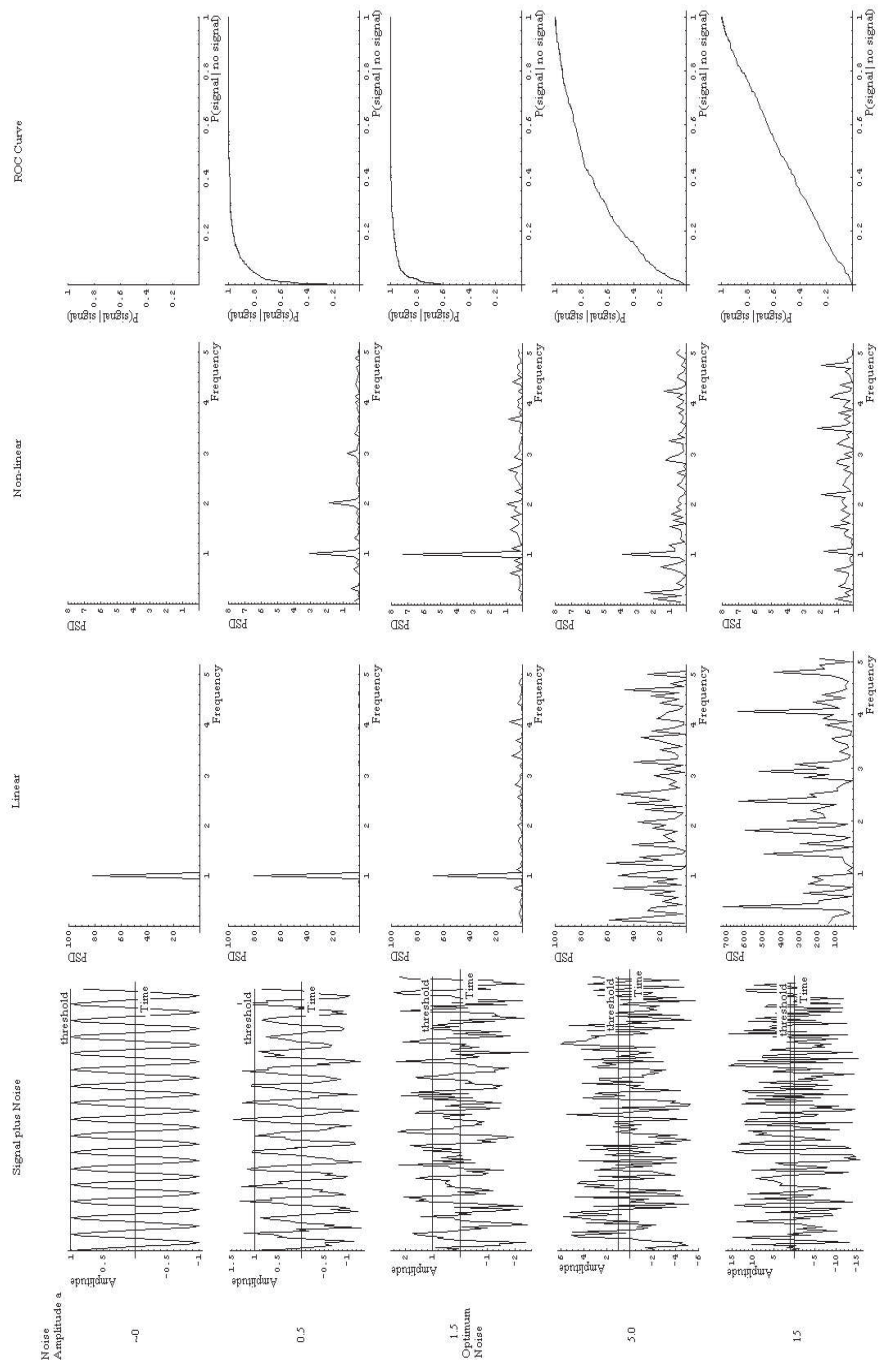


Figure 3.9: ROC curves and power spectra for both linear and non linear systems with different values of added noise. In the first column input stimuli are shown, relative to the threshold, for different values of added noise. The second and third columns show a single realisation of the noise, before and after the non-linearity respectively. The final column shows ROC curves based on 1000 realisations of the noise.

Chapter 4

Experimental Evidence for Stochastic Resonance

4.1 Introduction: What is Psychophysics?

In order to verify experimentally the effect noise has on vision, we need a robust way of measuring perception. The experimental methods used by neuroscientists are long established [16, 47], and *psychophysics* is the name given to the science of relating physical stimulation to perceptual events.

Psychophysics was named by its founder, Gustav Theodor Fechner (1801-1887) (figure 4.1), in his landmark book ‘Elements of Psychophysics’ [13], which was published in 1860 after the culmination of ten years of study. Fechner’s aim in this work was to find the scientific relationship between mind and body. He discussed the difficulties of the task, recognising that sensitivity cannot be directly measured. Only the effects of sensitivity are apparent, in a similar way the energy of a body is inferred only by its effect on the world. For this reason, Fechner and psychophysics since have had to rely on recording reactions to measured stimuli. However, in 1860, nineteen years before the electric light bulb was invented, Fechner had none of the advantages of calibrated electrical equipment to help him, instead he used cleverly devised experiments like those using the shadows cast by candles and involving the perception of clouds, for example. His most extensive experimental work was concerned with

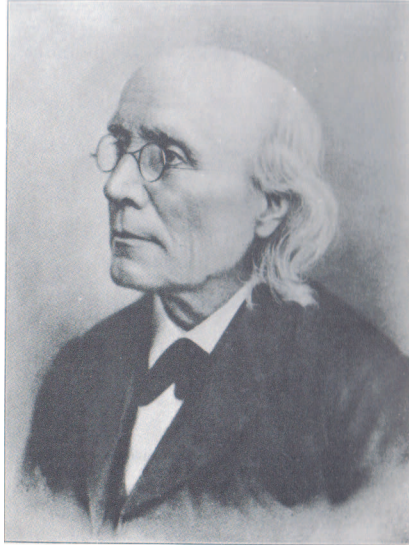


Figure 4.1: Gustav Theodor Fechner (1801-1887)

the perception of weight. He worked one hour per day over a two year period lifting weights and recording his perception of them. For this he devised three experimental methods which have formed the basis on which future psychophysics have had to build.

Fechner proposed a function that could be used to show the relationship between stimulus and sensation. Today this is called the *psychometric function* (figure 4.2), and it can be obtained by plotting stimulus intensity against percentage perceived.

Two quantities define the psychometric function: the *threshold*, below which a stimulus cannot be reliably perceived; and the *slope*, which defines how sudden the transition is between perceptible and imperceptible stimuli. Psychometric functions can be used to compare sensitivities between different tasks.

Historically, the most important law in psychophysics relating stimuli and perception is *Weber's Law*:

Theorem 1 (Weber's Law) *The difference between two stimuli is always perceived equal if its ratio to the stimuli remains the same, regardless of how absolute size changes.*

It was Fechner who attributed this to Weber. He quotes Bernoulli's financial example to illustrate it:

without doubt, the gain of 1000 ducats is far more important for poor

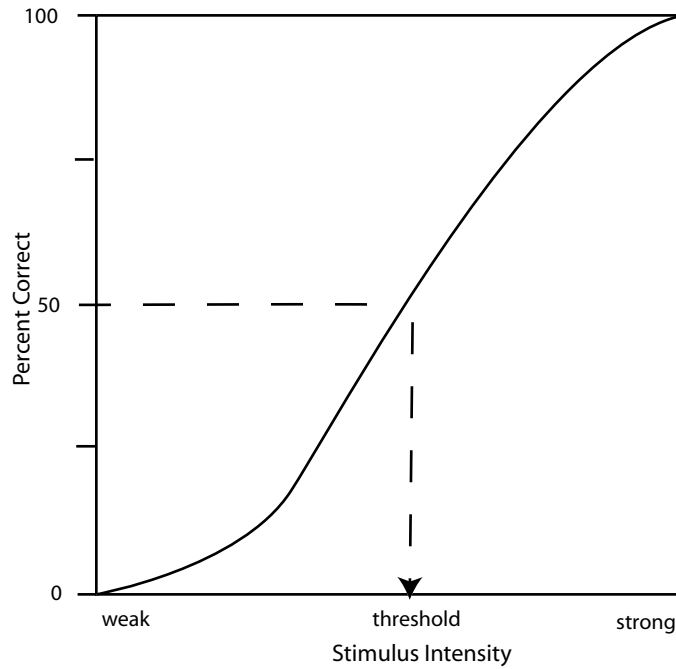


Figure 4.2: An example of a psychometric function

persons than for rich persons, although the amount is the same for both.

After publication of his book, Fechner turned his attention to other areas of science, leaving his legacy of psychophysics for others to develop.

4.1.1 Psychophysics and Statistical Decision Theory

In our world of noise and uncertainty, psychophysicists were forced to ask themselves what event or series of events must a stimulus provoke in order to be perceived. To explore their ideas about perception they turned to statistical decision theory which examines the statistics (both risk and uncertainty) related to an event and makes a decision based on the *most likely* option.

In section 3.1 the theory was applied to simple yes-no experiments and the process of producing ROC curves was described. While ROC curves are useful in the analysis of psychophysics experiments, they are very expensive to measure. Each point on the ROC curve may require hundreds of measurements and many points are required for a smooth curve. We require a more efficient method and the two alternative forced choice (2AFC) method provides this by eliminating the observer imposed criterion.

In a 2AFC experiment an observer is asked to make a decision between two pre-

defined alternatives. Here, the observer must prove that they can detect a stimulus by answering some question about it, such as the timing or spatial location of the stimulus. The only sensible strategy for this type of experiment is to choose the most likely alternative, that is, the observer chooses alternative A if

$$P(\text{signal presented in A}) > P(\text{signal presented in B}) \quad (4.1)$$

and chooses alternative B if

$$P(\text{signal presented in B}) > P(\text{signal presented in A}) \quad (4.2)$$

thus eliminating user imposed criteria. The exception to this is the case when both alternatives are equally likely, when the observer may apply a criterion as to how to distribute ‘guesses’ between alternatives. In the experiments devised here, however, this should not have an effect ¹. Psychometric functions can again be plotted, although now since an observer is forced to choose between two alternatives and thus will be correct on average 50% of the time when they cannot see the signal, the threshold is taken at the 75% correct point. This threshold is not affected by observer imposed criteria and can be used as a measure of perception. Thresholds or percentage correct results can be compared between experiments or observers to analyse performance.

There are other formats for psychophysics experiments, which have been devised to probe different aspects of perception, although in this study we will use the 2AFC method.

4.2 Experimental Design

4.2.1 Experimental Conditions and Dark Adaptation

Stochastic resonance is believed to exploit threshold mechanisms existing early in the retina. These thresholds control the quantity of light necessary to stimulate the visual system and their variable nature allows for the detection of light at very low

¹In threshold determination experiments: because an adaptive approach is used with half the signals in each alternative.

In SR experiments: because half of the signals are given to each alternative for each noise level.

light levels [50]. It is at these levels that noise may become a significant factor in the signal reaching the brain. Perhaps the most influential type of noise is *dark light* which arises as a result of the spontaneous isomerism of photoreceptors and can be seen as bright spots when the eyes are closed tight.

These experiments attempted to reproduce low light level conditions, where noise could have a significant effect on a signal. To achieve this, experiments were carried out in a dark windowless room, where the only light was provided by the computer VDU when images were displayed.

It is well known that prolonged exposure to bright light effects visual sensitivity significantly, as is demonstrated by the difficulty in visualising objects when walking from bright sunlit conditions into a dark room. The effect, called *dark adaptation*, is a consequence of the time taken for visual pigments to regenerate from a bleached to an unbleached state after exposure to light. It can be quantified and curves of the recovery of sensitivity (decrease of threshold) with time, can be drawn as in figure 4.3. In this graph, the dotted line represents the adaptation of cones while the solid

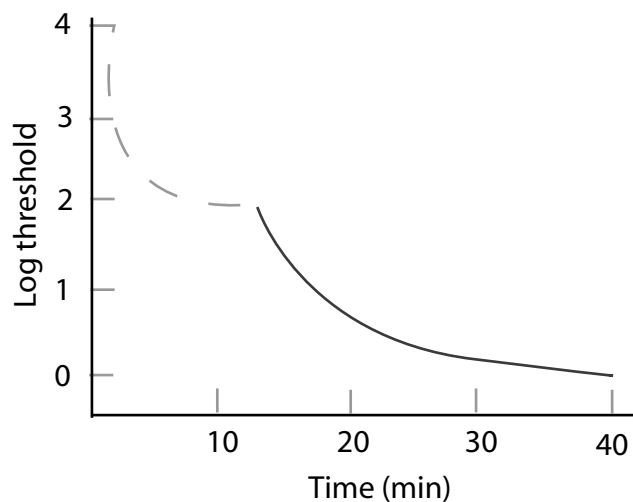


Figure 4.3: Dark Adaptation Curve, taken from [11]

line represents rod adaptation. The graph illustrates the rapid adaptation of cones to their new conditions reaching a maximum sensitivity after about five minutes, rods however don't reach maximum sensitivity until thirty minutes after dark exposure. Dowling [11] remarks that after being exposed to a bright light bleaching "virtually all" the receptor pigment, sensitivity took more than ninety minutes to recover in rats.

With these factors in mind I had to consider whether to include dark adaptation as a phase of the experiments. On reviewing previous work undertaken by the Manchester group, two projects were found with similar experimental design, one of these, carried out by Otterpohl [35] utilised dark adaptation, the other, carried out by Palladres [36] did not. Although the results of these experiments are not exactly comparable there do not appear to be any advantageous effects resulting directly from dark adapting observers. In fact the results of Palladres show a significant SR effect without its use. In view of this evidence, coupled with the fact that some of the experiments were tedious and sometimes extremely fatiguing, the decision was made not to dark adapt observers. Initial results (gathered for the grating experiment), where thresholds were measured both before and at the end of an experimental SR run, showed no apparent increase in sensitivity over the course of an experiment.

Another consequence of dark adaptation is raised by the issue of *after-images*. After-images arise because of uneven bleaching of the retina, which then takes differing times to recover. This results in an image being preserved in an area of the retina and a reduced sensitivity to further stimuli. Dowling [11] states that adaptation to dim intensities is complete within a minute, but in the experiments undertaken as part of this project, images in a duo are flashed on the screen after a half second gap and even between pairs the gap is much less than a minute (approximately two seconds), making after-images a distinct possibility. In fact, observers reported occasionally seeing the stimulus in both intervals of the 2AFC task, a possible consequence of this. However, in experiments where the gap between presentations was large (the delay was caused by the difficulty in generating the moving noise patterns, see 4.2.2), observers reported increased difficulty in maintaining concentration. This difficulty in concentration and the related inability to hold images in the mind for later comparison, outweighed any issues with afterimages.

4.2.2 The Experiments

These experiments were initially devised to demonstrate SR in the human visual system. They have been extended in an attempt to explore for which stimuli and tasks sub-threshold signals can be detected and also the extent of this detection. The tasks were divided into two forms; those of detection, where the aim was simply to

detect the presence of a signal and discrimination tasks, where an observer was asked to identify some property of the signal. We also examined whether using moving as opposed to static noise had a differential effect. In all eight kinds of experiment were carried out, these were divided into detection and discrimination tasks as follows:

Detection	Grating experiment	
	Square experiment	
	Grating with time varying noise experiment	
Discrimination	Single Interval	Triangle experiment
		Displaced Square Discrimination Experiment
		Angled grating experiment
	Triangle with time varying noise experiment	
Two Interval	Square wave discrimination experiment	

Table 4.1: Detection and discrimination experiments.

All experiments followed a 2AFC format, whereby an observer was asked to make a decision between two alternatives. Sometimes the alternatives differed in a temporal nature, sometimes spatial. In all experiments an equal number of each alternative was presented. All stimuli were presented on a VDU screen and were surrounded by a dark square frame, 20 degrees (of visual angle²) along each edge and 80% darker than the background luminance. The frame was presented only with the stimulus, thus providing a cue to the stimulus presentation, which alone may not have been visible. All images were fed through the green channel of the VDU (see 4.2.3), making the stimulus appear in differing shades of green. The screen was viewed binocularly through natural pupils. Decisions were indicated by the use of a switch or keyboard key.

Each experiment was divided into two parts; the first being a measurement of the *contrast detection threshold* (CDT), that is the minimum contrast at which the signal is detectable; while the second phase sought to determine the extent and magnitude of the SR effect. For some experiments two stimuli were presented and the observer had to choose the one with the desired property. For many of the discrimination

²The visual angle of an object on the retina is defined as the angle the object subtends to the eye

experiments, only one stimulus was presented and the observer had to identify some property of the signal. Here, a typical two interval experiment is described, the single interval alternative is similar.

For the CDT task a number (typically 75) of stimulus pairs were presented in the absence of noise. The first stimulus was presented for 500ms, then there was a 500ms gap then the second stimulus was presented for 500ms. Only one of these stimuli contained the signal, the other was a *blank*, with each pixel equal to the average intensity of the stimulus image. A typical set of presented images is shown in figure 4.4, where the image on the left contains the *blank* and the image on the right contains a grating signal. The observer's task was to choose which interval was most likely to have contained the signal. The software waits for this choice to be made before continuing with the next presentation. The signals were of differing intensity, the magnitude of which was calculated by a Bayesian adaptive method (See [22] and section 4.2.6) in order to provide the most information about the psychometric function while reducing the number of presentations required for an acceptable level of accuracy.

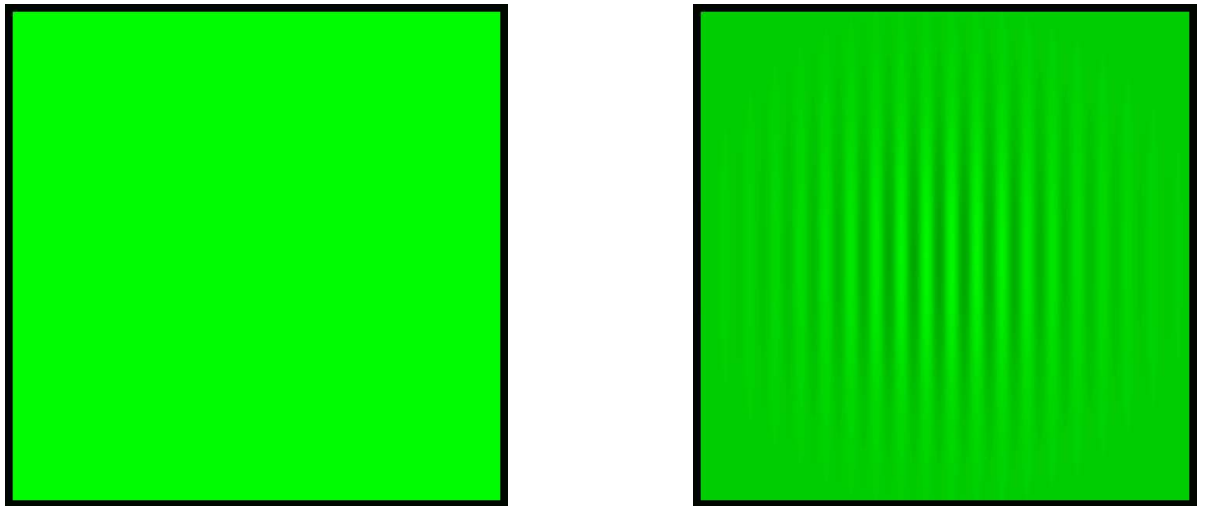


Figure 4.4: A typical pair of images used to determine a CDT

In the second part of the experiment, a signal was presented at a specified intensity (typically 0.2dB) below the CDT determined in part one. Noise of the same form was added to both signal and *blank* (no signal) presentations. Again, the order of presentation was; stimulus one for 500ms, 500ms gap, stimulus two presented for

500ms. A typical set of images for an SR experiment is shown in figure 4.5. The observer's task was to identify the interval which was most likely to contain the signal (right here), the software again waits for this decision to be made before presenting the next pair. A number of different (average) noise intensities were used, these were linearly spaced between specified minimum and maximum values, the case of no noise was also tested. There were many presentations, typically 40 though sometimes as many as 100, of each noise level which were arranged randomly.

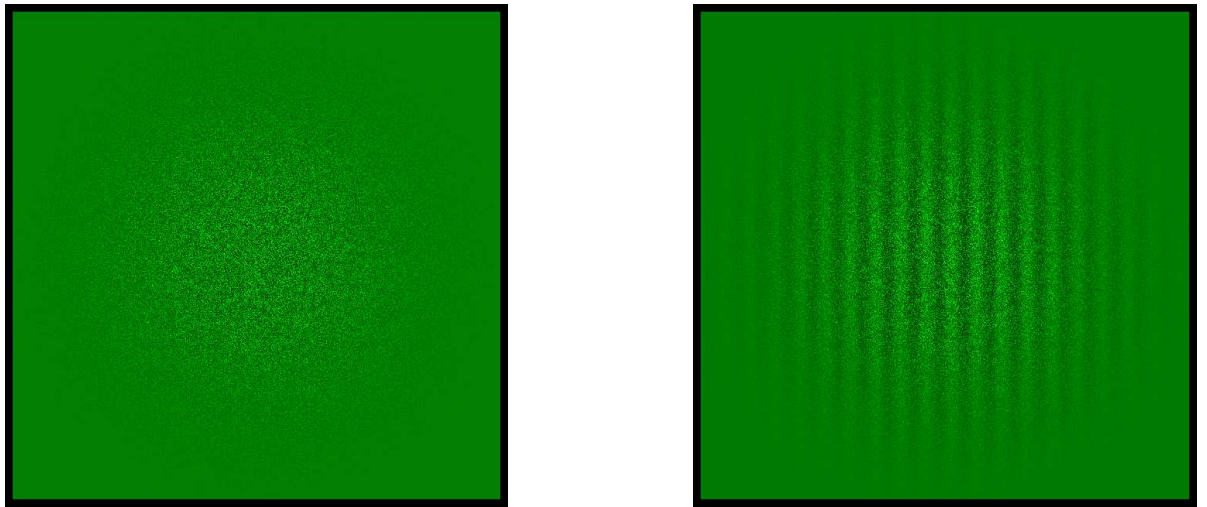


Figure 4.5: A typical pair of images used for an SR experiment

There are several differences between the single interval and double interval forced choice tasks. The first is the mode of presentation, which, for the single interval task was: present the stimulus for 500ms then wait for the observer's reply before presenting the next stimulus. Thus, a signal is always presented. This limits the type of perception that can be tested to discrimination tasks. The advantages of single interval experiments are that the experiments are quicker, leading to less fatigue, and also, the observer is not required to hold an image in memory for comparison: all the information is presented at the same time. The main disadvantage of this method is that an observer may miss the presentation and be forced to guess their decision, where in a two interval task she may be able to make an informed decision based on only one of the two presentations.

Each experiment is described in more detail below, with results given in section 4.3.

Grating Experiment

This experiment is essentially a repeat of those carried out by Otterpohl [35] and Pallares [36] in their demonstrations of SR. It is a two interval detection task where the observer is asked to identify which of the two intervals contained the sine wave grating

$$s(x) = \sin(2\pi fx) \quad (4.3)$$

with specified spatial frequency f . The signal is presented within a Gaussian envelope

$$g(r) = \exp\left(\frac{-r^2}{2\sigma^2}\right) \quad (4.4)$$

where σ is the envelope width, usually set to 4 degrees; this is designed to soften the edges of the stimulus and help it blend with the background. The stimulus is shown in figure 4.4 above.

In all 5 spatial frequencies were tested: 1 c/deg, 2 c/deg, 3 c/deg, 4 c/deg and 5 c/deg. 75 pairs were used to determine the CDT, which was taken to be the 75% correct point. To test for SR 40 pairs were presented 0.2dB below the measured CDT, for each of 9 noise magnitudes including zero.

Angled Grating Experiment

This is a discrimination task that uses the grating signal and inbuilt properties of the visual system in order to demonstrate SR. Even in the retina, the visual system distinguishes between lines of different orientation and passes this information onto the brain for image reconstruction. Here, this property is used to test possibly the simplest discrimination task, and the limits of our ability to discriminate between lines of differing orientation.

For this single interval experiment, a grating pattern of spatial frequency 3 c/deg, was presented within a 4 degree Gaussian envelope as described by equations 4.3 and 4.4. However, here the grating was sometimes oriented by angle $\theta = 90\text{deg}$, 45deg , 30deg , 20deg , 15deg , 10deg , 5deg , 3deg and 2deg , where each angle was tested individually in separate runs of the experiment. Examples of typical vertical and angled gratings are shown in figure 4.6. The observer's task was to say if the grating was vertical (left on the switch or 1 on the keyboard) or off from vertical (right or 2).

In the CDT phase of a trail, the observer was presented with 75 stimuli. For the SR phase the signal was presented 0.2dB below the CDT, 9 noises including zero were tested with 40 examples of each noise.

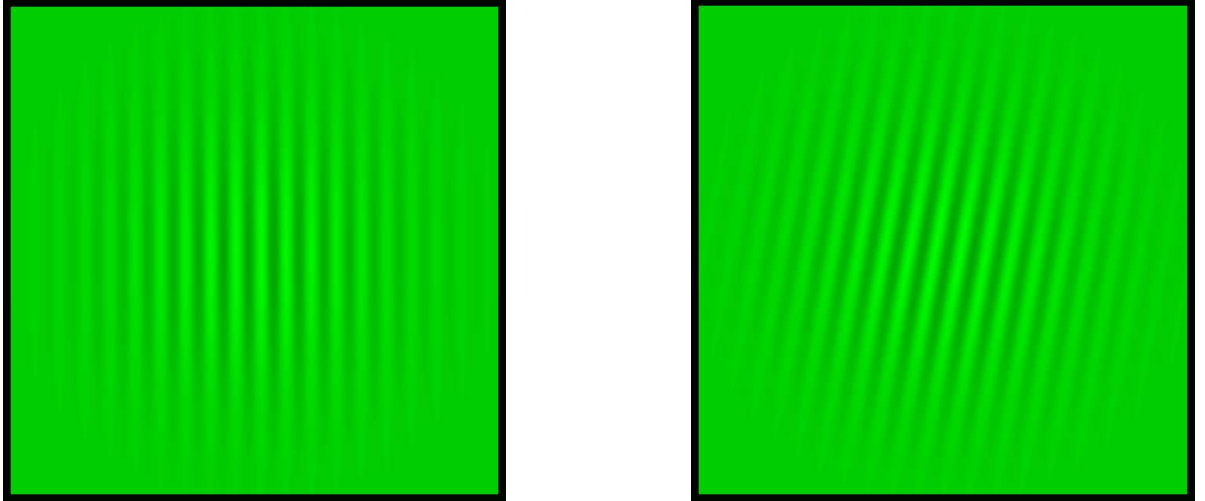


Figure 4.6: A typical pair of images used for angled grating experiment

Oriented Triangle Experiment

This was the first discrimination task tested. The results were somewhat disappointing and motivated other tasks which were devised to in an attempt to discover for what tasks SR is evident.

In this single interval task a triangle is presented that points either to the left or right, see figure 4.7, and the observer must decide on the direction and indicate their choice with the switch or keyboard. In different trials, different size triangles were presented, these were 0.5 deg, 1.0 deg and 1.5 deg, where the size is defined as the length of a side. The triangle was presented within a Gaussian envelope as described by equation 4.4 with $\sigma = 4$ degrees, which helped to soften the noise on SR trials.

In all 75 presentations were made for CDT measurement. For the SR phase the signal was presented 0.2dB below the CDT, 5 noise samples were tested (including zero) with 100 examples of each noise.

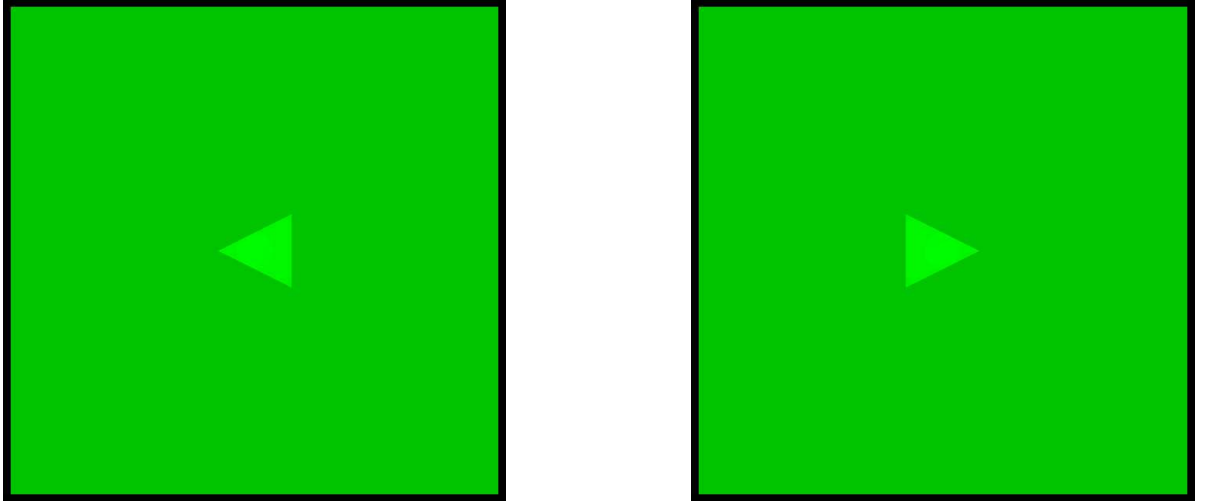


Figure 4.7: A typical pair of images used for the oriented triangle experiment

Square Detection Experiment

This detection task used the harder to perceive (relative to a grating) geometric square shape to explore whether SR is task (detection versus discrimination) or stimulus dependent. This shape is easier to detect than the triangle, because it has two pairs of parallel sides and four corners for an observer to pick out.

For this two interval detection task, an observer was asked if a square shape appeared in the first or second interval of the pair. Decisions were recorded with the switch or keyboard. The size of the square was defined by the length of one of its sides and in all two sizes of square were tested (1 deg and 1.5 deg) in separate runs of the experiment. A typical square signal is shown in figure 4.8.

In the CDT phase of a trail, the observer was presented with 75 stimulus pairs. For the SR phase the signal was presented 0.2dB below the CDT, up to 9 noises including zero were tested with either 40, 50 or 100 examples of each noise.

Displaced Square Discrimination Experiment

This discrimination experiment uses the geometric square shape again and asks on which side of the screen it is presented. This question of location is perceptually easier to answer than the one of orientation in the earlier oriented triangle experiment,

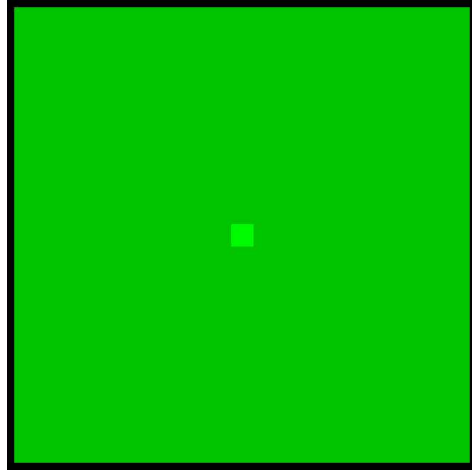


Figure 4.8: A typical square stimulus

the square shape is also easier to perceive.

In this single interval task, a square shape (1.0 deg) was presented along the horizontal centre-line of the screen off-set from the centre by an amount (1 deg, 2 deg or 3 deg in separate trials), see figure 4.9. The observer had to indicate whether they thought the shape appeared to the left or right of the screen, using the switch or keyboard.

In the CDT phase of a trail, the observer was presented with 75 stimuli. For the SR phase the signal was presented 0.8dB below the CDT (due to the difficulty in measuring CDT), 5 noises including zero were tested with 100 examples of each noise.

Square Wave Discrimination Experiment

The experiments in this section were motivated by the work of Campbell and Robson [8] and Abadi and Kulikowski [1], where the now widely-accepted proposal is made that, within the visual system, separate frequency channels exist, each detecting only those signals that lie within a narrow range of spatial frequencies.

The experiment was designed to utilise visual system properties to distinguish between sine and square waves. The Fourier series for the square wave of contrast C , depicted in figure 4.10 is given in equation 4.5

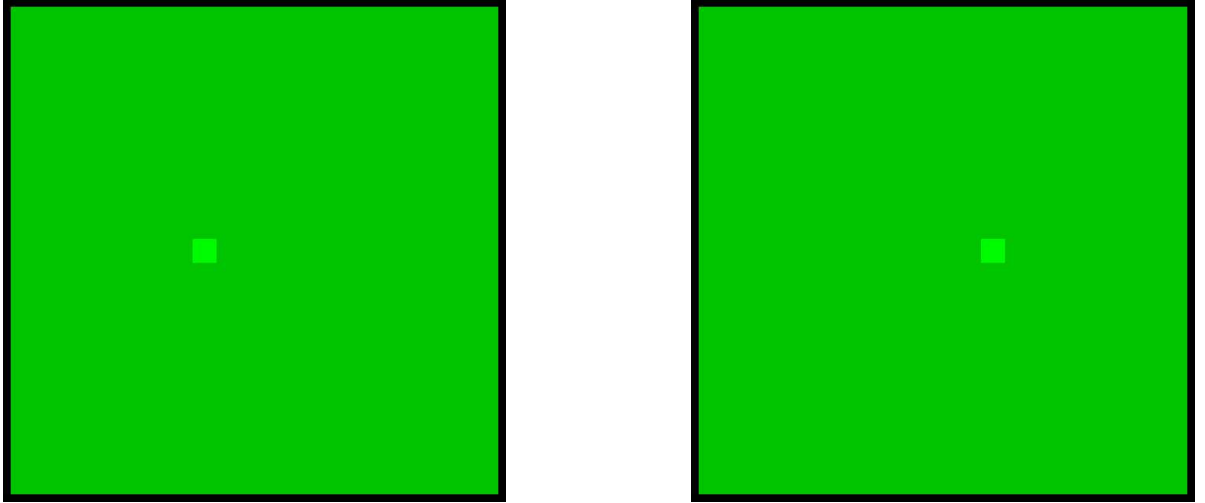


Figure 4.9: A typical pair of images used for the displaced square discrimination experiment

Square wave
$$f(x) = \begin{cases} -C & -\frac{\pi}{\omega} < x < 0 \\ C & 0 \leq x \leq \frac{\pi}{\omega} \end{cases}$$

Fourier series
$$f(x) = \frac{4C}{\pi} \sin(\omega x) + \frac{4C}{3\pi} \sin(3\omega x) + \frac{4C}{5\pi} \sin(5\omega x) + \dots \quad (4.5)$$

The sine wave of contrast C is given by

$$g(x) = C \sin(\omega x) \quad (4.6)$$

Now, suppose the threshold for a sinusoid of angular frequency ω is θ_1 , while that for a sinusoid of angular frequency 3ω is θ_3 , so that

θ_1 : is the value of C for which $C \sin(\omega x)$ becomes visible

θ_3 : is the value of C' for which $C' \sin(3\omega x)$ becomes visible

Then:

- The square wave will become **detectable** when $C = \frac{\pi}{4}\theta_1$. This is when the contrast of the first harmonic reaches θ_1 . Note, this implies that a square wave is more easily detected than a sinusoid of the same frequency.
- The square wave will become **distinguishable** from the sine wave when $C = 3\frac{\pi}{4}\theta_3$. This is when the contrast of the third harmonic reaches θ_3 .

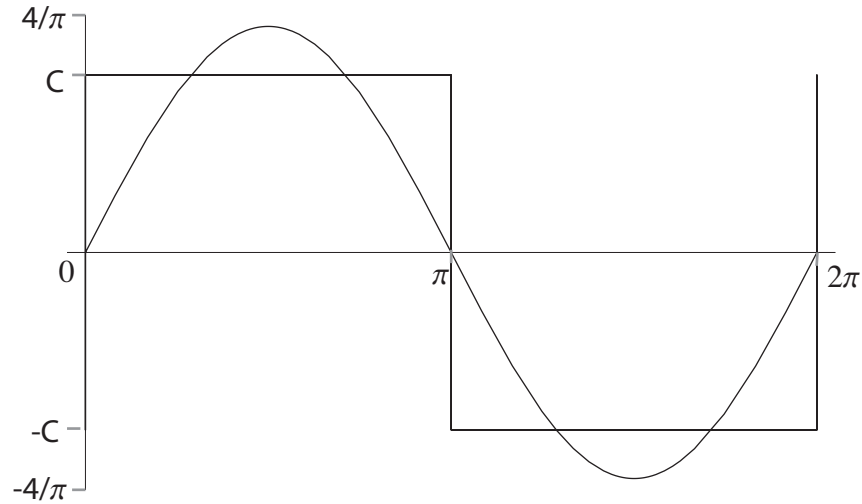


Figure 4.10: A square wave and its fundamental frequency

For this two interval experiment two signals were presented, one in each temporal interval. The signals were either a sine wave or a square wave³ and any of the following four combinations were possible: two sine waves, two square waves, a sine wave then a square wave (see figure 4.11) or a square wave then a sine wave. Each of these pairs were equally likely and appeared in random order. The observer's task was to say if the signals were identical (left on the switch or 1 on the keyboard) or different.

For the CDT measurement 76 stimulus pairs were presented. In the SR experiment 7 noise levels including zero were tested with 40 examples of each level. Both signals were presented 0.2dB below the measured CDT (taking into account that the square wave is reduced in contrast by $\frac{\pi}{4}$).

Grating with Time Varying Noise Experiment

The visual system monitors input over time, noting any changes to visual signals that occur. If the noise on an image varies over time, it would be expected that SR would highlight different parts of an image at different times. Integration of these differing noisy signals could further aid vision. The following two experiments were devised to show if time varying noise had any differential effect on perception. The first is essentially a repeat of the grating experiment with flickering noise.

³The square wave has a fundamental frequency equal to that of the sine wave and amplitude $\frac{\pi}{4}$ times that of the sine wave, in order for the two signals to appear at the same contrast.

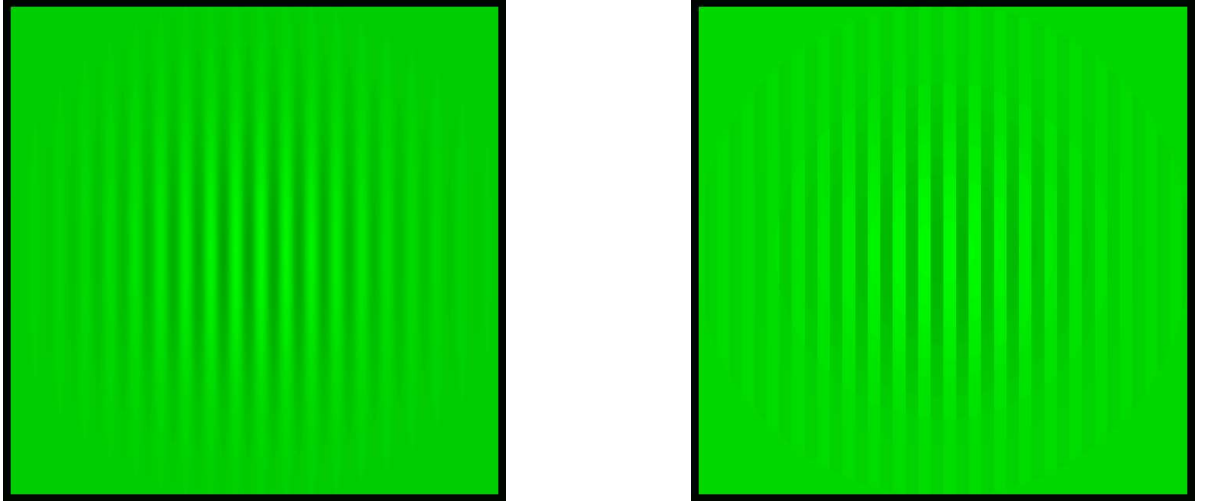


Figure 4.11: A pair of images used for the square wave discrimination experiment, where the first image (left here) contained the sine wave and the second (right) contained the square wave.

The experiment was carried out in exactly the same manner as described above. The spatial frequencies tested were 1 c/deg, 3 c/deg, 4 c/deg and 5 c/deg. For CDT measurement 75 samples were used and for the SR phase 5 noise samples were tested with 50 examples of each noise. Each stimulus was presented for 500 ms. Again the software waited for the observer's reply before presenting the next stimulus pair. There were hardware restrictions on how fast the noise could be generated and this slowed down the experiment considerably, so where for the stationary noise experiment a typical SR experimental run took 16 minutes, here a run took 55 minutes, and was therefore considerably more tiring.

Triangle with Time Varying Noise Experiment

This was a repeat of the oriented triangle experiment but used flickering noise .

4.2.3 Equipment

The following equipment was used for the experiments:

- Apple powerbook G3 233MHz laptop (with a serial port), running Denis Pelli's Video Toolbox software [39]

- High resolution Sony 200sf colour monitor
- Video attenuator, to convert three 8-bit DAC channels into one 12-bit (green) channel. This is used to increase ‘gray’ levels from 256 to 4096
- A bimodal switch (or alternatively a keyboard press), used to record decisions
- An RS-232 (model 232DA12 of B&B Electronics) 12-bit A\D data acquisition module
- A PR-1500 Spotmeter from Photo Research, a photometer used to calibrate the VDU
- A chin rest to ensure the observer remained stable

4.2.4 Software Review

To undertake psychophysics experiments stimuli need to be accurately drawn with known luminance (contrast) values. Modern computers have many pixels that can be individually set to create detailed and complicated stimuli. The process of setting the colour on a monitor, as well as the timing of a presentation, is controlled by the computer’s video card, which cannot be accessed directly and therefore is not easily manipulated.

To address these issues Denis Pelli has developed a suite of freely available C routines called *VideoToolbox* [39, 37]. These enable the generation of calibrated colour lookup tables that can be read by the video card and can also synchronize experiment timings with that of the video card’s internal clock. The Video Toolbox software enables a video attenuator to be used during the experiments. This attenuator is used to combine the video card’s three colour RGB channels into a single monochrome channel of higher grayscale resolution. The software includes examples of psychophysics experiments that can be run.

The software used for this project was written by Mark Muldoon using Denis Pelli’s Video Toolbox software. New stimuli have been written by the author along with new code that implements a single stimulus presentation (as opposed to the usual two presentations).

4.2.5 Calibration Procedure

In order to send luminance values to the computer’s video card a calibrated colour lookup table needs to be generated. This was achieved using a suite of programs called *CalibrateMonitor* within the VideoToolbox, and a photometer, the PR-1500 Spotmeter mentioned above. The photometer was focused on a central spot on the computer monitor and then reported back the measured luminance, to create the lookup table. The monitor was calibrated before the start of the reported experiments. It was not calibrated again as the calibration had proved stable over a period of many months during a previous set of experiments [35]. Additionally Pelli reports the calibration is stable (in a comment on the file *CalibrateLuminance.c*)

4.2.6 Bayesian Adaptive Method for Determination of CDT

To carry out the SR experiments a *contrast detection threshold* (CDT) measurement is required. The CDT is the contrast below which an observer cannot perceive a signal. To determine an observer’s CDT a separate CDT experiment was carried out immediately before each SR experiment.

A naive approach to determining CDT would be to use a *staircase* method: reduce the stimulus contrast until the observer can no longer see the stimulus (answers incorrectly) then increase the contrast until the stimulus is again seen (indicated by a correct answer); repeat this procedure until the difference between seeing and not seeing is sufficiently small. There are several problems associated with this approach: firstly, in a 2AFC experiment an observer would be correct 50% of the time even when they cannot perceive the signal; secondly, it may take many trials to accurately determine the threshold; and thirdly, this type of experiment makes no prediction for the slope of the psychometric function, which is not a simple step function as this method may suggest.

For the CDT experiments carried out under this project, a *Bayesian adaptive* method is implemented as suggested by Kontsevich and Tyler [22]. The method is reviewed in more detail in appendix B. The methodology of their approach is to look ahead to the next trial and predict which signal contrast would provide the greatest

confidence in the estimation of parameters that define the psychometric function. This is achieved by finding the contrast that gives the minimum of the expected entropy over all possible values of contrast. This test contrast is presented with the result being used to assist in calculating the next test contrast. The results of a typical CDT measurement experiment are shown in figure 4.12.

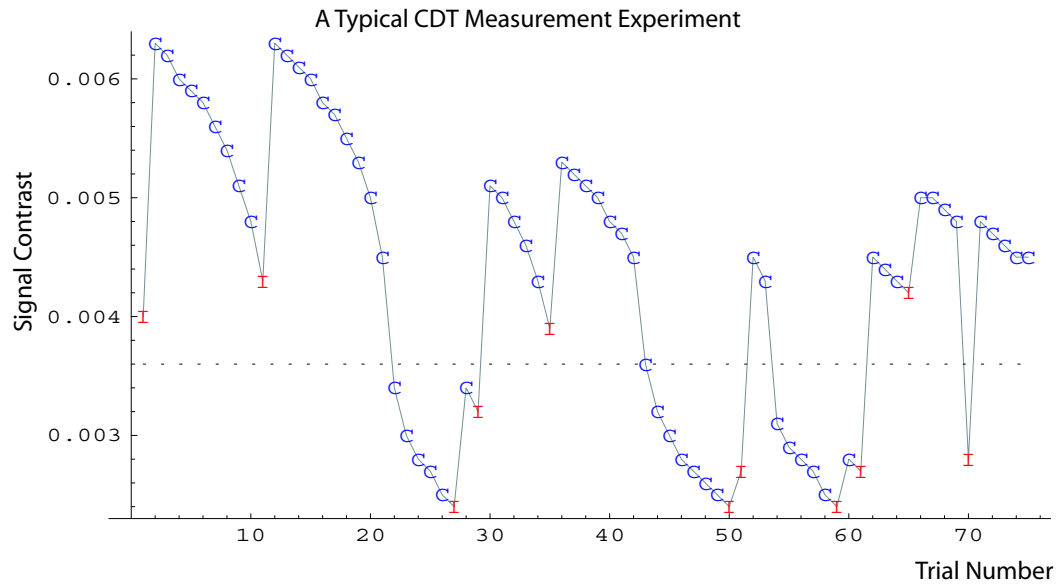


Figure 4.12: A Typical CDT measurement experiment using an adaptive Bayesian approach. In the graph: C indicates a correct answer, I an incorrect answer. After 75 trials the estimate of the CDT (see Appendix B) was 0.0036; this is shown in the figure by the horizontal dotted line.

Although one approach suggested by Kontsevich and Tyler [22] as the most accurate, is to run the experiment until the parameters are predicted to within a specified error, they rule this out as being impracticable. They instead suggest carrying out a fixed number (> 30) of trials, as then an experienced observer develops the ability to predict the duration of the experiment, thus, reducing possible uncertainty caused by a potentially endless experiment. In this project we have used this fixed number of stimuli approach, with 75 stimuli.

4.2.7 Generating the Noise

In order to carry out SR experiments noise patterns had to be generated and added to signals to create a stimulus. In her study Blackwell [7] states that the SR effect does

not depend on the form of the noise. She uses log-normally distributed noise in her experiments as this ensures that images look the same when scaled in intensity. All the experiments described here followed Blackwell’s prescription and used approximately log-normally distributed noise with a mean luminance equal to that of the stimulus as a whole. In this we were motivated by Weber’s law 1—that perceptibility is a matter of ratios: we wanted to use noise parameterised in such a way that its influence on perception would be the same for a broad range of stimulus intensities.

Stimuli are created by modifying individual pixels in the image (or on the screen), since these pixels are controlled individually and each has the same range of intensities, they can be said to be *independent and identically distributed* (IID). It is therefore sufficient to discuss how to generate the intensity (luminance) of a single pixel, with this intensity drawn from a log-normal distribution of the prescribed mean and variance.

Random numbers were generated using a pseudo-random number generator called the Mersenne Twister [26]. This produces a stream of integers uniformly distributed over the range $0 - (2^{32} - 1)$ with very long cycle times ($2^{19937} - 1$). These integers are normalised, so that they are uniformly distributed on the interval $(0, 1)$.

Pairs of uniformly distributed numbers can then be converted to normally distributed random numbers by a standard technique, the Box-Muller method, (see appendix C for more details)

$$\begin{aligned} y_1 &= \sigma_y \sqrt{-2 \ln x_2} \cos(2\pi x_1) \\ y_2 &= \sigma_y \sqrt{-2 \ln x_2} \sin(2\pi x_1) \end{aligned} \tag{4.7}$$

where the x ’s are uniformly distributed and the y ’s have a normal distribution of mean $\mu_y = 0$ and variance σ_y^2 . These intensities are translated and scaled (by taking the natural logarithm) to give a log-normal distribution of random numbers of specified mean and variance.

While all this sounds feasible several problems arise with the implementation. The first is concerned with displaying the full range of pixel intensities generated by the algorithm. Real monitors are restricted to certain minimum and maximum luminances, L_{min} and L_{max} . This gives rise to a maximum noise variance of

$$\sigma^2 \leq \left(\frac{L_{max} - L_{min}}{2} \right)^2 \tag{4.8}$$

which in turn affects the statistics of the distribution. We require our noise pattern to have a specified mean μ_z and variance σ_z^2 , which, taking into account the limitations on pixel intensities are given by

$$\begin{aligned}\mu_z &= \int_{\ln(L_{min})}^{\ln(L_{max})} e^y \left(\frac{e^{-\frac{(y-\mu_y)^2}{2\sigma_y^2}}}{\sqrt{2\pi\sigma_y^2}} \right) dy \\ \sigma_z^2 &= \int_{\ln(L_{min})}^{\ln(L_{max})} (e^y - \mu_z)^2 \left(\frac{e^{-\frac{(y-\mu_y)^2}{2\sigma_y^2}}}{\sqrt{2\pi\sigma_y^2}} \right) dy\end{aligned}\tag{4.9}$$

Given a target mean luminance μ_z and variance σ_z this pair of integrals can be solved numerically using Newton's method for the parameters μ_y and σ_y , which are used for the scaling.

The second problem affecting noise generation is the long time needed to solve equation 4.9, which makes it impossible to generate a new realisation of the noise for each stimulus presentation. Instead a new noise pattern was generated for each noise level and the noise pattern displayed for a stimulus of given mean noise was simply a shuffled version of the previous pattern displayed for that noise. The shuffling took place for 80% of the rows used to make up the stimulus, and involved interchanging randomly selected pairs of rows. Of these swapped rows, half had their pixels flipped from left to right. With the large number of pixels involved in making up a stimulus all presentations *looked* different, but had identical statistics.

Making the Noise Move

To make the noise move in the time varying noise versions of the experiments a new realization of the noise was used in each frame of the presentation. These new noise patterns were created by the shuffling procedure described above (section 4.2.7). With a frame rate of approximately 12 frames per second and a half second stimulus presentation time, this meant 6 noise patterns were used. During the presentation the noise appeared to flicker in a similar way to the noise on an untuned T.V. set.

4.2.8 Observers

I obtained results from three observers, a summary appears in table 4.2

Observer	Eyesight	Experiments
A Female 31 years old	corrected to 20/20	Grating experiment Angled grating experiment Oriented triangle experiment Square experiment Displaced Square Discrimination Experiment Grating with time varying noise experiment Triangle with time varying noise experiment
B Male 47 years old	corrected to 20/20	Grating experiment Angled grating experiment Oriented triangle experiment Displaced Square Discrimination Experiment Grating with time varying noise experiment Triangle with time varying noise experiment
C Female 26 years old	corrected to 20/20	Grating experiment Oriented triangle Square experiment

Table 4.2: Observers used for experiments

4.3 Results

Results are presented in the form of graphs of *inferred* probability correct against RMS noise. The actual number of correct answers isn't used as I wanted a probabilistic measure of the chance of being correct, taking into account the 2AFC paradigm. The inferred probability correct is taken to be the median of the posterior probability distribution (see Appendix D). This probabilistic approach also enables error bars to be drawn. The process used for calculating the error bars is also explained in Appendix D.

In the plots, the CDT measured for each experiment is given under the plot symbol in the legend at the right hand side of each graph. Also, note that some of the data points have been displaced slightly in the $\pm x$ direction. This is to prevent symbols

lying on top of each other and hence give a clearer picture of the results.

4.3.1 Grating Experiment

In this detection experiment the observer had to indicate which of two intervals was most likely to contain a grating signal (see 4.2.2 above). 75 pairs were used to determine the CDT and 40 pairs were presented for each noise level in the graphs below. A typical experimental run took approximately sixteen minutes.

Observer A

The results for 1 c/deg were obtained three days before those for 2 c/deg and those for 3 c/deg, 4 c/deg and 5c/deg were obtained 4 days later over a seven hour period.

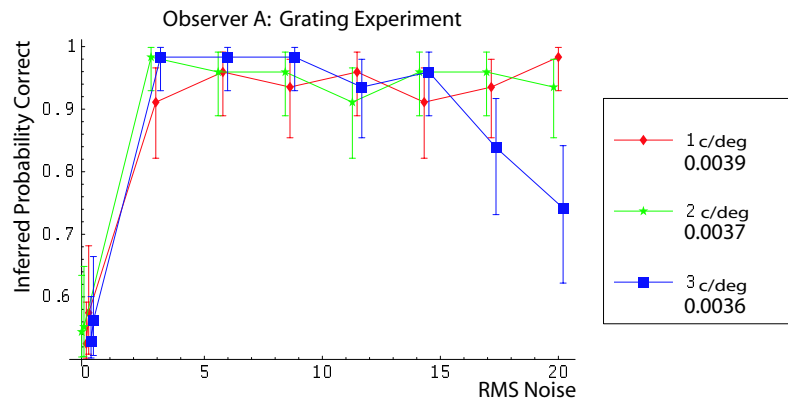


Figure 4.13: Observer A's results for the grating experiment with spatial frequencies 1 c/deg, 2 c/deg, 3 c/deg. The CDT for each frequency is given below that frequency label in the key.

Observer B

These results were obtained on separate days over a five month period.

Observer C

The results in graph 4.17 were obtained on 23rd August, 1st August and the 7th of July 2005, while those in graph 4.18 were obtained on the 1st August and the 23rd August. Where two experiments took place on the same day, these were carried out consecutively.

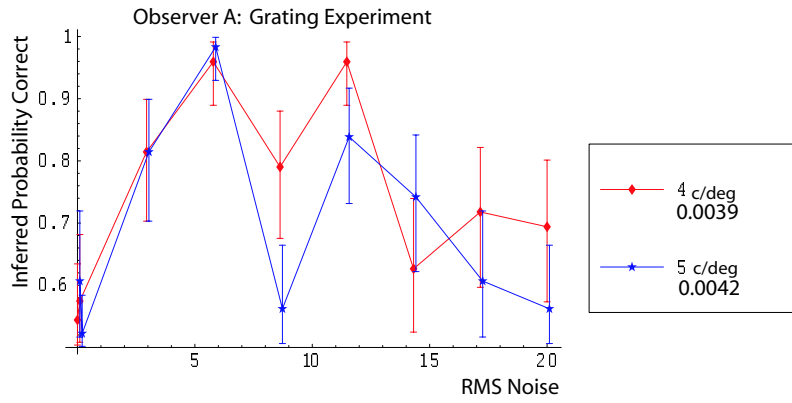


Figure 4.14: Observer A's results for the grating experiment with spatial frequencies 4c/deg, 5 c/deg

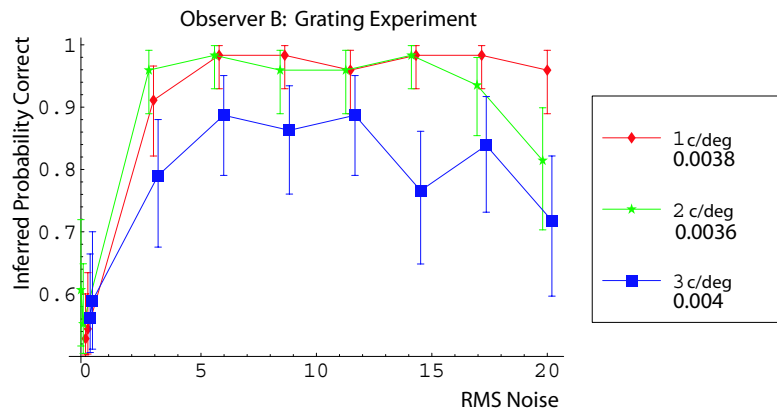


Figure 4.15: Observer B's results for the grating experiment with spatial frequencies 1 c/deg, 2 c/deg, 3 c/deg

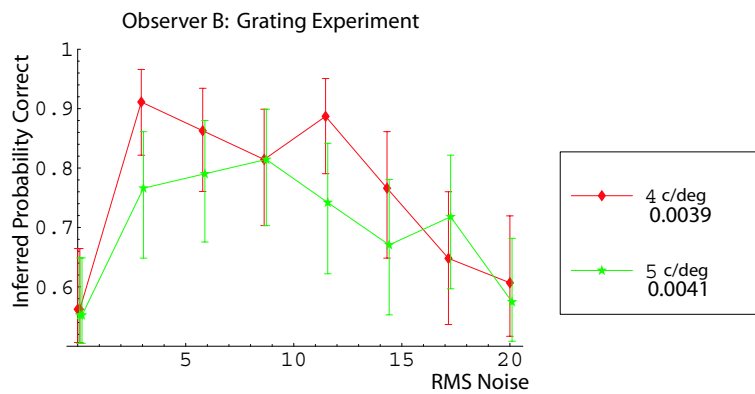


Figure 4.16: Observer B's results for the grating experiment with spatial frequencies 4 c/deg, 5 c/deg

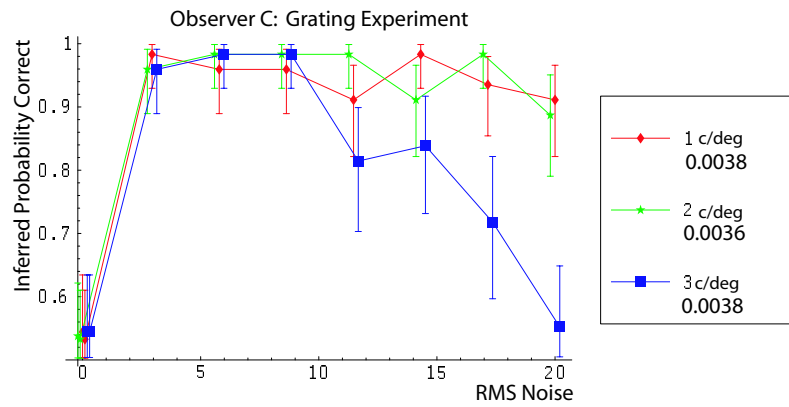


Figure 4.17: Observer C's results for the grating experiment with spatial frequencies 1 c/deg, 2 c/deg, 3 c/deg

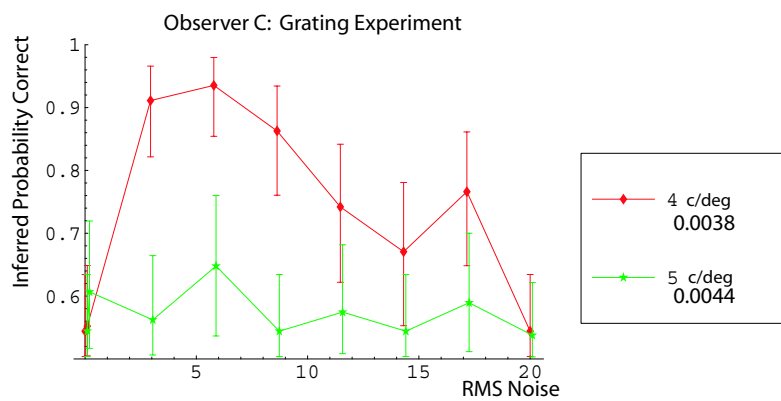


Figure 4.18: Observer C's results for the grating experiment with spatial frequencies 4c/deg, 5 c/deg

Comment

With the exception of observer C's 5 c/deg run, all experimental runs show a significant increase in perceptibility when noise was added to the signal. In particular, for observers A and C, the probability of a correct answer increased from less than 60% to more than 90% for low (≤ 2 c/deg) frequency signals, with the addition of noise. The results also show a decrease in the perceptibility of noisy signals with increasing noise for grating frequencies 3 c/deg or more, for all observers.

4.3.2 Angled Grating Experiment

In this discrimination experiment the observer was asked to indicate whether a presented signal was vertical or off from vertical. 75 stimuli were used to determine the CDT and 40 stimuli were presented for each noise level in the graphs below. A typical experimental run took approximately 22 minutes.

Observer A

The results in graph 4.19 were obtained on one day over a seven hour period, those in graph 4.20 were obtained three days later over a eight hour period and those in graph 4.21 were obtained on two consecutive days, seventeen days later than those in graph 4.20.

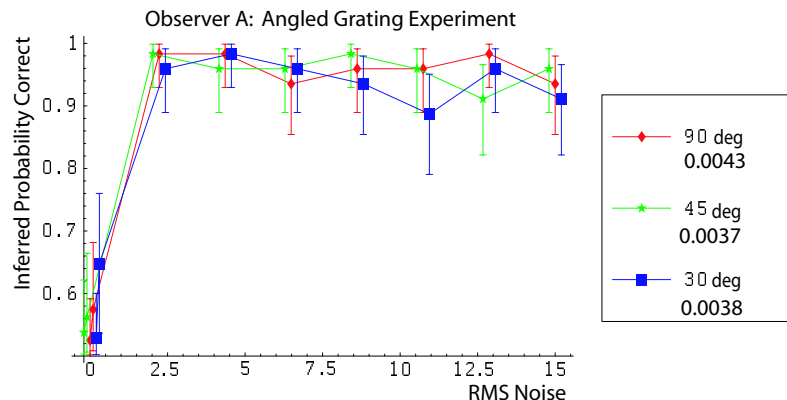


Figure 4.19: Observer A's results for the angled grating experiment with angles 90, 45, and 30 degrees

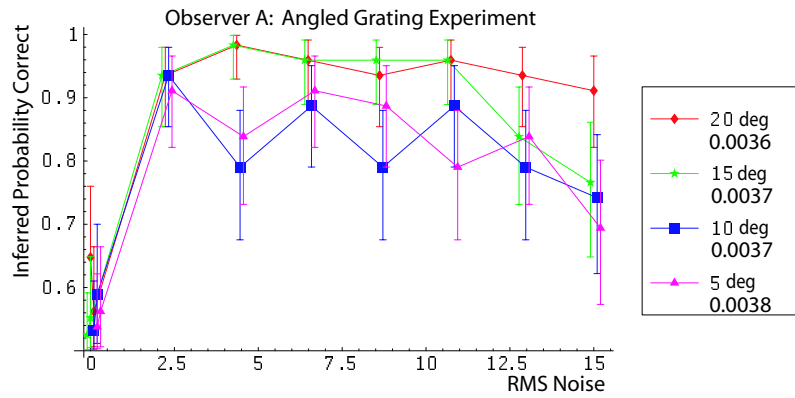


Figure 4.20: Observer A's results for the angled grating experiment with angles 20, 15, 10, and 5 degrees

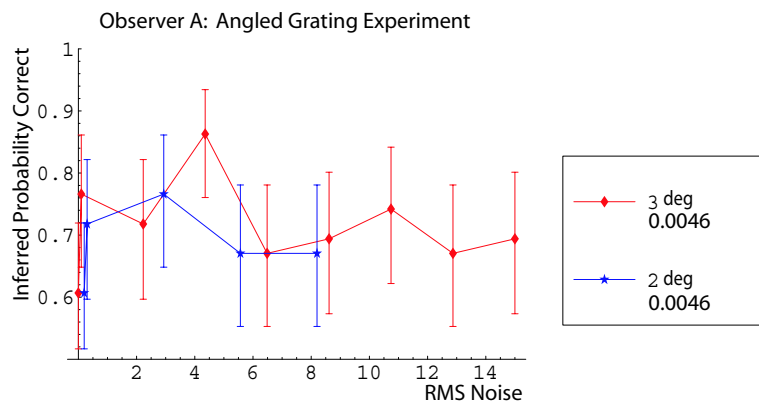


Figure 4.21: Observer A's results for the angled grating experiment with angles 3, and 2 degrees

Observer B

The results in graph 4.22 were obtained on two days over a ten day period.

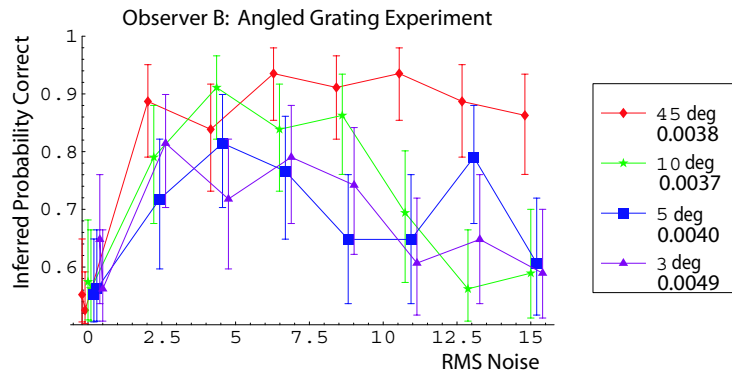


Figure 4.22: Observer B's results for the angled grating experiment with angles 45, 10, 5 and 3 degrees

Comment

In this experiment the task has changed from purely identifying the presence of a signal (detection) to identifying some property of it (discrimination). It is interesting to note that the CDT's measured in this experiment do not differ greatly from those measured in the grating experiment, perhaps an indication of the existence of separate frequency channels [8, 1] .

The results presented in figures 4.19 and 4.20 show a significant increase in distinguishability when noise was added to the signal. The effect was much less pronounced for a small off-set angle (3° and 2°) perhaps because of the difficulty of accurately measuring the CDT (the results are significantly above chance for the addition of a very small amount of noise) which may result from the increased difficulty of the task when both signals are detected by the same receptors within the retina.

4.3.3 Oriented Triangle Experiment

For this discrimination task a triangle was presented, the observer had to indicate whether it pointed to the left or the right. 75 stimuli were used to determine the CDT and 40 stimuli were presented for each noise level in the graphs below.

Observer A

The results in graph 4.23 were obtained on two days, more than a month apart, while those in graph 4.24 were obtained on separate days covering a six day period.

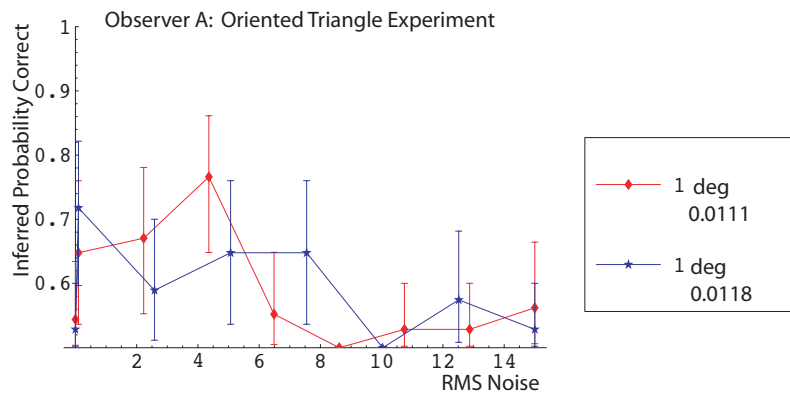


Figure 4.23: Observer A's results for the oriented triangle experiment with a one degree triangle

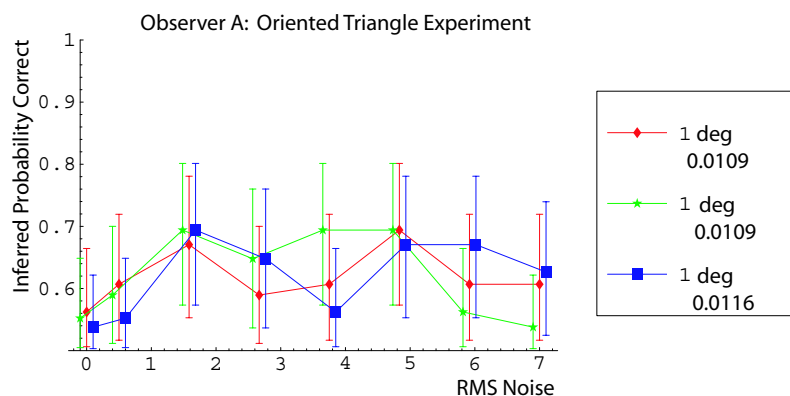


Figure 4.24: More of observer A's results for the oriented triangle experiment with a one degree triangle

Observer B

The result in graph 4.25 was obtained for observer B.

Observers A and C

The results in graph 4.26 were obtained for observers A and C for a 0.5 degree triangle.

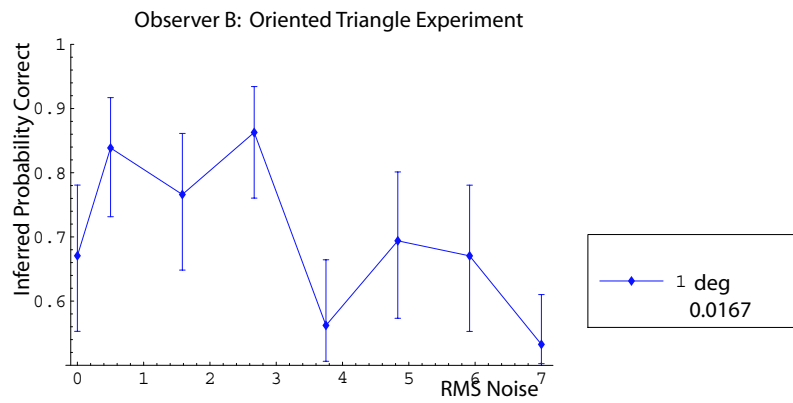


Figure 4.25: Observer B's results for the oriented triangle experiment with a one degree triangle

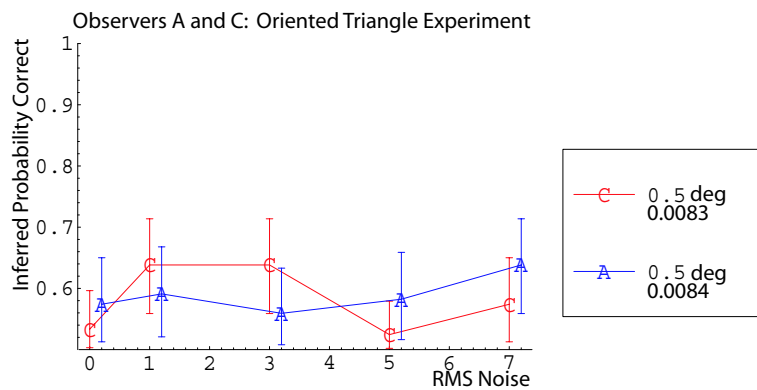


Figure 4.26: Observers A and C, results for the oriented triangle experiment with a 0.5 degree triangle

Comment

In this discrimination task the stimulus has changed from a simple grating pattern (detected by the frequency channels of the visual system) to a more complex geometric shape, a triangle. The task was to determine if the triangle pointed to the left or the right of the screen. An indication of the difficulty of this task can be taken from the increase in CDT. All observers also reported the increased difficulty of the task and felt fatigued after a relatively short time experimenting. It is interesting to note that the smaller triangles yielded a lower CDT (i.e. were more discriminable) than the larger ones, this maybe because the corners of the larger triangles are obscured slightly from the softening effect of the Gaussian envelope.

One problem with this experiment was the accurate measurement of CDT's. Figures 4.23 and 4.25 appear to show good discrimination, but the zero (or very low) noise level stimulus is also well detected (the observer was correct more than 65% of the time). In figure 4.24 the CDT appears more accurately measured (with around 55% of answers correct) and the stimuli are correctly discriminated more often (about 15% more) when noise is added. In Figure 4.26 for the smaller triangle, observer C shows some increased discriminability (around 10% more correct answers) while observer A showed no significant increase. In none of the valid experiments does the number of correct answers exceed 75%, the point at which we could conclude that the observer does correctly discriminate the stimuli. Therefore, the results of this experiment indicate that there may be a slight SR effect for the discrimination of complex stimuli, although there is no definitive proof.

4.3.4 Square Detection Experiment

In this detection task a square shape was presented centrally on the screen in one of two intervals. The observer had to say if the square appeared in the first or second interval. 75 pairs were used to determine the CDT and 50 pairs were presented for each noise level in graph 4.27, 100 pairs for the 1 degree square in graph 4.28 and 40 pairs for the 1.5 degree square in graph 4.28.

Observer C

The results in graph 4.27 were obtained for observer C with a 1 degree square.

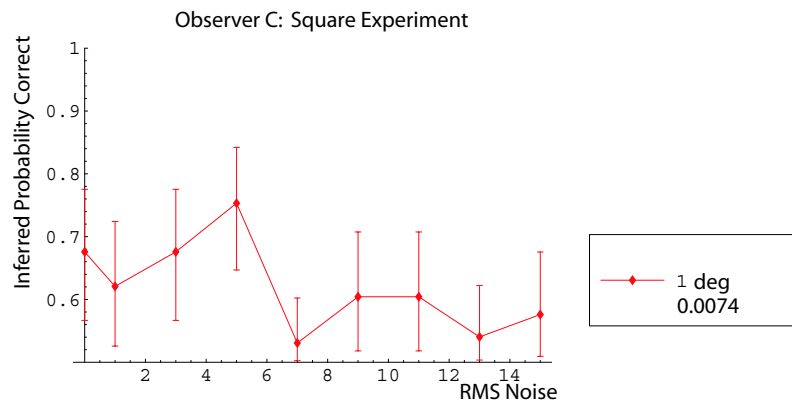


Figure 4.27: Observer C's results for the square experiment, with a 1 degree square.

Observer A

The results in graph 4.28 were obtained for observer A over a six day period.

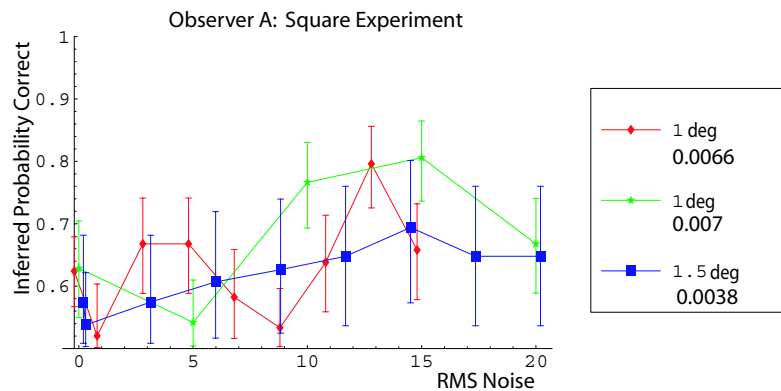


Figure 4.28: Observer A's results for the square experiment, with a 1 degree and 1.5 degree square.

Comment

For this experiment the observer had to detect a square, which having two pairs of parallel sides and four corners should be easier than the triangle to perceive. The results do indeed show a reduction (compared to the triangle) in measured CDT.

The experiments again show a difficulty in accurately measuring the CDT, with that of observer C being significantly above chance. The trials involving observer A with a 1 degree square show some improvement in detection while for the 1.5 degree square the improvement was less substantial and almost linear with added noise. Again, these results give an indication of an SR effect, but do not provide definitive proof.

4.3.5 Displaced Square Discrimination Experiment

For this discrimination task an observer was asked if a square shape was presented on the left or right hand side of the screen. 75 pairs were used to determine the CDT and 40 pairs were presented for each noise level in the graphs below.

Observer A

The results in graph 4.29 for the 2 degree and 3 degree displacement were obtained on the same day over a five hour period, while those for 1 degree displacement were obtained the following day.

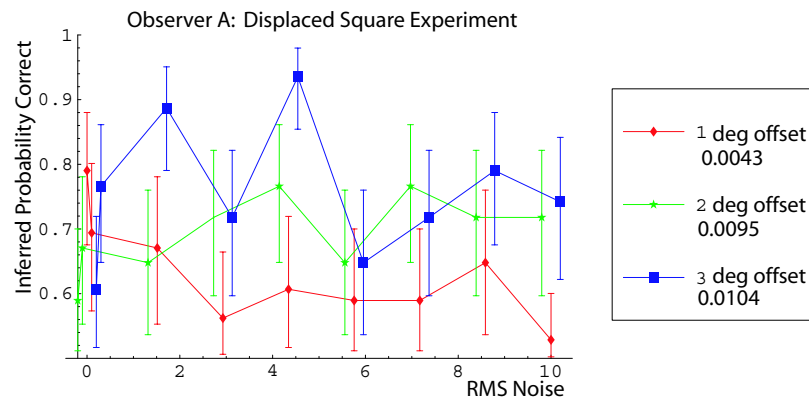


Figure 4.29: Observer A's results for the Displaced Square Discrimination Experiment with a one degree square and different displacements/ offsets

Observer B

The results in graph 4.30 were obtained for observer B, on a single day over a three hour period.

Comment

This was another discrimination task with a geometric object (a square), where this time the task was to determine the location of the object. The measured CDT's were again high and the stimulus appears to be presented above threshold in all trials.

Both observers show an increase in discrimination for one offset (3 degrees for observer A and 1 degree for B), with the other results remaining fairly flat or showing a decrease in discriminability.

4.3.6 Square Wave Discrimination Experiment

In this experiment an observer had to discriminate between a sine wave and a square wave. They did this by indicating whether they believed the stimuli presented in two intervals were the same or different. Four possible combinations of stimuli were given: two sine waves, two square waves, a sine wave then a square wave or a square wave then a sine wave. In the CDT experiment 76 presentations were made. For the SR experiment 40 presentations were made for each of 7 noise levels, with an equal number of each stimuli combination for each noise.

Observers A and B

All results were gathered on one day over a period of less than one hour for each observer.

Comment

In this experiment, the observer was supposed to detect higher frequency components of the square wave to enable discrimination of the signals. However, the task proved very difficult with observers becoming tired very quickly and CDT's were elevated from the grating experiment.

In three of the experiments (A - 1 c/deg and both of B's results) the stimulus appears to be presented above the actual CDT and there is no increase in discriminability with noise. In observer A's 3 c/deg experiment the stimulus seems below threshold and there is increased discriminability, although less than 70% of the stimuli are correctly discriminated and only one noise value gives rise to this increase. This experiment illustrates the limitations of the SR effect in the visual system.

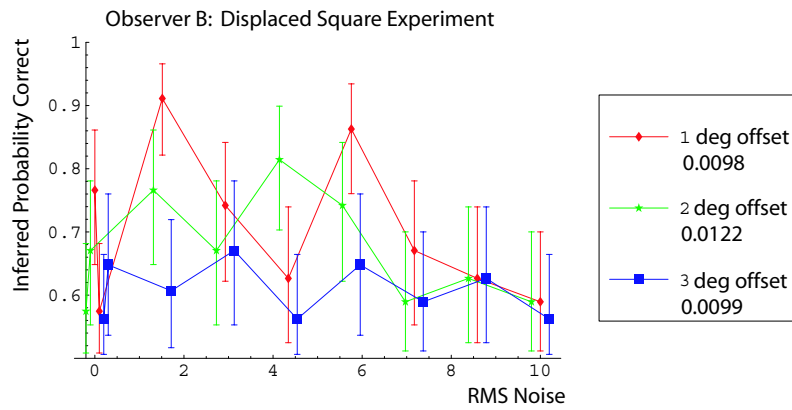


Figure 4.30: Observer B's results for the Displaced Square Discrimination Experiment with a one degree square and different displacements/ offsets

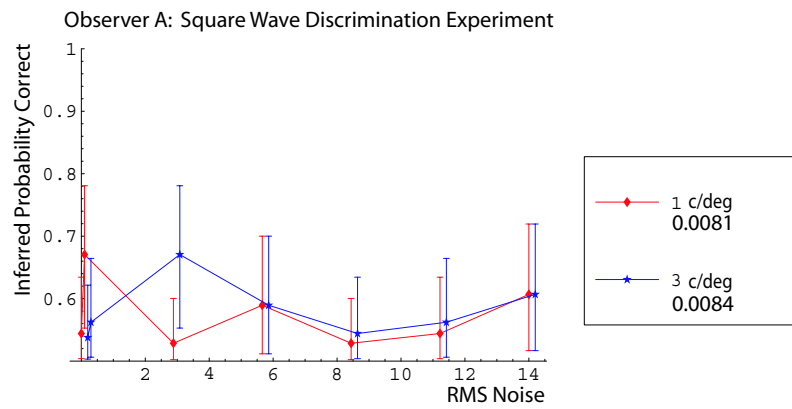


Figure 4.31: Observer A's results for the square wave discrimination experiment

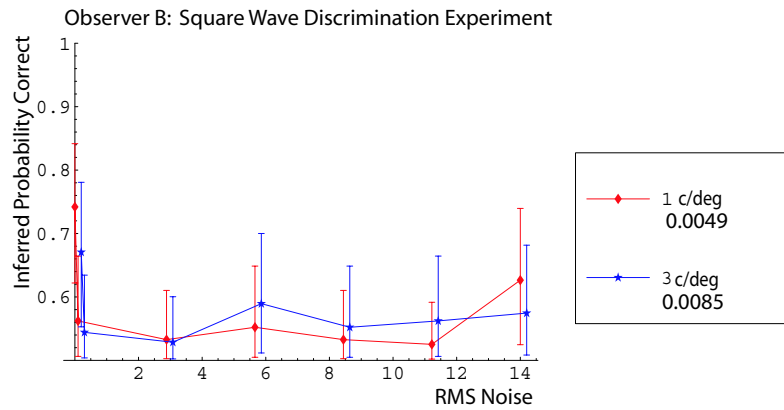


Figure 4.32: Observer B's results for the square wave discrimination experiment

4.3.7 Grating with Time Varying Noise Experiment

This is a repeat of the grating experiment described in section 4.3.1, here a grating was presented within a Gaussian envelope in one of two temporal intervals. The observer had to determine which interval contained the signal. The noise used in this experiment flickered in time. 75 pairs were used to determine the CDT and 50 pairs were presented for each noise level in the graphs below.

Observer A

The results for 1 c/deg, 3 c/deg and 5 c/deg were obtained on the same day over a six hour period, while those for 4 c/deg were obtained three days later.

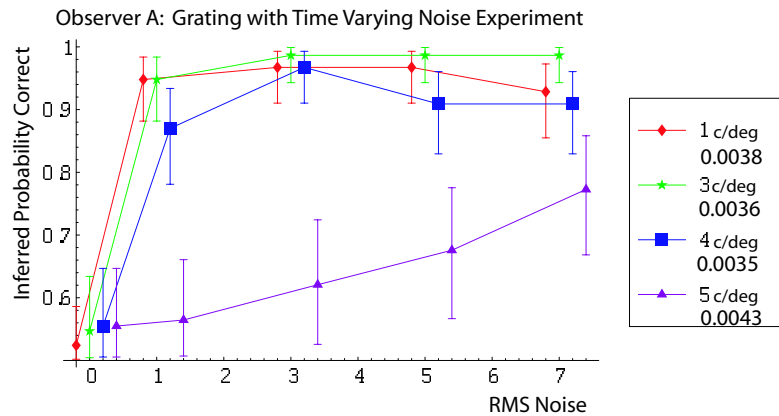


Figure 4.33: Observer A's results for the grating with time varying noise experiment, for spatial frequencies 1 c/deg, 3 c/deg, 4 c/deg and 5 c/deg

Observer B

Observer B's results are shown in graph 4.34.

Comment

In this repeat of the grating experiment, time varying noise was added to the stimulus. The addition of moving noise does not seem to have had an effect on CDT measurements which remained similar to those measured in static noise experiments.

The addition of noise has had a significant effect on the detectability of grating signals for both observers and all frequencies (with the exception of the 5 c/deg result

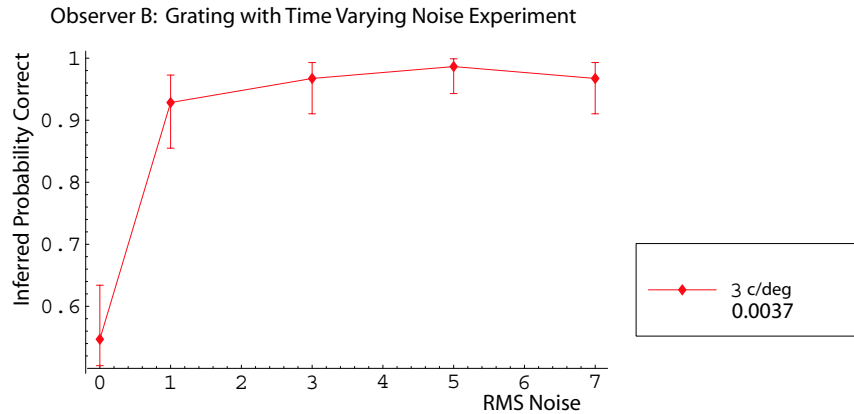


Figure 4.34: Observer B’s results for the grating with time varying noise experiment, for a spatial frequency of 3 c/deg

for observer A, which appears anomalous). The 5 c/deg experiment took place at the end of a day where two other time varying noise experiments were carried out. The lack of effect and anomalous shape of the curve could be due to observer fatigue. It is also possible that the actual CDT was higher than measured, so only higher noise variances increased detectability.

Overall, this experiment confirms an SR effect in grating detectability.

4.3.8 Triangle with Time Varying Noise Experiment

This is a repeat of the oriented triangle experiment described above, here a 1 or 0.5 deg triangle was presented that pointed either to the left or right side of the screen. The observer had to say which way the triangle pointed. The noise used in this experiment flickered in time. 75 stimuli were used to determine the CDT and 50 stimuli were presented for the experiment in graph 4.35 and 20 stimuli were used for graph 4.36, for each noise level.

Observer A

Observer A’s results were collected on two days spanning a twenty two day period.

Observer B

Observer B’s results are shown in graph 4.35

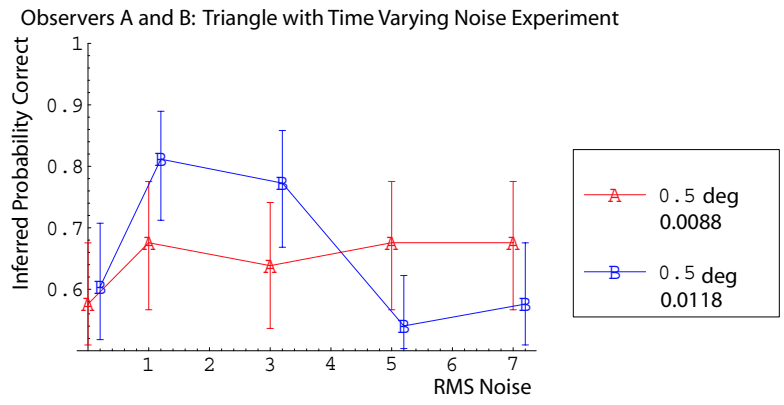


Figure 4.35: Results for observers A and B in the triangle experiment with time varying noise, with a 0.5 degree triangle.

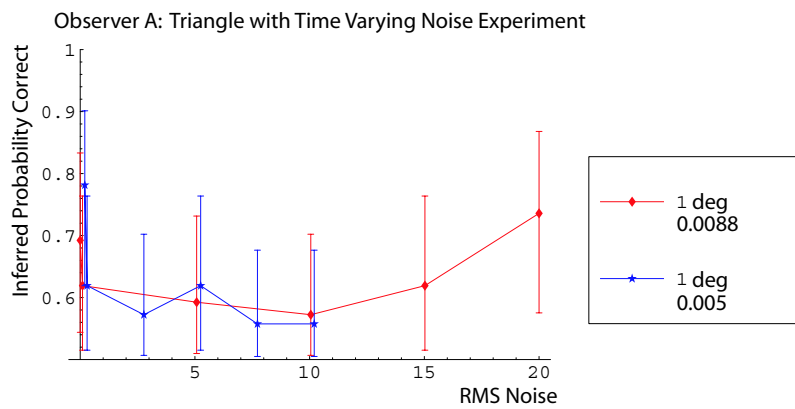


Figure 4.36: Observer A's results for the triangle experiment with time varying noise, with a 1 degree triangle.

Comment

The thresholds measured for the 0.5 degree triangle were similar to those measured in the static noise experiment, although CDT measurements for the 1 degree triangles were reduced. This experiment also suffered from the same difficulty in correctly determining the CDT's as the static noise experiment (an identical procedure was used in both experiments). In an attempt to rule out lengthy experiments with supra-threshold signals, observer A carried out no noise trials using a small number of stimuli before undertaking the full experiment.

The results of the experiment show no discernable SR effect for observer A. Observer B does show an effect with a 20% increase in the number of correct answers which was similar to the static noise case, although here the number of correct answers was closer to chance at zero noise. It is also worth noting that the results in 4.3.3 were selected from quite a large sample while observer B only undertook this experiment once (due to time constraints and the difficulty of the experiment).

4.4 Discussion

These experiments show that while SR does occur in the retina it is a fragile phenomenon. The phenomenon itself seems tied to tasks involving gratings that are of a fairly primitive nature (that is tasks processed in the retina, like grating detection and angled grating discrimination). For more complicated targets (like the geometric shapes tested here) SR seems absent, or the addition of noise had only a small effect, even when the task was low level (retinal based), identifying the position or the presence of an object for example (see the tasks involving the square shape in sections 4.3.4 and 4.3.5).

One thing crucial to the success of the experiments was accurate measurement of the CDT. For grating experiments CDT's were low (relative to other experiments) and remained fairly stable. For more difficult tasks, where CDT's were elevated, they were much less stable. This is illustrated in figure 4.37 where the CDT has been measured over time for the two types of task. As well as indicating the wide range of measured CDT's possible within a short space of time, this graph shows that over the course of an experimental SR run the signal may lie significantly above or

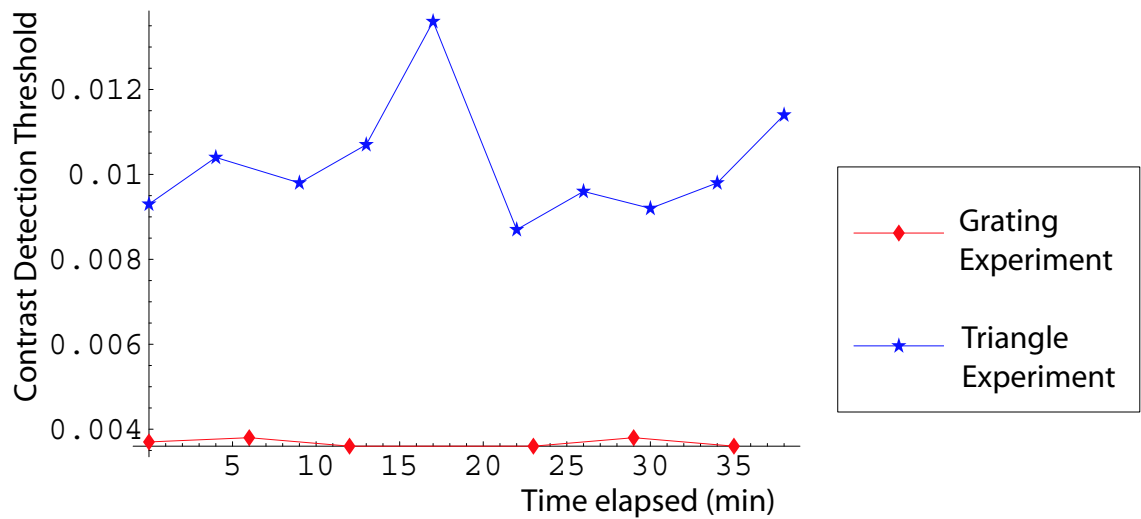


Figure 4.37: CDT against time for the grating and triangle experiments on observer A

below threshold for some of the presentations, this could be a possible cause of the *saw-toothed* appearance of some of the graphs.

During the course of carrying out these experiments it became apparent that some of the tasks were far more tiring than others. The degree of fatigue appeared to be linked to the difficulty of the task (in terms of how hard it was to correctly identify the signal) and to a lesser extent on the duration of the experiment. This effect could have given rise to the variability of CDT.

Perhaps an anomalous result was obtained for the square wave discrimination experiment (see section 4.3.6) task. This experiment proved very difficult, with observers reporting having “no idea” what signals were presented. Only a limited number of experimental runs were carried out and perhaps the results would have been more consistent with other experiments if participants had been given more practice at identifying the different signals.

Chapter 5

Conclusions

In this project I began by exploring the historical development of SR from a theory to explain the periodic occurrence of ice ages to more recent applications in biological sensory systems. The structure of the retina was described and mathematics was used to explore why this structure might lead to SR.

The most extensive and time consuming aspect of this work was concerned with the experimental demonstration and exploration of the phenomenon (see chapter 4). This study showed significant increments in the detectability of grating patterns with added noise (see 4.3.1) while also indicating the limitations of the phenomenon to low level processes. In particular, experiments involving simple geometric shapes (see 4.3.4) showed little if any increment in detectability. When the task was changed to a discrimination problem results continued to show little improvement (in discriminability) with the addition of noise, only for the simpler grating task (see 4.3.2) did increased discriminability occur. When the noise was made to move (see 4.3.8) some improvement was seen, if only for one observer, despite the prolonged nature of this experiment.

Overall, the experiments demonstrate the existence of the SR effect in the human visual system, although they also indicate its limitation to low level visual processing. This limits the scope for practical applications. For example, adding noise to night vision aids would be unlikely to improve performance and as to the development of prosthetic aids, I feel that SR would be of no assistance.

As part of this project I hoped to produce some modeling results. Several different models were explored before the Watson model [58, 56, 57] was discovered towards

the end of the project. We have developed a simplified version of their model which reproduces the main processes occurring in the retina. These are sketched out in figure 5.1. A slightly more detailed description of each of these stages is given in appendix E.

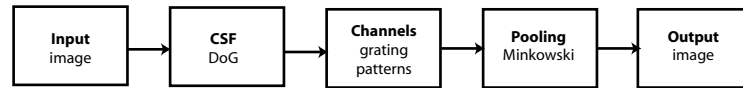


Figure 5.1: Stages of the retina model

The work in this project is still ongoing and in the future I hope to produce some results tying the modeling work to the experimental results.

Appendix A

The Variance of the Power Spectrum

In this appendix we obtain an expression for the variance of an entry P_k in the power spectrum of the signal discussed in the later sections of chapter 3. We already have an expression for $\langle P_k \rangle$ and so need only an expression for:

$$\begin{aligned}\langle P_k^2 \rangle &= \langle (a_k^2 + b_k^2)^2 \rangle \\ &= \langle (a_k^4 + 2a_k^2 b_k^2 + b_k^4) \rangle \\ &= \langle a_k^4 \rangle + 2\langle a_k^2 b_k^2 \rangle + \langle b_k^4 \rangle\end{aligned}$$

The quartic terms are, from a computational point of view, identical, but the cross term requires separate consideration. The strategy for constructing these formulae is much the same as that used in formula (3.20) for $\langle a_k^2 \rangle$: here we'll start with $(\mathbf{p} \cdot \mathbf{u}_k)^4$ and then add and subtract certain sums to eliminate unwanted terms and replace them with correct ones.

A.1 Constructing formulae

The quantities we want are all powers of dot products of some vector with the entries of a random Boolean vector. The goal is to obtain formulas for the expectation that consist of sums of terms that, individually, look like dot products: this permits us to compute the desired expectation in $O(N)$ time, where N is the dimension of the vector.

To simplify the notation, we will refer to the vector as \mathbf{a} and indicate its components by a_j . Also, when writing sums we will suppress the limits on the index. The components of the Boolean vector will be x_j and p_j will indicate the probability that $x_j = 1$. Then one of the things we want to compute is $\langle (\mathbf{a} \cdot \mathbf{x})^4 \rangle$ or

$$\begin{aligned} \left\langle \left(\sum_j a_j x_j \right)^4 \right\rangle &= \sum_j a_j^4 \langle x_j^4 \rangle + 4 \sum_{j \neq k} a_j^3 a_k \langle x_j^3 x_k \rangle + 6 \sum_{j < k} a_j^2 a_k^2 \langle x_j^2 x_k^2 \rangle \\ &+ 12 \sum_{j < k \neq l} a_j a_k a_l^2 \langle x_j x_k x_l^2 \rangle + 24 \sum_{j < k < l < m} a_j a_k a_l a_m \langle x_j x_k x_l x_m \rangle \end{aligned} \quad (\text{A.1})$$

Then, using the facts that the x_j are independent and that $\langle x_j^r \rangle = p_j \forall r \neq 0$, we find:

$$\begin{aligned} \langle (\mathbf{a} \cdot \mathbf{x})^4 \rangle &= \sum_j a_j^4 p_j + 4 \sum_{j \neq k} a_j^3 a_k p_j p_k + 6 \sum_{j < k} a_j^2 a_k^2 p_j p_k \\ &+ 12 \sum_{j < k \neq l} a_j a_k a_l^2 p_j p_k p_l + 24 \sum_{j < k < l < m} a_j a_k a_l a_m p_j p_k p_l p_m \end{aligned}$$

We would like to compute this using sums of a special form, for which it's handy to define a concise notation:

$$a^m p^n \equiv \sum_j a_j^m p_j^n$$

Our starting point is clearly $(\mathbf{a} \cdot \mathbf{p})^4$, but comparison with (A.1) shows that this will include many terms with many unwanted powers of the p_j . For example, we need to replace terms of the form $a_j^4 p_j^4$ with ones of the form $a_j^4 p_j$. This is a fairly easy matter, involving adding a correction of the form

$$-a^4 p^4 + a^4 p = - \sum_j a_j^4 p_j^4 + \sum_j a_j^4 p_j$$

A more typical correction is the one required to replace terms of the form $a_j^3 a_k p_j^3 p_k$ (where $j \neq k$) with ones of the form $a_j^3 a_k p_j p_k$. The product $(a^3 p^3)(a^1 p^1)$ generates many of the terms we want to remove, but it also produces a new, unwanted, contribution $a^4 p^4$. Similarly, $(a^3 p^1)(a^1 p^1)$ generates most of the desired replacement terms, but also produces a spurious contribution of $a^4 p^2$. Thus the complete correction for terms of the form $a_j^3 a_k p_j^3 p_k$ is

$$\sum_{j \neq k} a_j^3 a_k p_j p_k - \sum_{j \neq k} a_j^3 a_k p_j^3 p_k = \{(a^3 p^1)(a^1 p^1) - a^4 p^2\} - \{(a^3 p^3)(a^1 p^1) + a^4 p^4\}$$

Expected fourth powers of dot products

Similar tedious, but essentially straightforward considerations allow one to formulate corrections for all the offending terms. Simplifying the result yields:

$$\begin{aligned}
\langle (\mathbf{a} \cdot \mathbf{x})^4 \rangle &= (a^1 p^1)^4 + (a^2 p^2)^2 - 7(a^4 p^2) + 12(a^4 p^3) - 6(a^4 p^4) - 12(a^3 p^2)(a^1 p^1) \\
&+ 8(a^3 p^3)(a^1 p^1) + 6(a^1 p^1)^2(a^2 p^1) + 3(a^2 p^1)(a^2 p^1) \\
&- 6(a^2 p^2)[(a^1 p^1)^2 + a^2 p^1] + 4(a^1 p^1)(a^3 p^1) + a^4 p^1
\end{aligned} \tag{A.2}$$

Expected products of pairs of squared dot products

In much the same way, one can also obtain an expression for the expectation of the cross term. Generalising the notation in a natural way:

$$\begin{aligned}
\langle (\mathbf{a} \cdot \mathbf{x})^2 (\mathbf{b} \cdot \mathbf{x})^2 \rangle &= ((p^1 a^1)^2 - p^2 a^2 + p^1 a^2)((p^1 b^1)^2 - p^2 b^2 + p^1 b^2) \\
&- 7(p^2 a^2 b^2) + 2(p^2 a^1 b^1)^2 + 12(p^3 a^2 b^2) - 6(p^4 a^2 b^2) \\
&- 6(p^2 a b^2)(p^1 a^1) + 4(p^3 a^1 b^2)(p^1 a^1) + p^1 a^2 b^2 - 4(p^2 a^1 b^1)(p^1 a^1 b^1) \\
&+ 2(p^1 a^1 b^1)^2 + 2(p^1 a)(p^1 a^1 b^2) - 6(p^2 a^2 b)(p^1 b^1) + 4(p^3 a^2 b^1)(p^1 b^1) \\
&- 4(p^2 a^1 b^1)(p^1 a^1)(p^1 b^1) + 2(p^1 a^2 b^1)(p^1 b^1) + 4(p^1 a^1)(p^1 a^1 b^1)(p^1 b^1)
\end{aligned} \tag{A.3}$$

A.2 Verifying the results

Although the original assembly of correction terms was done by hand, using reasoning of the sort sketched in the previous section, we also tested these expressions with automatic symbolic computations in *Mathematica*. First, one needs to be able to generate vectors of distinct symbols. The following fragment does this job.

```
vectorOfSymbols[n_, baseStr_] :=
  Table[Symbol[baseStr <> ToString[j]], {j, 1, n}] ;
```

A typical application is

```
In[454] := vectorOfSymbols[3, "a"]
Out[454] := {a1, a2, a3}
```

We then wrote a function to generate the desired expressions by direct means, computing, for example $(\mathbf{a} \cdot \mathbf{p})^4$ for symbolic vectors and replacing powers of p_j^k with p_j in the result. The function that does this is defined by

```
targetExpression[a_, p_] := Module[
  {k, targetExpr},

  targetExpr = Expand[(a.p)^4] ;
  For[k = 1, k < Length[p], ++k,
    targetExpr = targetExpr /. p[[k]]^2 -> p[[k]] ;
    targetExpr = targetExpr /. p[[k]]^3 -> p[[k]] ;
    targetExpr = targetExpr /. p[[k]]^4 -> p[[k]] ;
  ] ;

  Return[targetExpr] ;
] ;
```

Finally, we tested the main function, which is called `expectedFourthPowerOfDotProduct` and is based on (A.2), with the following sequence:

```
In[500] := a = vectorOfSymbols[4, "a"] ;
In[501] := p = vectorOfSymbols[4, "p"] ;
In[502] := Simplify[
  targetExpression[a, p] -
  expectedFourthPowerOfDotProduct[a, p]
]
```

and got the result

```
Out[502] := 0
```

establishing that `expectedFourthPowerOfDotProduct` worked correctly. Although it is sufficient to do this test for vectors of four symbols—four is large enough that representatives of every possible pattern of term are generated—we also did tests for vectors of 6 and 8 symbols. The companion function `expectedProductofSquaresOfDotProducts` was tested in a similar way.

Appendix B

Implementation of Bayesian Adaptive Method

This appendix gives an overview of how the Bayesian adaptive method was implemented to determine CDT in the experiments reported as part of this thesis. The method is the one used by Kontsevich and Tyler [22]

The psychometric function is given by

$$\Psi_\lambda(x) = (1 - \delta) - (0.5 - \delta) e^{-\left(\frac{x}{\alpha}\right)^\beta} \quad (\text{B.1})$$

where $\lambda = (\alpha, \beta)$ gives the assumed threshold (α) and slope (β) of the psychometric function, x is the contrast of the stimulus presented and 2δ is the *probability of lapse* used to account for an observer answering incorrectly even though he perceives the stimulus correctly. This function tends to 0.5 (50% correct) for low contrasts and $(1 - \delta)$ for high contrasts.

For the CDT experiments α , β and δ were varied uniformly across the ranges

$$\begin{array}{llll} \log(0.001) & \leq \log(\alpha) & \leq \log(1) & 61 \text{ points} \\ 0.5 & \leq \beta & \leq 4.0 & 31 \text{ points} \\ 0.1 & \leq \delta & \leq 0.03 & 5 \text{ points} \end{array} \quad (\text{B.2})$$

These parameters are used to calculate a look-up table of conditional probabilities $p(\text{result}|\lambda, x)$ where

$$\begin{aligned} p(\text{correct}|\lambda, x) &= \Psi_\lambda(x) \\ p(\text{incorrect}|\lambda, x) &= 1 - \Psi_\lambda(x) \end{aligned} \quad (\text{B.3})$$

A prior probability distribution $P_0(\lambda)$ is set to an initial value. The Bayesian adaptive method then utilises the following steps

- 1.) For each test contrast x , calculate the probability of getting response r

$$p_t(r|x) = \sum_{\lambda} p(r|\lambda, x) p_t(\lambda)$$

- 2.) Use Bayes rule to estimate the posterior probability of each psychometric function

$$p_t(\lambda|x, r) = \frac{p_t(\lambda) p(r|\lambda, x)}{p_t(r|x)}$$

- 3.) Estimate the entropy of the pdf over the space of psychometric functions

$$H_t(x, r) = - \sum_{\lambda} p_t(\lambda|x, r) \log(p_t(\lambda|x, r))$$

- 4.) Estimate the expected entropy for each test contrast x

$$E[H_t(x)] = H_t(x, \text{correct}) p_t(\text{correct}|x) + H_t(x, \text{incorrect}) p_t(\text{incorrect}|x)$$

- 5.) Find the contrast x that has the minimum expected entropy $E[H_t(x)]$

- 6.) Run trial with contrast x_{t+1} to get response r_{t+1}

- 7.) Let the posterior probability (step2) that corresponds to the completed trial become the new prior over the hypothesis

$$P_{t+1}(\lambda) = P_t(\lambda|x_{t+1}, r_{t+1})$$

- 8.) Find a new estimate for the psychometric function based on $P_{t+1}(\lambda)$ i.e.

$$\lambda_{t+1} = \sum_{\lambda} \lambda P_{t+1}(\lambda)$$

- 9.) Repeat from step one until the specified number of trials has been carried out.

Appendix C

Creating Normally Distributed Noise From Uniformly distributed Noise

This explanation is based on the one given in section 7.2 of [41]. We have uniformly distributed x 's and wish to generate normally distributed y 's. Usually this is done by selecting an x

$$x = F(y) = \int_0^y p(y) dy \quad (\text{C.1})$$

and inverting to find y (i.e. $y = F^{-1}(x)$), see figure C.1.

The pdf for the normal distribution is

$$p(y) = e^{-\frac{y^2}{2}} \quad (\text{C.2})$$

which is not integrable, however, the product

$$p(y_1) p(y_2) = e^{-\frac{(y_1^2 + y_2^2)}{2}} \quad (\text{C.3})$$

is integrable by a change to polar coordinates r, θ such that

$$y_1 = r \cos \theta \quad (\text{C.4})$$

$$y_2 = r \sin \theta$$

The cumulative density function (CDF) is then given by

$$\begin{aligned} F(x_1 x_2) &= \int_0^{2\pi} \int_0^{\frac{r}{\sigma}} u e^{-\frac{u^2}{2}} du d\theta \\ &= 2\pi \left[-e^{-\frac{u^2}{2}} \right]_0^{\frac{r}{\sigma}} \\ &= 2\pi \left(1 - e^{-\frac{r^2}{2\sigma^2}} \right) \end{aligned} \quad (\text{C.5})$$

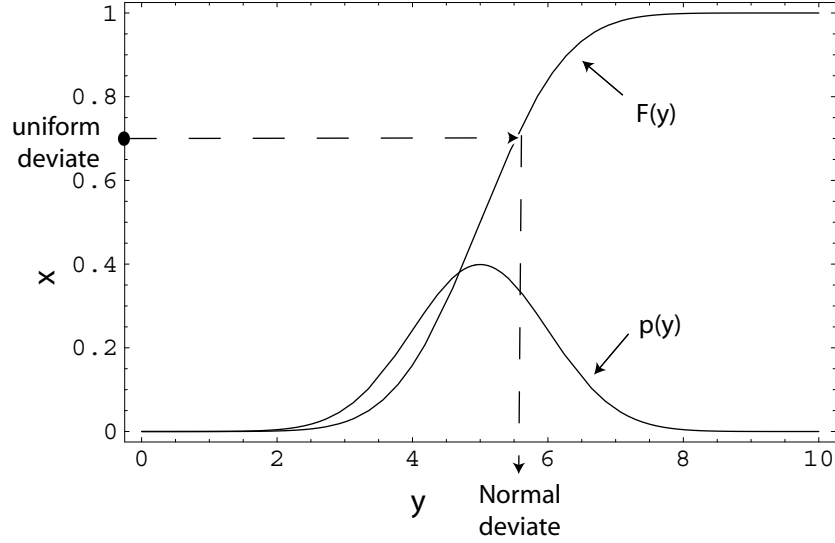


Figure C.1: Illustration of the transform method for generating normal deviate from a uniform deviate. A uniform deviate x is chosen between 0 and 1, the corresponding y on the definite integral curve is the normal deviate. Based on diagram 7.2.1 of [41].

So generate random variables $(x_1, x_2) \in (0, 1) \times (0, 1)$ and think of x_1 as a random angle

$$x_1 \rightarrow 2\pi x_1 \equiv \theta \quad (\text{C.6})$$

and x_2 as a value of the CDF for r

$$\begin{aligned} x_2 &= \left(1 - e^{-\frac{r^2}{2\sigma^2}}\right) \\ 1 - x_2 &= e^{-\frac{r^2}{2\sigma^2}} \\ \ln(1 - x_2) &= -\frac{r^2}{2\sigma^2} \\ r^2 &= -2\sigma^2 \ln(1 - x_2) \\ r &= \sigma \sqrt{-2 \ln(1 - x_2)} \end{aligned}$$

but $(1 - x_2)$ is also uniform in $(0, 1)$, so

$$r = \sigma \sqrt{-2 \ln x_2} \quad (\text{C.7})$$

we have

$$\begin{aligned} y_1 &= r \cos \theta = \sigma \sqrt{-2 \ln x_2} \cos(2\pi x_1) \\ y_2 &= r \sin \theta = \sigma \sqrt{-2 \ln x_2} \sin(2\pi x_1) \end{aligned} \quad (\text{C.8})$$

where the y 's are normally distributed and the x 's are uniformly distributed.

Appendix D

Bayesian Estimation of Frequencies

In this section *Bayes theorem* is used to calculate the probability of achieving k correct answers in a 2AFC experiment with N trials¹. The probability of a correct answer, p is assumed to be greater than $\frac{1}{2}$, since an observer has a 50% chance of being correct if she guessed.

Let:

p be the probability of a correct answer

k be the total number of correct answers

N be the number of trials

D represent the data, k correct for N trials

H represent the hypotheses, or assumptions about p

Then Bayes theorem states that

$$P(H|D) = \frac{P(D|H) P(H)}{P(D)} \quad (\text{D.1})$$

The parts of equation D.1 have standard names:

$P(H|D)$ is the *posterior distribution* over the parameters

$P(H)$ is the *prior distribution* over the hypotheses

$P(D)$ is the *prior* over the data

Consider two cases:

¹Note that in this analysis, the only variable is whether the signal is present, or not. Each noise level is treated as a separate experiment

D.1 Case I - Make no assumptions about p

As each experiment can be thought of as a *Bernoulli process*, we have

$$P(D|H) = p^k (1-p)^{N-k} \binom{N}{k} = p^k (1-p)^{N-k} \frac{N!}{k!(N-k)!} \quad (\text{D.2})$$

The probability of a correct answer, p , can take any value in the range $0 \leq p \leq 1$, no value being more likely than another. To preserve area one under the curve of the prior over the hypotheses (see figure D.1), set

$$P(H) = 1 \quad (\text{D.3})$$

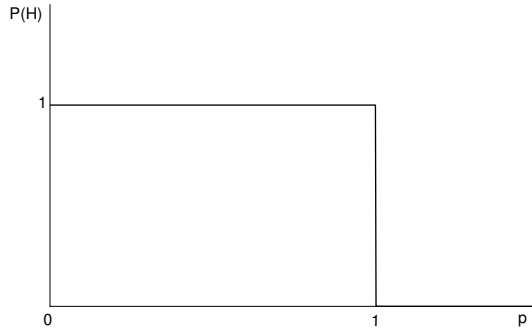


Figure D.1: The prior distribution over the hypotheses

Now²,

$$P(D) = \int_{\text{all hypotheses } H} P(D|H) \rho(H) dH = \frac{1}{N+1} \quad (\text{D.4})$$

where $\rho(H)$ is the pdf of H . Using Bayes theorem D.1, we have

$$P(H|D) = p^k (1-p)^{n-k} \frac{(N+1)!}{k!(N-k)!} \quad (\text{D.5})$$

A plot of the posterior distribution for $k = 13$, $N = 20$, is given below.

Now consider the more interesting 2AFC case when

D.2 Case II - p lies in the range $\frac{1}{2} \leq p \leq 1$

In the psychophysics experiments of this project, an observer is always presented a signal and is asked some question about it, for which there are two possible answers.

² k can take values from $0 - N$ all of which are equally likely, so $1 = (N+1)P(D)$

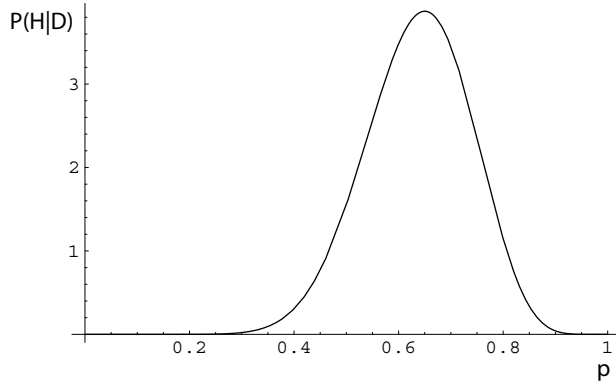


Figure D.2: The posterior distribution.

When the observer can not see the signal she is forced to guess. The probability of a correct answer, p , when guessing, is $\frac{1}{2}$. On the other hand, when the observer is able to use some of the information contained in the signal $\frac{1}{2} < p \leq 1$.

Now, the prior over the hypothesis becomes

$$P(H) = 2 \tag{D.6}$$

to preserve area 1 under the curve of $P(H)$. Since the experiments still constitute a

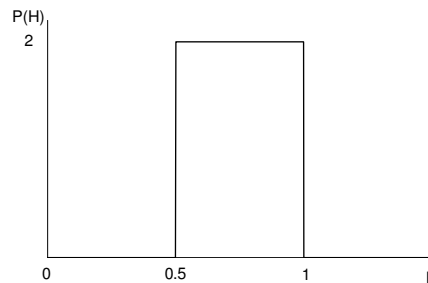


Figure D.3: The prior distribution over the hypotheses, with the restricted range of probabilities $\frac{1}{2} \leq p \leq 1$

Bernoulli process, equation D.2 remains unchanged. This gives rise to

$$P(D) = \int_{\frac{1}{2}}^1 2p^k (1-p)^{N-k} \frac{(N)!}{k!(N-k)!} dp \tag{D.7}$$

so

$$P(H|D) = \frac{p^k (1-p)^{n-k}}{\int_{\frac{1}{2}}^1 p^k (1-p)^{N-k} dp} \tag{D.8}$$

which can be calculated numerically using Mathematica [42]. Below (figure D.4) is a plot of the posterior distribution for the case $k=13$, $N=20$, with the restricted range of probabilities $\frac{1}{2} \leq p \leq 1$

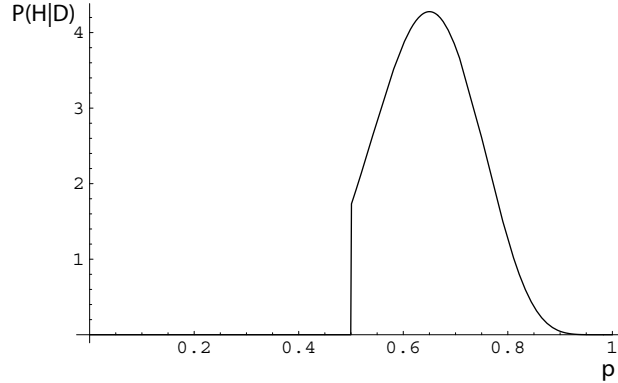


Figure D.4: The posterior distribution with the restricted range of probabilities $\frac{1}{2} \leq p \leq 1$

It is possible to calculate the integral D.8 using *Mathematica*, although the integrand becomes singular when N and k are large. In practice the calculation is not feasible for $N > 50$. Instead the (built in) *Beta* and *incomplete Beta* functions

$$B(m, n) = \int_0^1 u^{m-1} (1-u)^{n-1} du \quad B(p; m, n) = \int_0^p u^{m-1} (1-u)^{n-1} du$$

can be used by re-writing D.8 in terms of them.

D.3 Error Bar Construction

The next task is to find the 90% confidence interval and construct error bars for the SR results. To do this, the values of p for which the area under the graph of the posterior probability (for a particular number, k correct) equals 0.05 (5% point) and 0.95 (95% point) are found. These form the range of the error bars. The point plotted as the *inferred probability correct* is then the value of p for which the area under the posterior probability curve equals 0.5 (50%) point. This will not correspond to the mid-point of the error bar as the curve is not symmetric (see figure D.4).

Appendix E

Watson's Model of Early Vision

E.1 The Model

This model is based on those developed by Watson *et al.* [58, 56, 57] that were evaluated using the *Model Fest* data set. These models closely resemble the early visual system and have been developed over several years. The different stages of the model are shown in figure E.1 and described below in greater detail.

E.1.1 Input

The input to the model is a small ($2^\circ \times 2^\circ$)¹ grayscale image which could be either a high frequency grating pattern, or a simple shape.

E.1.2 Contrast sensitivity Filter

A *difference of Gaussians* (DoG) mask is then applied to the input image. The DoG is chosen because its shape best replicates the centre-surround nature found in certain cells in the retina[25]. Watson [57], who tested several forms of contrast sensitivity function (CSF) , suggests it is not the most representative for the visual system as a whole, instead recommending use of a log-sensitivity interpolation mask. As here the aim is to model the retina as closely as possible, so we use the DoG.

¹where $^\circ$ means degrees of visual angle

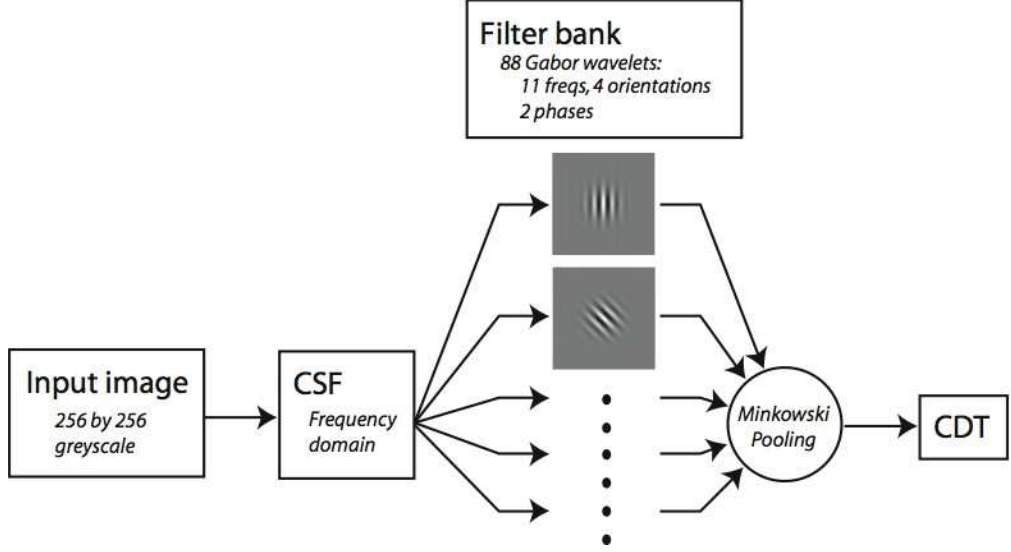


Figure E.1: Watson’s model for early vision: the input is a greyscale image with unit contrast. The contrast sensitivity function (CSF) is implemented as an orientation-independent filter in the spatial frequency domain and the result of this stage is fed through a bank of 88 filters whose impulse responses are Gabor wavelets. The 88 filtered results are then pooled and the L^β norm of their summed results is used to estimate a contrast detection threshold (CDT).

The DoG is given by

$$S_{DoG}(f; f_0, f_1, a) = \exp\left[-\frac{f^2}{f_0^2}\right] - a \exp\left[-\frac{f^2}{f_1^2}\right] \quad (\text{E.1})$$

where, the parameters f_0, f_1 define the widths of two gaussians and a defines the degree of overlap. These parameters are found by fitting a DoG curve to a measured CSF, where each point of the measured CSF is found using the same procedure as was used for measuring the contrast threshold in the grating experiment (see section 4.2.2).

E.1.3 Channels

The filter bank in figure E.1 consists of 8 filters at each of 11 spatial frequencies. The frequencies are spaced uniformly in log from a maximum of 30 cpd down to a minimum of $(30 / 32)$ cpd. At each fixed frequency there are two basic forms of filter

$$F_{j,k,1}(x, y) = \lambda_j \cos(2\pi f_j(x \cos \theta_k + y \sin \theta_k)) e^{-(x^2+y^2)/\sigma_j^2}$$

$$F_{j,k,2}(x, y) = \lambda_j \sin(2\pi f_j(x \cos \theta_k + y \sin \theta_k)) e^{-(x^2+y^2)/\sigma_j^2}$$

Here λ_j is a frequency-dependent normalization constant that will be discussed further below while the θ_k determine the orientation of the grating and are one of $0, \pi/4, \pi/2$ or $3\pi/4$. The parameter σ_j is related to the frequency by

$$\sigma_j = \frac{2^{b-1}}{\sqrt{2}f_k}$$

and the *bandwidth* parameter $b = 1.4$. Choosing the parameter for the Gaussian envelope in this frequency-dependent way means that the Gabor wavelets look like scaled versions of each other, independent of frequency.

E.1.4 Pooling

The outputs of the filter bank are combined via an L^β norm to produce an estimated threshold for the input image: Watson refers to this step as “Minkowski pooling” If we say that the output of the channel defined by $F_{j,k,l}$ has pixel values $r_{j,k,l,x,y}$, where x and y range over the width and height of the image, respectively, then the estimated threshold is

$$\Theta = \left(\sum_{j=1}^{11} \sum_{k=1}^4 \sum_{l=1}^2 \sum_{x,y} \Delta x \Delta y |r_{j,k,l,x,y}|^\beta \right)^{-1/\beta} \quad (\text{E.2})$$

where Δx and Δy are the dimensions of a pixel.

Frequency-dependent normalization

The normalization constant λ_j is chosen in such a way as to yield a net response—in the sense of the multiple sum over responses in (E.2)—of 1.0 when the 8 filters at a given frequency are applied to an image consisting of $F_{j,0,1}$ scaled to have unit contrast. The idea behind this normalization is to concentrate the frequency dependence of the model in the initial, CSF stage.

Bibliography

- [1] R. V. Abadi and J. J. Kulikowski. Linear summation of spacial harmonics in human vision. *Vision Research*, 13:1625–1628, 1973.
- [2] F. Apostolico, L. Gammaitoni, F. Marchesoni, and S. Santucci. Resonant trapping: a failure mechanism in switch transitions. *Physical Review E*, 55(1):36–39, 1997.
- [3] Robert Benzi, Giorgio Parisi, Alfonso Sutera, and Angelo Vulpiani. Stochastic resonance in climatic change. *Tellus*, 34:10–16, 1982.
- [4] Robert Benzi, Alfonso Sutera, and Angelo Vulpiani. The mechanism of stochastic resonance. *Journal of Physics A*, pages L453–L457, 1981.
- [5] Sergey M. Bezrukov and Igor Vodyanoy. Noise-induced enhancement of signal transduction across voltage dependent ion channels. *Nature*, 378:362–364, 1995.
- [6] Sergey M. Bezrukov and Igor Vodyanoy. Stochastic resonance in non-dynamical systems without response thresholds. *Nature*, 385:319–321, 1997.
- [7] Kim T Blackwell. The effect of white and filtered noise on contrast detection thresholds. *Vision research*, 38(2):267–280, 1998.
- [8] F. W. Campbell and J. G. Robson. Application of Fourier analysis to the visibility of gratings. *J. Physiol.*, 197:551–5664, 1968.
- [9] François Chapeau-Blondeau. Stochastic resonance in the Heaviside nonlinearity with white noise and arbitrary periodic signal. *Physical Review E*, 53(5):5469–5472, 1996.

- [10] John K. Douglass, Lon Wilkens, Eleni Pantazelou, and Frank Moss. Noise enhancement of information transfer in crayfish mechanoreceptors by stochastic resonance. *Nature*, 365:337–340, 1993.
- [11] John E Dowling. *The Retina: An Approachable Part of the Brain*. The Belknap Press of Harvard University Press, 1987.
- [12] S. Fauve and F. Heslot. Stochastic resonance in a bistable system. *Physics Letters*, 97A(1,2):5–7, 1983.
- [13] Gustav Fechner. *Elements of Psychophysics*, trans. by Helmut E Adler. Henry Holt Editions in Psychology, 1860 trans. 1966.
- [14] Luca Gammaitoni, Peter Hanggi, Peter Jung, and Fabio Marchesoni. Stochastic resonance. *Reviews of modern physics*, 70(1):223–287, 1998.
- [15] Ilse Christine Gebeshuber. The influence of stochastic behaviour on the human threshold of hearing. *Chaos, Solitons and Fractals*, 11:1855–1868, 2000.
- [16] Davig M. Green and John A. Swets. *Signal Detection Theory and Psychophysics*. John Wiley and Sons, 1966.
- [17] Mattias H. Henning, Nicolas J. Kerscher, Klaus Funke, and Florentin Wörgötter. Stochastic resonance in visual cortical neurons: does the eye-tremor actually improve visual acuity. *Neurocomputing*, 44-46:115–120, 2002.
- [18] Jenny Hogan. Eye can see better when it’s noisy. *New Scientist*, 2521:20–21, 2003.
- [19] Fernan Jaramillo and Kurt Wiesenfeld. Mechanoelectrical transduction assisted by Brownian motion: a role for noise in the auditory system. *Nature neuroscience*, 1(5):384–388, 1998.
- [20] Keiichi Kitajo, Daichi Nozaki, Lawrence M. Ward, and Yoshiharu Yamamoto. Behavioral stochastic resonance within the human brain. *Physical Review Letters*, 90(21):218103, 2003.
- [21] Helga Kolb, Eduardo Fernandez, and Ralph Nelson. Webvision, the organization of the retina and visual system. webvision.med.utah.edu, 2003.

- [22] Leonid L. Kontsevich and Christopher W. Tyler. Bayesian adaptive estimation of psychometric slope and threshold. *Vision Research*, 39:2729–2737, 1999.
- [23] Andre Longtin, Adi Bulsara, and Frank Moss. Time-interval sequences in bistable systems and the noise-induced transmission of information by sensory neurons. *Physical Review Letters*, 67(5):656–659, 1991.
- [24] Jitendra Malik. Recognizing people, objects and actions. Lecture 2 at www.cs.berkeley.edu/~malik, 2004.
- [25] David Marr. *Vision: A computational investigation into the human representation and processing of visual information*. W. H. Freeman and company, 1980.
- [26] Matsumoto and Nishimura. Mersenne twister. <http://www.math.sci.hiroshima-u.ac.jp/m-mat/MT/emt.html>.
- [27] Bruce McNamara and Kurt Wiesenfeld. Theory of stochastic resonance. *The American Physical Society*, 39:4854–4869, 1989.
- [28] Bruce McNamara, Kurt Wiesenfeld, and Rajarshi Roy. Observation of stochastic resonance in a ring laser. *Physical Review Letters*, 60(25):2626–2629, 1988.
- [29] Toshio Mori and Shoichi Kai. Noise-induced entrainment and stochastic resonance in human brain waves. *Physical Review Letters*, 88(21):218101, 2002.
- [30] Robert P. Morse and Edward F. Evans. Enhancement of vowel coding for cochlear implants by addition of noise. *Nature medicine*, 2(8):928–932, 1996.
- [31] Frank Moss, Faye Chiou Tan, and Rainer Klinke. Will there be noise in their ears? *Nature medicine*, 2(8):860–862, 1996.
- [32] Frank Moss, Lawrence M. Ward, and Walter G. Sannita. Stochastic resonance and sensory information processing: a tutorial and review of application. *Clinical Neurophysiology*, 115:267–281, 2004.
- [33] C. Nicolis. Stochastic aspects of climatic transitions - response to a periodic forcing. *Tellus*, 34:1–9, 1982.
- [34] C. Nicolis and G. Nicolis. Stochastic aspects of climatic transitions - additive fluctuations. *Tellus*, 33:225–234, 1981.

- [35] Jens R. Otterpohl. The role of stochastic resonance in visual pathways at low light levels. Thesis submitted for the degree of Diplom-Physiker, Bergische Univerität Wuppertal, Wuppertal, Germany, 1999.
- [36] Cristina Pallares. Noise-induced perceptual enhancement for (barely) subliminal signals. Thesis submitted for the degree of MSc., UMIST, Manchester, UK, 2001.
- [37] Denis Pelli. Videotoolbox. <http://vision.nyu.edu/videoToolBox>.
- [38] Denis G. Pelli. Uncertainty explains many aspects of visual contrast detection and discrimination. *J. Opt. Soc. Am A*, 2(9):1508–1532, 1985.
- [39] Denis G. Pelli. The videotoolbox software for visual psychophysics: Transforming numbers into movies. *Spatial Vision*, 10:437–442, 1997.
- [40] Donatella Petracchi. What is the role of stochastic resonance. *Chaos, solitons and fractals II*, pages 1827–1834, 2000.
- [41] William H. Press, Saul A. Teukolsky, William T. Vetterling, and Brian P. Flannery. *Numerical Recipes in C*, chapter 12. Camberage University Press, 1992.
- [42] Wolfram Research. Mathematica 4.2, 2002.
- [43] Jyrki Rovamo, Rauli Franssila, and Risto Nasanen. Contrast sensitivity as a function of spatial frequency, viewing distance and eccentricity with and without spatial noise. *Vision research*, 32(4):631–637, 1991.
- [44] Jyrki Rovamo, Helja Kukkonen, and Risto Nasanen. Effects of luminance and exposure time on contrast sensitivity in spatial noise. *Vision research*, 33(8):1123–1129, 1992.
- [45] David F. Russell, Lon A. Wilkens, and Frank Moss. Use of behavioural stochastic resonance by paddle fish for feeding. *Nature*, 402:291–294, 1999.
- [46] Steven H Schwartz. *Visual Perception, A Clinical Orientation*. McGraw-Hill, 1999.
- [47] R Sekuler and R Blake. *Perception*, chapter Appendix. McGraw-Hill, 1994.

- [48] Enrico Simonotto, Massimo Riani, Charles Seife, Mark roberts, Jennifer Twitty, and Frank Moss. Visual perception of stochastic resonance. *Physical Review Letters*, 78(6):1186–1189, 1997.
- [49] Richard S. Snell and —Michael A. Lemp. *Clinical Anatomy of the Eye*. Blackwell Science Inc., 1998.
- [50] Peter Sterling. *The Synaptic Organisation of the Brain*, chapter 6 Retina. Oxford University Press, 1998.
- [51] N. G. Stocks. Suprathreshold stochastic resonance in multilevel threshold systems. *Physical Review Letters*, 84(11):2310–2313, 2000.
- [52] Hugo Touchette and Seth Lloyd. Information-theoretic limits of control. *Physical Review Letters*, 84(6):1156–1159, 2000.
- [53] Jakob Tougaard. Signal detection theory, detectability and stochastic resonance effects. *Biological Cybernetics*, 87:79–90, 2002.
- [54] Gautam Vemuri and Rajarshi Roy. Stochastic resonance in a bistable ring laser. *Physical Review A*, 39(9):4668–4674, 1989.
- [55] Robert A. Wannamaker, Stanley P. Lipshitz, and John Vanderkooy. Stochastic resonance as dithering. *Physical Review E*, 61(1):233–236, 2000.
- [56] Andrew B. Watson. Visual detection of spatial contrast patterns: Evaluation of five simple models. *Optics Express* 12, 6(1):12–33, 2000.
- [57] Andrew B. Watson and Jr. Albert J. Ahumada. A standard model for foveal detection of spacial contrast. *Journal of Vision*, 5:1534–7362, 2005.
- [58] Andrew B. Watson and Joshua A. Solomon. Model of visual contrast gain control and pattern masking. *Journal of the Optical Society of America*, 14(9):2379–2391, 1997.
- [59] Fan-Gang Zeng, Qian-Jie Fu, and Robert Morse. Human hearing enhanced by noise. *Brain Research*, 869:251–255, 2000.

Index

- 2AFC, 24, 51, 54, 55, 66, 70
- After-image, 54
- Amacrine cell, 30
- Angled Grating Experiment, 58, 74
- Bayes theorem, 99
- Bayesian adaptive method, 56, 66
- Bipolar cell, 29, 30
- Bistable Ring Laser, 19
- Brownian motion, 22
- Calibration, 66
- CDF, 43
- CDT, 22, 24, 55, 58–61, 63, 64, 66, 67, 70, 76, 79, 80, 82, 85, 87
- Centre-surround, 29, 30
- Climate change, 17
- Cone, 26, 53
- Crayfish Mechanoreceptors, 20
- Criterion (observer imposed) , 35, 51, 52
- CSF, 103
- Dark adaptation, 53
- Dark light, 27, 53
- Detectable, 62
- Detection, 55, 58, 60, 71, 79, 84, 87
- DFT, 36–38
- Discrimination, 55, 58–61, 74, 76, 81, 82, 85, 87, 88
- Displaced Square Discrimination Experiment, 60, 81
- Distinguishable, 62
- Dithering, 31
- DoG, 103
- Double well potential, 13, 17–19
- Equipment, 64
- Excitable system, 15, 20
- Fechner, Gustav Theodor, 49
- Fourier analysis, 14
- Frequency channels, 61, 76, 104
- Ganglion cell, 30
- Generating noise, 67, 69
- Grating, 24, 30
- Grating Experiment, 58, 71
- Grating with Time Varying Noise Experiment, 63, 84
- Hearing, 22
- Horizontal cell, 29
- Ice ages, 17
- Ideal observer, 35
- ISIH, 20, 22
- Noise, 27
- NSR, 42, 43
- Observers, 69

Optic nerve, 31

Oriented Triangle Experiment, 59, 76

Paddle Fish, 20

Photoreceptor, 26, 27, 53

PSD, 14, 19, 20, 24, 36–39, 41, 44

Psychometric function, 35, 50, 56, 66

Psychophysics, 49, 51, 65

Results, 70

Retina, 25–28, 31, 54, 58

ROC curve, 33, 35, 36, 41, 42, 46, 48, 51

Rod, 26, 28, 53

Schmitt Trigger, 18, 19, 22

SDT, 33–35, 51

Sensitivity, 28, 29, 49, 53, 54

Single interval task, 57

Square Detection Experiment, 60, 79

Square Wave Discrimination Experiment,
61, 82

Synapse, 28

Time varying noise, 55, 63, 64, 69

Triangle with Time Varying Noise Exper-
iment, 64, 85

Two interval task, 57

Vision, 22–24, 27

Weber's law, 28, 50